A Study of Variable Friction Base Isolation Systems

Sandip Timsina

A thesis
submitted in partial fulfillment of the
requirements for the degree of

Master of Science in Civil Engineering

University of Washington

2017

Committee:
Paolo M. Calvi
Richard Wiebe
Jeffrey W. Berman

Program Authorized to Offer Degree:
Department of Civil and Environmental Engineering

University of Washington

Abstract

A Study of Variable Friction Base Isolation Systems

Sandip Timsina

Chair of the Supervisory Committee:
Assistant Professor Paolo M. Calvi
Civil and Environmental Engineering

Variable Friction Systems (VFS) have been recently proposed as possible alternatives to traditional base isolation devices. The main benefit of VFS over other systems lies in their superior energy absorption properties that comes from the greater encompassed area of the hysteresis loops.

Greater energy dissipation results in higher damping and, in turn, in lower seismic demand on the system. More specifically, more dissipative base isolation systems offer better seismic protection in that they lower the overall displacement demand and limit the lateral forces and accelerations transmitted to the isolated structure.

Recent numerical studies of VFS employing both flat and curved sliding surface systems with variable friction coefficients indicate that VFS are theoretically capable of high seismic performance, and preliminary results suggest that they represent promising solutions.

However, the available studies are limited to two kinds of VFS with specific characteristics. As a consequence, a generalized design process for VFS is currently missing. In addition, the design process that was proposed for VFS makes use of a number of empirical equations, particularly for the calculation of the equivalent damping associated to these devices, which have not been sufficiently validated.

This thesis presents an extensive discussion on VFS, in the attempt of leading to a better understanding of their seismic behavior and performance. More than 500,000 non-linear time history analyses are conducted to study and characterize the damping properties of VFS, and to investigate their effectiveness at protecting SDOF and MDOF case study structures from the effects earthquakes. The results of the analyses are also used to extend and generalize the current design approach for VFS.

TABLE OF CONTENTS

Page

LIST OF FIGURES

LIST OF TABLES

ACKNOWLEDGMENT

I would like to thank my friends and family for their continued support, and being there when I needed them to be.

I would also like to thank Dr. Richard Wiebe and Dr. Jeffrey Berman for, not just being a part of my defense committee, but also being key professors during my time at the graduate school.

Finally, I would like to thank my advisor Dr. Paolo Calvi for funding the project, and putting the extra effort to help me understand the scientific process, and guiding me through my thesis. Without him, this work would not have been possible, and I am glad to have worked with him.

Chapter 1

INTRODUCTION

1.1 Background

Earthquakes are amongst the deadliest and most costly natural catastrophes that affect our society. Over the years, earthquakes have been the cause of thousands of casualties and very high economic losses. In the US alone, the annual earthquake losses are estimated at $4.4B [FEMA, 1999]. Often, the loss of life is considerable. For example, in the Nepal earthquake of 2015 with a magnitude of 7.8 Richter scale, more than 9000 casualties were reported, with damages worth millions of dollars [Rai et al., 2016].

Recent seismic events, such as the Darfield earthquake of September 2010 [Dhakal, 2010] as well as past earthquakes, such as the Nisqually earthquake of 2001 [Filiatrault, 2003], have shown that even if modern seismic design techniques may be able to limit the damage to main structural elements during intense earthquakes, the damage to secondary structural and non-structural elements can be extensive, costly, and in some cases can lead to loss of life. In the 2010 M7.1 Darfield (New Zealand) earthquake, that imposed seismic demands comparable to the design level earthquake in the Christchurch region, total losses have been estimated at NZ$5billion [Bollard and Ranchhod, 2011], even though there was no loss of life. In the context of past seismic design philopsophies, which had life safety and collapse prevention as two main objectives, such outcomes were considered acceptable. However, as the desire for high performance buildings increases, it is increasingly evident that engineers require reliable methods and tools to mitigate the effects of earthquakes on both structural and non-structural elements, enhancing the overall resiliency and reducing the vulnerability of the built environment.

In today's "performance based" context, an effective way of protecting structures, and

achieving a desired performance, is to mitigate the seismic demand on the system itself. To this end, base isolators represent a promising solution and are now recognized as effective tools to ensure a high level of building performance under earthquake-induced lateral loads. Base isolators consist of low lateral stiffness devices installed beneath key supporting points of the structure they are intended to protect. The goal of base isolation is to prevent the structure from damage, by absorbing the full displacement demand induced by seismic ground motions at the isolation layer. Isolating a structure results in a more controlled structural response, lower floor accelerations and lower lateral forces transmitted to the structure.

1.2 Motivation

A number of base isolation solutions have been proposed and implemented over the years and are now potentially available for practical use. Friction devices and laminated lead-rubber bearings are perhaps the most popular devices in use. While quite stable and relatively efficient at dissipating energy, lead-rubber bearings integrate somewhat poorly in today's performance-based design context in which design objectives are no longer limited to preventing structural collapses. They have two main limitations: the lack of self-centering properties (i.e. significant residual displacements are expected at the end of an earthquake) and the likely need to replace all devices that have been stressed beyond the yielding of the lead element (a necessary condition to allow energy dissipation). Further, lead-rubber bearings are affected by rotational equilibrium constraints, which limit the allowable lateral displacement to approximately 1/3 of the bearing size (taken in the direction parallel to the motion).

On the other hand, current friction devices are somewhat limited in that a device with given characteristics (e.g. a Friction Pendulum with certain radius of curvature and friction coefficient) can only guarantee a high building performance with respect to some of the parameters of interest. More specifically, the objective of a base isolation system should be to reduce the seismic forces and accelerations transmitted to the structure while achieving the lowest possible maximum displacement and residual displacement at the isolation layer.

However, such objectives cannot be met simultaneously.

For example, the use of a smaller radius of curvature (i.e. high post-activation stiffness) has the advantage of limiting the residual displacement and the maximum lateral displacement in case the system is hit by an event of greater magnitude than the design earthquake. At the same time, the use of low friction tends to produce devices which "activate" (and are therefore beneficial) for more frequent (less intense) earthquakes. In contrast, high-friction low-curvature devices may not activate for minor earthquakes and may be subjected to excessive displacement demand in case of rare events. A nontrivial downside of using small radius of curvature devices, however, is that the system will experience larger induced vertical accelerations as the lateral displacement demand increases [Calvi et al., 2016].

In general, the "optimal" solution a designer would often select is an intermediate one. It should be further pointed out that the solution adopted as "optimal" under the design earthquake demand may not work for more or less intense seismic events.

In this context, the pursuit of more efficient base isolation systems has triggered the interest of many investigators and has been the object of numerous research projects all across the world. For instance, recent studies have explored the possibility of employing flat or curved sliding-surface base isolators with variable friction coefficients [Calvi et al., 2016; Calvi and Ruggiero, 2016]. Preliminary studies performed on these new types of devices have shown that they are capable of high seismic performance, and that they can theoretically improve upon traditional sliding isolators in light of their higher energy-absorption capacity.

Although promising, the development of these newly proposed systems is in its infancy, and further numerical, analytical and experimental work is required before Variable Friction Systems (VFS) can be brought into practice.

1.3 Objectives

The objectives of this thesis are motivated by the discussion presented in the previous sections. In particular, it has been emphasized that there are still many knowledge gaps associated to the properties and performance of VFS, which prevent this technology from being

developed and implemented for practical use. In this context, the main objectives of this research can be summarized as follows:

- To provide some insight into the damping properties of generic VFS, developing suitable equations to be used in a detailed design framework;
- To study the performance of VFS with arbitrary radius of curvature and frictional properties, possibly establishing preliminary criteria for selecting the characteristic of the "optimal" device;
- To provide some preliminary evidence of the effectiveness of VFS at protecting buildings from the effects of earthquakes of various magnitudes.

These objectives are achieved numerically, via 2D non-linear time history analyses, conducted considering a number of single-degree-of-freedom (SDOF) and multi-degree-of-freedom (MDOF) base-isolated case study structures, and a large suite of input ground motions of varying magnitudes and characteristics.

The results of the analyses are used to draw some preliminary conclusions about the performance and the design methodology proposed for VFS, simultaneously assessing their energy absorption properties and calibrating suitable design equations for the estimation of equivalent damping factors. The results are also used to illustrate the key differences in performance of the different VFS considered, emphasizing apparent advantages and drawbacks.

The work presented in this thesis fits into a more ambitious research project that aims at a full development and implementation of this innovative family of base isolation devices. The achievement of this greater objective, will clearly require further efforts including more advanced numerical analyses and laboratory experiments under more complex real-world conditions.

1.4 Thesis Content

This thesis is organized as follows:

- Chapter 2 : Literature Review. Chapter 2 examines existing base isolation systems, with particular focus on the evolution of Variable Friction Systems (VFS). To this end, a detailed discussion on mechanics, numerical modeling and design philosophies, is presented.

- Chapter 3: Verification of the damping properties of VFS. Chapter 3 focuses on studying the damping properties of this new family of base isolators. Through extensive non-linear time history (NLTH) analyses, the effective damping properties of VFS are characterized and design equations are calibrated. Considerations on the relationships between effective damping and demand reductions are also included.

- Chapter 4: Performance of VFS base isolated SDOF systems. Chapter 4 investigates the performance of base isolated SDOF case study structures, through a very large number of NLTH analyses. A series of important parameters are included in the numerical study. In addition, the results presented in Chapter 4 provide some evidence on the reliability of the preliminary design approach proposed for VFS.

- Chapter 5: Multiple degree of freedom structures. Chapter 5 looks at the response of a set of MDOF case study structures, isolated using VFS with different characteristics. Even though the results presented in this chapter are meant to be of preliminary nature, they provide some insight into aspects of the response of VFS that could not be observed while the study was limited to SDOF systems.

- Chapter 6: Conclusions and future work. Chapter 6 summarizes the findings of this work, pointing out potential advantages and drawbacks of VFS, and outlines future work for this project.

Chapter 2

LITERATURE REVIEW

2.1 Existing Base Isolation Systems

The following section briefly discusses current research that provides foundation for this proposed work. Since there is a large volume of literature available on the topic of base isolation, this chapter focuses on seismic isolation as practiced in the US, and more specifically on friction bearings.

Base isolators consist of low lateral stiffness devices installed beneath key supporting points of the structure that they are intended to protect. The goal of base isolation is to prevent the isolated structure from damage, by shifting the fundamental period of the structure to the long period range, and by absorbing the full displacement demand induced by the seismic ground motions at the isolation layer. Isolating a structure results in a more controlled structural response, lower floor accelerations, and lower lateral forces transmitted to the structure.

The reduced seismic demand allows the superstructure to remain elastic, or nearly elastic, following a design level event. Furthermore, isolating a structure contributes to reducing the likelihood of damage to displacement sensitive and acceleration sensitive equipment, nonstructural components, and content.

Though the concept of seismic isolation dates back more than a hundred years, the modern era of base isolation began in the mid 1960s with the New Zealand Department of Scientific and Industrial Research [R.I. Skinner, 1993] and the development of rubber isolation bearings equipped with sufficient vertical stiffness to resist service loading. The first modern building to incorporate base isolation was the Pestalozzi School in Skopje, Macedonia, constructed in 1969, while the first rubber-base isolated building in the US was constructed in 1985 [Naeim

and Kelly, 1999].

Modern rubber bearings are composed of elastomeric rubber layers alternating with steel plates joined together through a process called vulcanization. The bearing's low lateral stiffness is solely linked to the height and the area of the rubber. The steel plates provide confinement and impede the bulging deformation of the rubber, greatly enhancing the vertical stiffness of the bearings [Charles Roeder, 1990].

Lead-rubber bearings were introduced in the 1970s in New Zealand [Robinson, 2011] as a more dissipative alternative to laminated-rubber bearings. Lead-rubber bearings consist of traditional elastomeric bearings with the addition of lead plug designed to yield under lateral deformation and to dissipate supplemental energy (figure 2.1(a)). A detailed description of the mechanical behavior of laminated elastomeric bearings typical of modern practice can be found in the work by Naeim and Kelly [1999]. Both laminated-rubber bearings and lead-rubber bearings have been proven capable of protecting structural systems from the effects of earthquakes and have been used for seismic isolation around the world [R.I. Skinner, 1993].

As the research into base isolation increased, modern sliding base isolators came about in the late 1980s. The first analytical and experimental studies on Friction Pendulum (FP) isolation bearings was conducted by Victor Zayas [1987]. A Friction Pendulum system is a friction type of sliding bearing that uses gravity as the restoring force. The system consists of an articulated friction slider that travels on a spherical concave sliding surface (figure 2.1(b)). In this context, the constant curvature sliding surface is characterized by a nominally single-valued friction coefficient. To date, devices from this general family have been extensively studied analytically and experimentally by a number of authors (e.g. [Victor Zayas, 1990; Constantinou et al., 1990; Mokha et al., 1990, 1991; Calvi et al., 2004; Casarotti and Pavese, 2014] amongst many others) and used in real-world applications for a variety of buildings, bridges, and other structures.

Alternatives to standard FP systems have been proposed, with the intent of improving the response and possibly reducing the size of the bearings. A key system with multiple sliding bearings is a Triple Pendulum Friction Bearing (figure 2.1(c)). Details on some multi-surface

devices derived from the FP can be found in the works of Fenz and Constantinou [2006, 2008] amongst others. Tension capable bearings have also been proposed by Roussis and Constantinou [2006]. Kasalanati and Constantinou [2005] proposed the use of pre-stressing tendons as a means of overcoming uplift issues.

Modern seismic codes incorporate provisions for the design of base isolated structures. To this end, ASCE 7-10 ASCE [2013], allows the adoption of three types of analysis: Equivalent Linear Analysis (ELA), Response Spectrum Analysis (RSA) or Nonlinear Time History Analysis (NLTHA). Because of its simplicity, limitations on the adoption of the ELA apply on the structural layout, on the seismicity of the site and on the isolator properties. The behavior of the isolation system within the ELA is represented by using equivalent damping and stiffness. The equivalent damping is used to estimate the response spectrum reduction factor. The process is more complex for RSAs and NLTHAs, as the code requires the use of a full 3D model, with full representation of bi-directional loading and torsional response.

A peer review process is mandatory for isolation projects and is generally managed through the local authorities, who often nominate an external team of peer reviewing engineers. Analogously, prototype tests and approval are required specifically for every single project unless similarity can be demonstrated with other units already approved in the past. The peer review team reviews the prototype test report and sometimes attend the tests [Pietra et al., 2015].

For modeling purposes within the context of NLTHA, the behavior of friction base isolators is typically derived from first principles and their force displacement response is typically idealized simplifying the isolators' behavior as piecewise-linear hysteresis, as shown in figure 2.1 for different devices.

It can be seen that a traditional FP system behaves essentially rigidly as long as the acting shear force is smaller than the weight of the structure multiplied by the friction coefficient characterizing the sliding surface. Upon activation, the tangent stiffness of the system decreases to a value equal to the ratio between the borne weight and the radius of curvature of the sliding surface. In an extreme simplification, and neglecting a number of

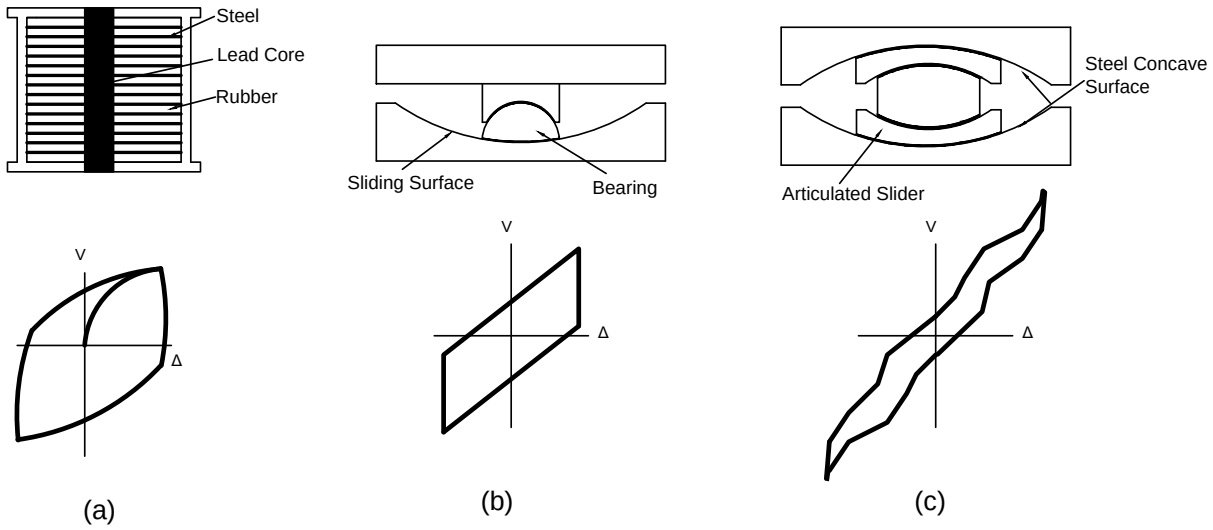

Figure 2.1: Model of isolator and corresponding hysteresis for (a) Lead Rubber Bearing, (b) Friction Pendulum, and (c) Triple Friction Pendulum devices

effects, such as the variation of the axial force [Calvi et al., 2004], the dependency of the friction coefficient on pressure and velocity, etc., the shear force that is transmitted by a FP system is merely a function of the friction coefficient (typically assumed constant in value), the borne weight, the radius of curvature, and the lateral displacement.

Extensive testing of individual bearings as well as shake table testing of base-isolated buildings have been conducted over the past three decades. The first Friction Pendulum system was tested on a 2-story frame [Victor Zayas, 1987]. Several tests on Friction Pendula have then been conducted in the early 1990s [Constantinou et al., 1990; Mokha et al., 1990], and these systems were found to provide effective horizontal isolation.

Comprehensive programs have evaluated the performance of multi-stage FP devices [Fenz and Constantinou, 2008; Morgan and Mahin, 2011]. A few experimental studies focused specifically on evaluation of secondary system response [Wolff and Constantinou, 2004; Kelly, 1982; Kelly and Tsai, 1985]. It was found that although lead-rubber bearings reduced the displacement demand in the base isolation system, they were less beneficial than linear

elastic bearings, with respect to the secondary system response. It was also observed that the isolation system was very effective in reducing the response of an oscillator tuned to the natural frequency of the fixed-base structure, but could slightly increase the response of the high frequency detuned oscillators. Wolff and Constantinou [2004] focused on secondary system response by evaluating floor accelerations and floor spectra in different isolation systems (friction pendulum bearings and flat sliders) with and without viscous dampers. The authors concluded that highly nonlinear systems incorporating friction pendulum bearings or flat sliders were reasonably effective at protecting non-structural elements and building contents.

More recently, two test programs on full scale isolated buildings have been conducted at the National Institute for Earth Science and Disaster Prevention (NIED) E-Defense shaking table of Japan [Warn and Ryan, 2012; Ryan et al., 2012]. From the first study, it was observed that elastomeric isolation systems could only guarantee the functionality of the structure in case of a near-fault motion but not for a long duration, long period ground motion generated from a subduction earthquake.

The main outcome of the second study was the significant influence of vertical excitation and the amplification of the horizontal accelerations recorded at the various levels of the building as a consequence of the multi-directional excitation. The findings of these experimental studies suggest that mitigation of the effect of multi-directional seismic excitations may be required to maintain functionality in critical base-isolated buildings, and that this may require the use of isolation devices capable of higher performance.

To this end, Variable Friction Systems (VFS) were recently proposed as promising seismic alternatives to currently available friction sliders such as FP systems etc. [Calvi et al., 2016; Calvi and Ruggiero, 2016]. The coexistence of materials with different frictional properties within the same device, the use of better-performing materials and a more clever combination of sliding surfaces, open the door to the possibility of new hysteretic responses, such as those shown in figure 2.2 (a).

The results of preliminary analytical studies showed that VFS can dissipate more energy

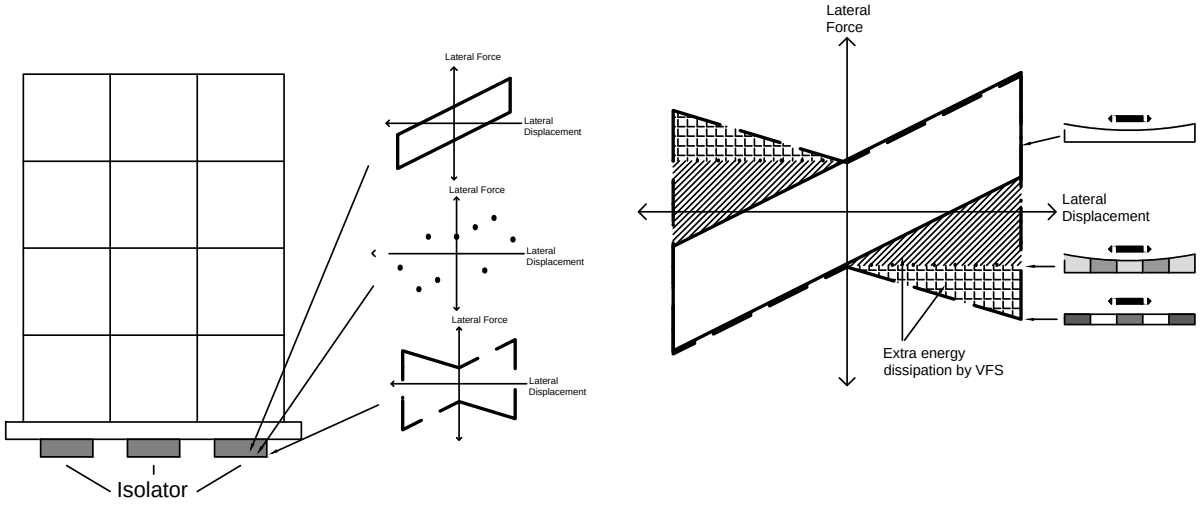

Figure 2.2: (a) Schematic view of base isolated structures with varying force-displacement loop shapes and (b) comparison of standard and innovative force-displacement loop shapes

and can be capable of higher performance with respect to their "traditional" counterparts. More specifically, smaller (i.e. less costly) and flatter (i.e. capable of reducing undesired vertical fluctuations and accelerations) devices, have been shown capable of protecting more efficiently the structures analyzed, at all levels of earthquake intensities. The larger area encompassed by the hysteresis of the innovative systems, as shown in figure 2.2 (b), indicates that more energy is dissipated by these system.

Even though flat VFS do not afford re-centering capabilities, their cost is approximately one third of that of a curved device, making them ideal to protect low-mass elements such as high-tech strategic pieces of equipment (e.g. MRI machines in hospitals) that need to remain functional during and immediately after a seismic event or to protect temporary structures or structures over the course of the construction phases.

A more detailed discussion on the mechanics and numerical modeling of VFS, which represent the focus of this research work, is presented in the next subsection.

2.2 Mechanics and Numerical Modeling of VFS

2.2.1 Mechanics of VFS

Two kinds of VFS have been studied thus far (referred to as "BowTie" and "BowC"), and their mechanics has been discussed in detail by Calvi et al. [2016] and Calvi and Ruggiero [2016]. For the reader's benefit, a brief overview of these two devices is reported below (mostly taken from the two papers just referenced).

The BowTie isolation device consists of a fixed base-plate overlaid by a sheet of stainless steel material with areas with different friction coefficients and a slider composed by a steel plate and a sliding pad of low friction material (e.g.: polytetrafluorethylene or polyamide) in contact with the stainless steel, as shown in Figure 2.3 [Calvi et al., 2016]. The slider is free to move with respect to the base-plate surface, treated specifically to form a number of bands arranged as a series of concentric rings. Each ring is characterized by different frictional properties, with the friction coefficient between the slider and the base plate progressively increasing moving outward from the center of the device.

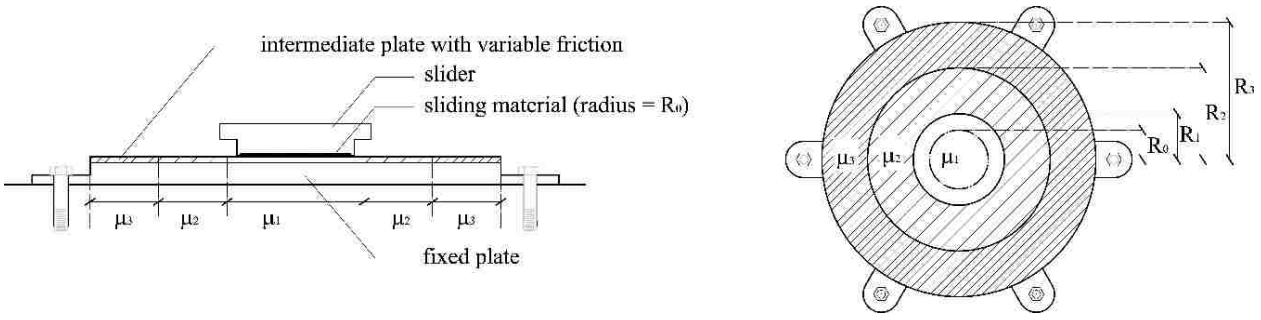

Figure 2.3: (a) Cross section view of a Bow C device, (b) aerial view of a Bow C device [Calvi et al., 2016]

In the example shown in Figure 2.3, the friction coefficient μ_1 would be lower than μ_2, which, in turn, would be lower than μ_3. Under lateral loads applied on the BowTie device, the friction between the low friction material and the stainless steel plate provides frictional

resistance and energy dissipation, after activation of lateral motion. Because of the geometry of the sliding surface, there is no restoring force.

The lateral force-displacement response of a BowTie device is shown in figure 2.4. In the figure, the hysteretic response for an isolator using a three-band base plate is shown, where the area of the slider corresponds to the area of the central ring. It is assumed that the axial stress on the BowTie device is uniform over the area of the slider, there is no difference between static and dynamic friction, and the value of the friction coefficient assigned to each band is well defined and perfectly stable. In reality, the friction coefficient may vary as a function of pressure, velocity, and surface temperature, which might cause the change of stiffness. However, the hysteretic response of built BowTie devices would exhibit the same phases.

As the lateral load applied on the system increases from zero (figure 2.4, step a), the BowTie exhibits a perfectly rigid response until motion is activated (i.e.until the applied lateral load equals the vertical load W multiplied by the friction coefficient μ_1 in the central ring of the plate). After this condition is reached, the top portion of the device begins its motion with respect to the bottom plate. As shown in steps (c) and (d) in figure 2.4, as the slider sits across the inner and middle bands, resistance comes from both the rings, proportional to overlapping areas times appropriate friction coefficients. As the slider moves, as shown in Figure 2.4 from step (c) to step (d), the slider transitions from sitting on ring 1 and 2 to sitting on ring 2 and 3. In between these phases, there may be a situation during which the lateral strength is provided by all three rings.

During these phases the force-displacement response of the system is non-linear, to an extent determined by the number of rings, their dimensions and their frictional properties [Calvi and Ruggiero, 2016].

If the lateral load is reduced and reversed (step e), the lateral displacement will remain unchanged until the motion is activated in the reverse direction, which is reached once the lateral load is equal (in magnitude) and opposite (in sign) with respect to the load responsible for causing the current displaced configuration. During the unloading-reloading phase, prior

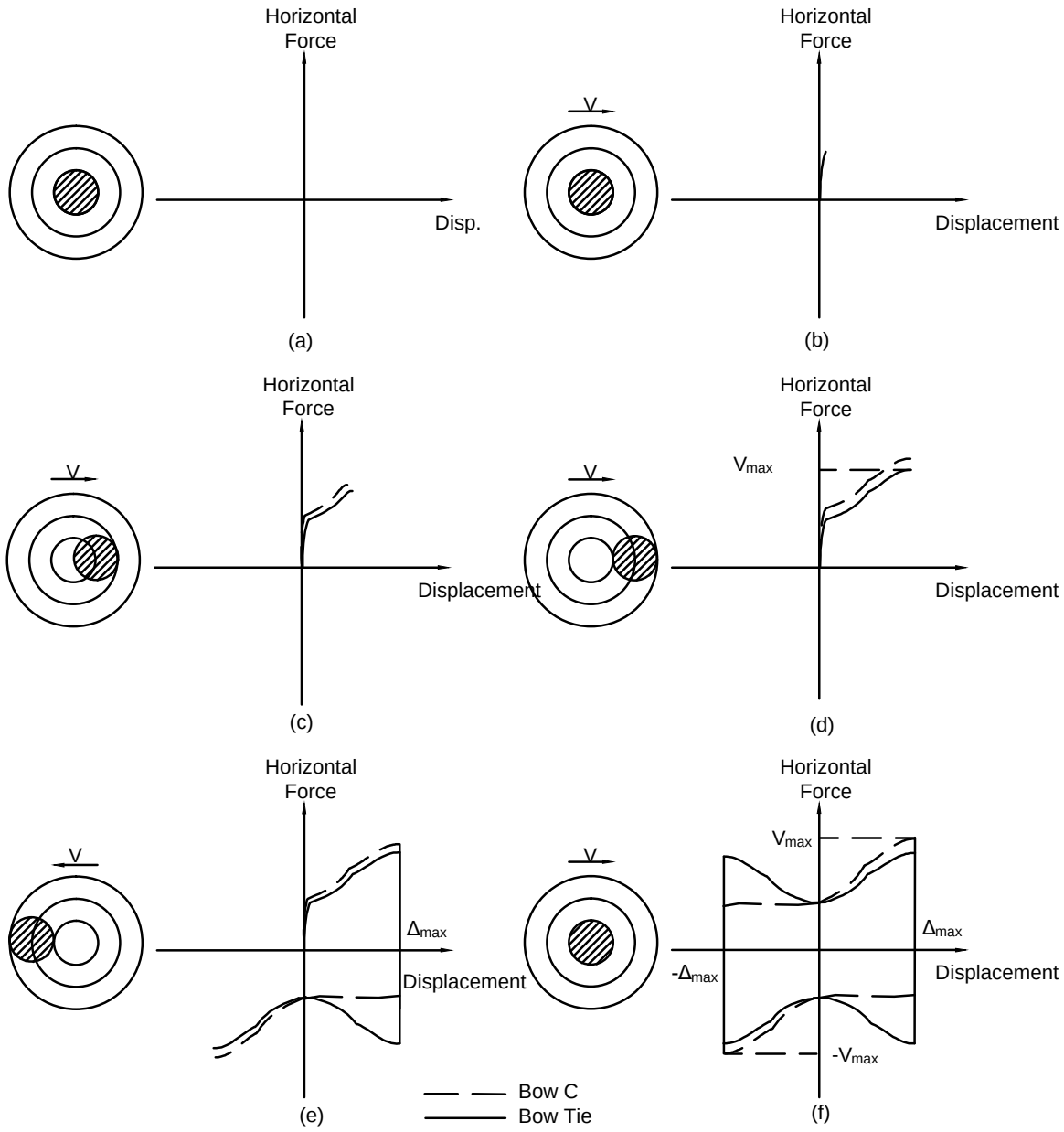

Figure 2.4: Force-displacement response of a BowTie (BT) device and a BowC (BC) device: (a) at rest; (b) pre-activation; (c) post-activation; (d) at maximum displacement; (e) lateral load reversal; (f) at initial position

(adapted from [Calvi et al., 2016])

to activation, the isolation device experiences a perfectly rigid response.

After the activation of the lateral motion in the reversed direction, the lateral load required to push the slider back to its initial position is progressively lower as shown in figure 2.4 (e). The force-displacement curve follows a trend which is symmetric to the loading branch, with respect to the displacement-axis of the graph. Returning the slider to its initial position comes from the application of a lateral load in the appropriate direction (step f) that is non-negligible.

A closed-form procedure for calculating the actual response of a BowTie device was derived by [Calvi and Ruggiero, 2016], who also showed that, for most applications, the hysteresis of a BowTie can be approximated using piecewise-linear hysteretic models.

To improve the BowTie on the lack of re-centering properties, a system referred to as the "BowC" device has been conceived by Calvi et al. [2016] and Calvi and Ruggiero [2016]. The BowC combines a traditional FP and a BowTie, so to take advantage of the characteristics of both systems.

The BowC isolation device is similar to a BowTie in essence, but like in the Friction Pendulum, the sliding surfaces are characterized by a radius of curvature (Figure 2.5). Under the application of lateral loads, after activating the lateral motion, the friction between stainless steel plate surface and low friction material layer provides increasing non-stepped frictional resistance and energy dissipation. Additional lateral strength is provided by the presence of the curvature at the sliding surfaces. Hence, both lateral strength and lateral stiffness of the device are a function of both the radius of curvature of the sliding surface and the frictional properties selected.

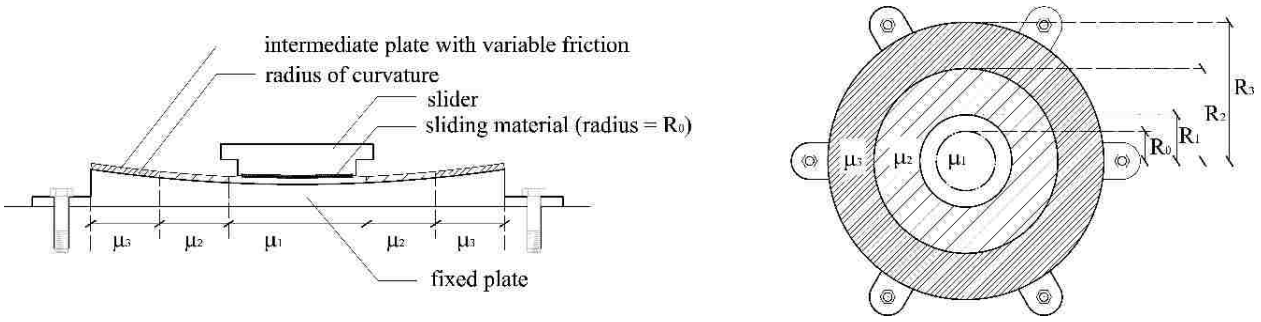

Figure 2.5: (a) Cross section view of a BowC device; (b) aerial view of a BowC device [Calvi et al., 2016]

Depending on the radius of curvature selected for the sliding surface, it is possible to "correct" the hysteresis loop shape of the BowTie, making it more or less self-centering and more or less "dissipative". It was suggested that the radius of curvature be calculated using the following equation:

$$R = \frac{2\Delta_d W}{V_d - \mu_1 W} \tag{2.1}$$

Where R is the radius of curvature of the surface, W is the seismic weight of the structure, Δ_d is the design displacement, V_d is the corresponding shear force and μ_1 is the initial (i.e. the lowest) friction coefficient.

The force-displacement response of a BowC device is shown in figure 2.4. The qualitative response is sketched for an isolator equipped with a three band base plate characterized by a radius of curvature calculated according to Equation 2.1. As for the case of the BowTie device described earlier, the area of the articulated slider corresponds to that of the central ring. Again, it is assumed that the axial stress on the BowC device is uniform over the area of the slider, that there is no stick slip, and that the value of the friction coefficient characterizing each band is well defined and perfectly stable [Calvi et al., 2016].

A BowC device subjected to increasing lateral load exhibits a perfectly rigid response until the applied load overcomes the activation load, i.e. the vertical load W multiplied by

the friction coefficient μ_1 (step (a) and (b), figure 2.4).

As the slider sits across the inner and the middle bands of the base plate (step c), the lateral resistance is provided by both the overlapped rings (in proportion to the overlapping area times the appropriate friction coefficient), as well by the "curvature component", whose stiffness corresponds to the weight of the structure divided by the radius of curvature of the sliding plate (K = W/R). As a consequence, in this phase the lateral stiffness increases, as a function of both the higher friction between slider and plate in the external rings and the radius of curvature R. The transition from step (c) to step (d) can be described in a similar way, so that the total lateral strength of the system can be generally expressed as:

$$V = \frac{W}{A}(A_1\mu_1 + A_2\mu_2 + A_3\mu_3) + \frac{W}{R}\Delta \tag{2.2}$$

Where R is the radius of curvature of the sliding surface, Δ is the displacement undergone, A is the area of the slider, A_1, A_2 and A_3 are the fractions of A overlapping ring 1, 2 and 3 and μ_1, μ_2 and μ_3 are the corresponding friction coefficients.

Again the degree of non-linearity of the response over the course of these phases depends on the number of rings, their dimensions and their frictional properties. If the lateral load is reduced and reversed (step e), the lateral displacement will remain unchanged until the motion is activated in the reversed direction. If the radius of curvature of the sliding surface has been determined in line with Equation 2.1, this condition is reached once the lateral load is equal (in magnitude) and opposite (in sign) with respect to the initial activation load. After the activation of the lateral motion, the lateral load required to push the slider back to its initial position is essentially constant as shown in figure 2.4 (e). Loading in the opposite direction results in a symmetric force-displacement response. Returning the slider to its initial position always implies the application of a lateral load equal in magnitude to the initial activation load (step f) Calvi et al. [2016].

As for the case of the BowTie, Calvi and Ruggiero [2016] showed that, for most applications, the hysteresis loop of a BowC can be idealized using simpler piecewise-linear hysteretic

models, as shown in figure 2.2 (b).

2.2.2 Numerical Modeling of VFS

In addition to describing the mechanics of VFS, Calvi and Ruggiero [2016] provided some insight into the integration of these new devices into the larger problem of nonlinear structural analysis. They suggested that, at least in the context of relatively simple non-linear dynamic analysis, the base isolators should be modeled using a lumped plasticity approach. In this case, the translational degree of freedom at the base of a structure is released and a single translational spring with an appropriate-shaped hysteresis may be used.

Typically, the hysteretic model is calibrated using experimental results or analytical approaches. In the present case, the isolators hysteretic models are entirely based on the mechanical considerations discussed in the previous sections, as no experimental evidence is currently available.

Table 2.1 summarizes the properties of a variable friction sliding base isolator element that must be specified during a NLTHA. The element is fully defined by a total of five functions used to trace the backbone curves as well as the reloading and unloading curves, as shown in Fig. 2.6.

Note that the curve identified as $F_2(x)$ in figure 2.6 should ideally be infinitely stiff, given that it represents the element's frictional response prior to activation. However, for numerical reasons, it is idealized using a linear function with an assigned stiffness on the order of 10000 times (or greater) than the post activation stiffness K_p. (Note also that the slope of F_2(x) is voluntarily exaggerated in the representation of figure 2.6).

The backbone curves are combined to give the final response according to:

$$F_r(x) = \begin{cases} max[min(F_1(x), F_2(x - x_p)), F_3(x)] & if \;\; x \geq 0 \\ max[min(F_4(x), F_2(x - x_p)), F_5(x)] & if \;\; x < 0 \end{cases}$$

All of the backbone functions ($F_1(x)$, $F_3(x)$, $F_4(x)$ and $F_5(x)$) may be either linear or

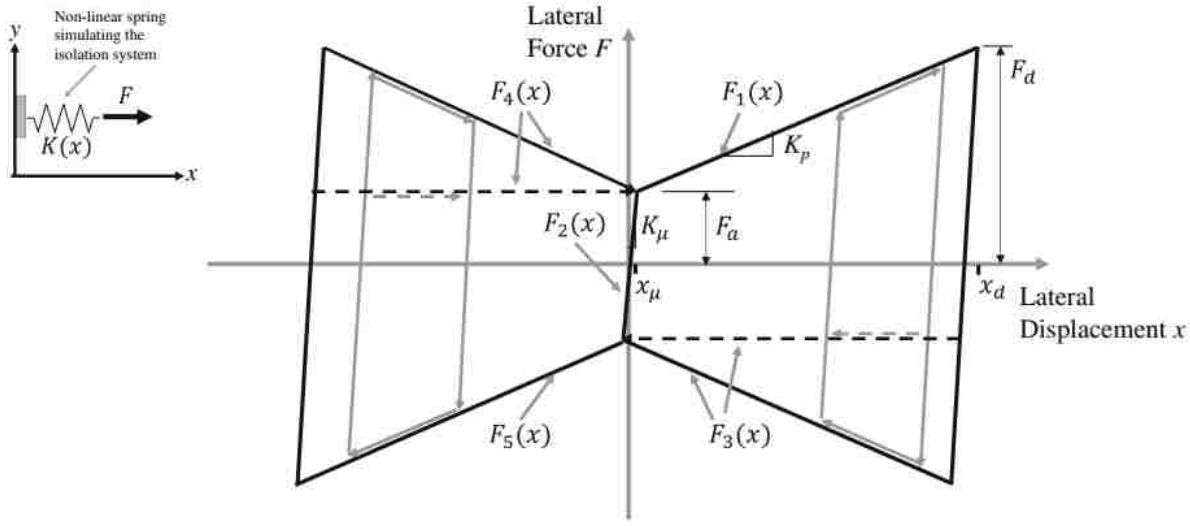

Figure 2.6: Hysteretic response (idealized as linear piecewise) of a BowTie bearing (continuous line) and of a BowC bearing (dashed line) [Calvi and Ruggiero, 2016]

nonlinear, depending upon the level of accuracy desired in the numerical analyses. Linear functions are expressed as:

$$F_1(x) = F_a + K_p x \tag{2.3}$$

$$F_2(x) = K(x - x_p) \tag{2.4}$$

$$F_3(x) = \begin{cases} -F_a - K_p x & for\ \ Bow\ Tie \\ -F_a & for\ \ Bow\ C \end{cases}$$

$$F_4(x) = \begin{cases} F_a - K_p x & for\ \ Bow\ Tie \\ F_a & for\ \ Bow\ C \end{cases}$$

$$F_5(x) = -F_a + K_p x \tag{2.5}$$

Table 2.1: Summary of the properties of a variable friction sliding base isolator element

Name	Symbol	Computation
Seismic Weight	W	User-specified
Initial friction	μ_L	User-Specified
Design displacement	x_d	Selected design demand
Design force	F_d	From design process (see chapter 3)
Post-activation stiffness	K_p	User-Specified (from design requirements)
Initial stiffness	K_μ	$10000K_p$
Activation displacement	x_μ	$x_\mu = \frac{F_a}{K_\mu}$
Activation force	F_a	$W\mu_{low}$

Where x_p is a plastic displacement offset calculated at each converged stage of the analysis as:

$$x_p = x - x_\mu \tag{2.6}$$

and V_{act}, K_0, K_p are the activation shear, pre-activation stiffness , and post-elastic stiffness respectively of the system.

In the context of a NLTHA, to minimize the occurrence of numerical errors, the instantaneous stiffness of the system can be evaluated, iteratively within each time step. This can be done by employing an iterative procedure of the Newton-Raphson "family".

It should be noted that Calvi and Ruggiero [2016] had only considered two kinds of VFS with specific characteristics (i.e. the BowTie and the BowC). However, VFS can be designed and theoretically built assigning arbitrary frictional properties and radius of curvature. Equations 3.1.2 can be adapted and generalized simply by introducing a new design parameter, β, which represents the ratio between re-centering and loading stiffness charac-

terizing the response of the device (this new parameter will be further discussed in later sections). Thus, equations 3.1.2, can be re-written for any arbitrary VFS as equation 3.1.2 where F_1, F_2, and F_5 are the same as described earlier, but :

$$F_3(x) = \begin{cases} -F_a - \beta K_p x & for\ all\ \beta\ systems \end{cases}$$

$$F_4(x) = \begin{cases} F_a - \beta K_p x & for\ all\ \beta\ systems \end{cases}$$

2.3 Displacement Based Design of VFS

2.3.1 Displacement Based Design of Base Isolated Structures

Calvi et al. [2016] and Calvi and Ruggiero [2016] recommended that the design of VFS be performed employing Direct Displacement Based Design (DDBD) criteria, as discussed in general terms by Priestley et al. [2007c] . The basic procedure for "traditional" base isolated structures is summarized in figure 2.7.

As shown in figure 2.7 (a), the structure is first idealized as a SDOF system. The equivalent SDOF structure is then based on a model that takes into account both the isolation system and the structure. For design purposes, the structure can be assumed to deform according to its yield displacement. This assumption allows the estimation of the displacement values at each floor level for all structural elements and consequently the yield displacement of the equivalent model. The yield displacement shape of the structure alone can be found using appropriate equations as suggested by [Priestley et al., 2007c] or by simply assuming a linear deformed shape. This assumption is often adequate given that the structural response is capacity protected and not expected to be critical. Therefore, the effective height (H_e) of the structure alone can be calculated as:

$$H_e = \frac{\sum_{i=1}^{n}(m_i \Delta_i H_i)}{\sum_{i=1}^{n}(m_i \Delta_i)} \tag{2.7}$$

Where m, Δ and H are mass, displacement and height respectively and i indicates the

floor level.

In conducting the conceptual design of the system, the displacement of the structure alone ($\Delta_{d,str}$) is assumed in the range of 80% of the calculated yield displacement. The starting point of the design process is the selection of the design displacement of the isolation system ($\Delta_{d,iso}$) and therefore the selection of the displacement of the global structural system (Δ_{sys}=$\Delta_{d,str}$+$\Delta_{d,iso}$). The second step, shown in figure 2.7 (b), consists of calculating the equivalent damping of the system. The equivalent viscous damping $\xi_{e,sys}$ is used to determine a spectral reduction factor, which is used to correct the displacement demand on the structure. The equivalent viscous damping ratio of the system can be estimated combining the contributions of the structure and of the isolation system, assuming that the same shear force is applied to both parts. For the structure, the equivalent viscous damping is normally assumed as 5% or lower, given that an elastic response will be enforced. For the isolation system, the equivalent damping is estimated as a function of the force-displacement relationship that characterizes the system. Normal values range between $\xi_{e,iso}$ of 0.2 and 0.3 (20%-30%). The system equivalent viscous damping ($\xi_{e,sys}$) can be computed as:

$$\xi_{e,sys} = \frac{\xi_{e,s}\Delta_{d,str} + \xi_{e,iso}\Delta_{d,iso}}{\Delta_{d,sys}} \tag{2.8}$$

The effective period $T_{e,sys}$ of the system can be obtained entering an appropriately corrected design displacement spectrum, as shown in figure 2.7 (c). The effective period of the structure is used to calculate the effective stiffness of the system ($K_{e,sys}$):

$$K_{e,sys} = \frac{4\pi^2 m_e}{T_{e,sys}^2} \tag{2.9}$$

Where m_e represents the effective mass of the system, computed as:

$$H_e = \frac{\sum_{i=1}^{n}(m_i\Delta_i)}{\Delta_{d,sys}} \tag{2.10}$$

In which m_i and Δ_i are mass and displacement of each floor, including the ground floor

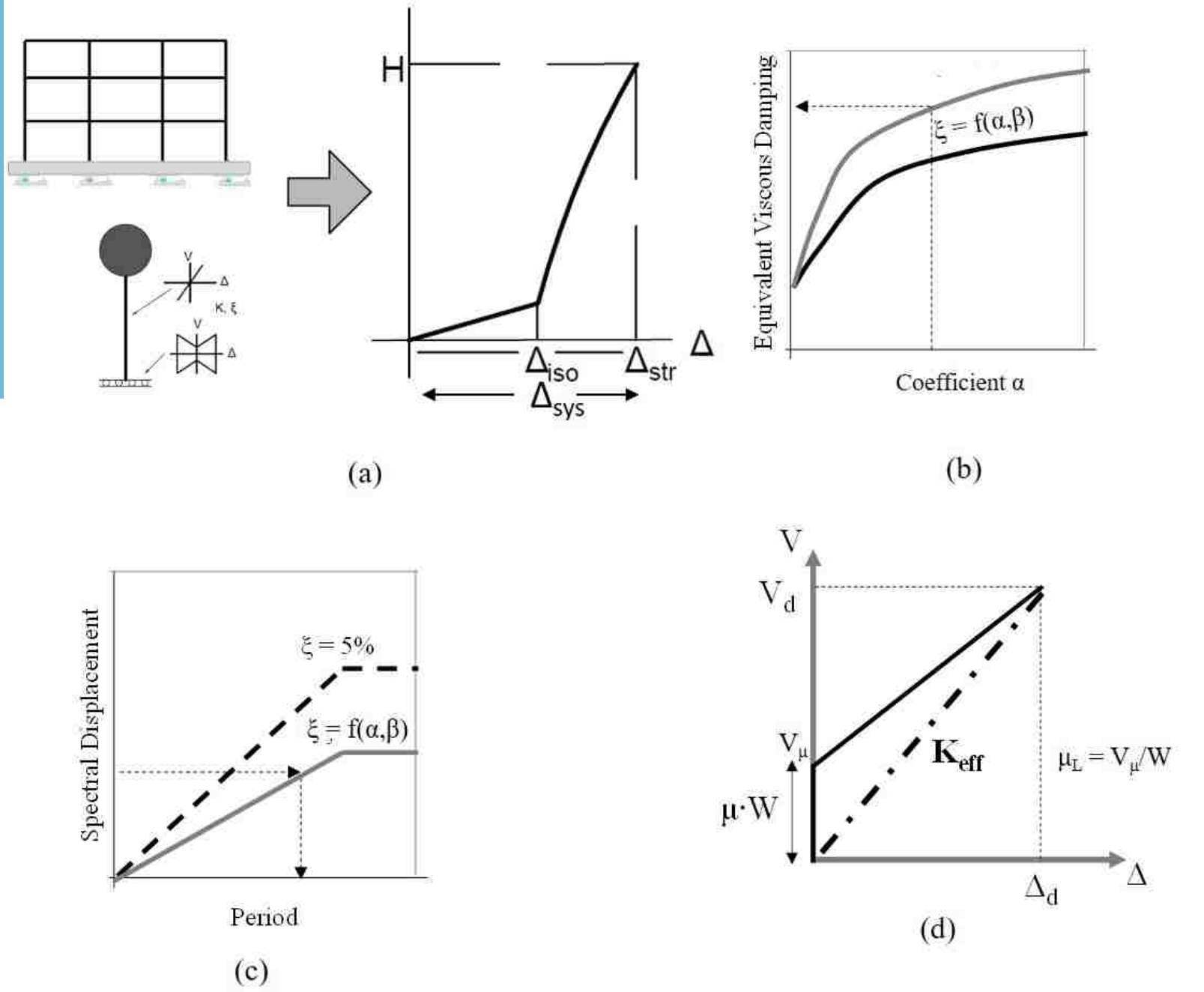

Figure 2.7: Basic DDBD procedure for base isolated structures. (a) Displacement shape; (b) Selection of equivalent damping coefficient; (c) Calculation of the effective period of vibration of the system; (d) Calculation of the design shear force

above the isolation system, and $\Delta_{d,sys}$ is the displacement of the equivalent isolated structure.

The effective stiffness of the system is used in combination with the design displacement to obtain the design base shear, which is the lateral force that the system must be capable of resisting (figure 2.7 (d)). The design base shear is computed multiplying equivalent stiffness and design displacement:

$$V_{d,sys} = K_{e,sys}\Delta_{d,sys} \tag{2.11}$$

2.3.2 Displacement Based Design of VF Base Isolated Structures

The design steps summarized in the previous section represent a general design approach that can be employed to design any arbitrary base isolated structures. While the general approach is applicable to VFS without the need for any notable modifications, some important questions need to be answered before the design of a VFS can be performed. These questions are:

- How should the equivalent viscous damping (EVD) of a generic VFS be estimated?
- How should the demand reduction factor be calculated?
- How should the actual properties of the VFS be determined, once the seismic demand on the system has been defined?

These three key aspects will be discussed in the following of this section.

Energy Dissipation Properties

Damping in real structures is typically represented by Equivalent Viscous Damping (EVD). This approach is based upon Jacobsen's energy equivalence between the energy dissipated in a vibration cycle of the actual structure and an equivalent viscous system [Chopra, 2014]. Relying on this principle, Emilio Rosenbleuth [1964] introduced the concept of representing

the response of a non-linear system analyzing the response of a linear system with equivalent properties that is an effective period computed proportionally to a secant stiffness and an equivalent viscous damping [Pennucci et al., 2011]. As discussed earlier, this approach has been adopted and incorporated in the Direct Displacement Based Design (DDBD) framework.

In light of the success that this idealization has had for many years when employed to estimate the damping properties of a variety of structural systems (including base isolated structures), Calvi et al. [2016] recommended that this approach should be extended to VFS.

Thus, EVD design equations for two types of VFS were derived and expressed as a function of a design parameter, α, representing the ratio between the design shear and the activation shear.

Note that the EVD can be directly estimated from the hysteretic response of the base isolator, as the ratio between the area under the force-displacement curve (shown in figure 2.8 for FP, BowC and BowTie systems) and the area of the ellipse that crosses the axes in correspondence of the force and displacement design values, using the following equation:

$$\xi_{hys} = \frac{E_d}{4\pi E_{so}} = \frac{A_{hys}}{2\pi V_{max}\Delta_{max}} \tag{2.12}$$

The vertical arrows at a sample displaced position indicate that a BT requires a similar shear force to increase or decrease the displacement, while BC and FP tend to move towards the center at lower shear force values.

The EVD equations derived over the course of previous studies, are reported below for the two systems considered thus far (the BowTie and the BowC, respectively):

$$\xi_{eBT} = \frac{1+\alpha}{\pi\alpha} \tag{2.13}$$

$$\xi_{eBT} = \frac{3+\alpha}{2\pi\alpha} \tag{2.14}$$

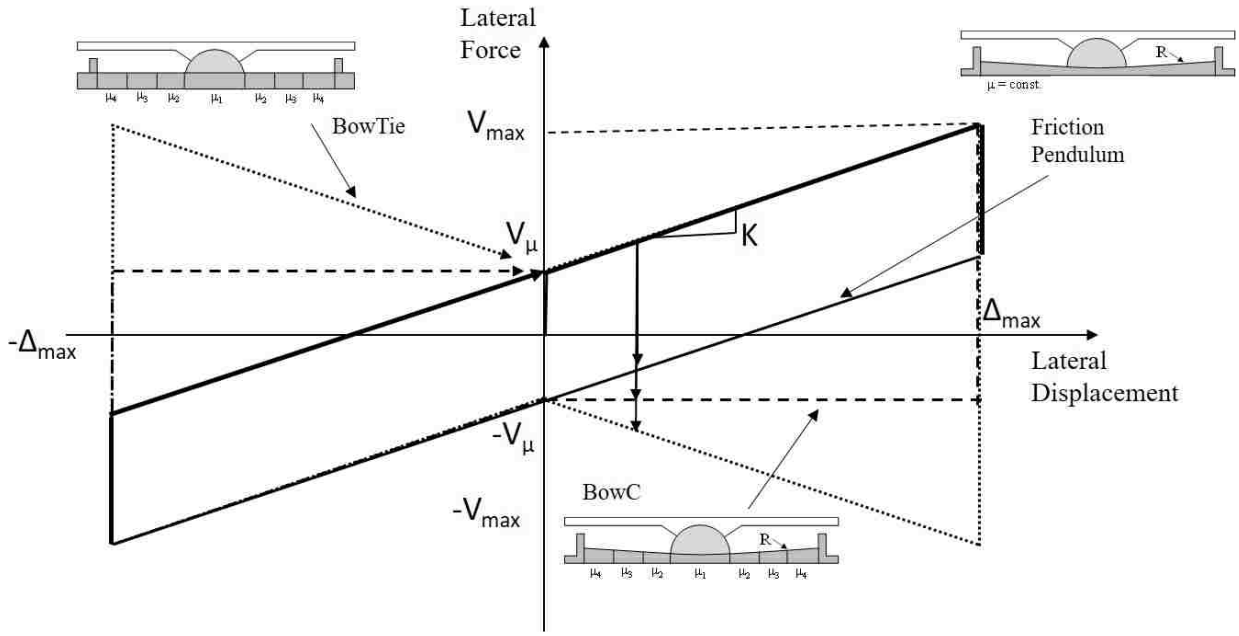

Figure 2.8: Comparison between the hysteresis of a BowC (BC), a BowTie (BT) and a Friction Pendulum (FP) device

It should be noted that, although only these two systems (with specific characteristics) have been studied in the past, VFS with arbitrary radius of curvature and frictional properties can be theoretically developed. Varying frictional properties and radius of curvature of a device, has the effect of modifying the hysteretic response and specifically of altering the magnitude of the re-centering stiffness with respect to the post activation stiffness of the device (as shown in figure 2.8).

By means of the new design parameter β (introduced earlier as the ratio between the re-centering stiffness and the post-activation stiffness), a general equation to estimate the EVD of VFS can be derived. First, the area under the hysteretic curve can be written as:

$$A_h = 4V_\mu\Delta_d + (V_d - V_\mu)\Delta_d + (V_\mu - V_{d1})\Delta_d \tag{2.15}$$

Where:

$$V_{d1} = K_{rec}\Delta_d + V_d \tag{2.16}$$

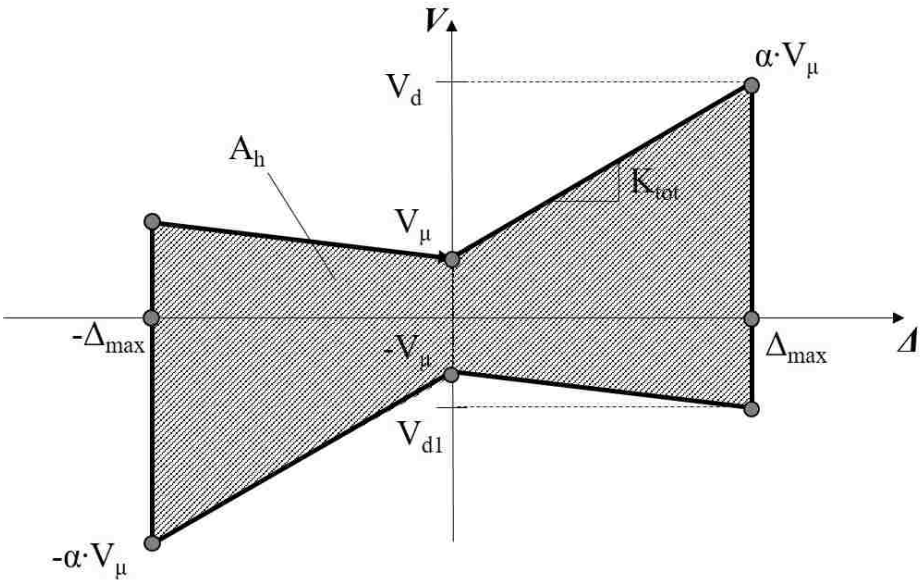

Figure 2.9: Hysteretic energy dissipated by a Variable Friction System

And the re-centering stiffness is given by:

$$K_{rec} = \beta K_{tot} \tag{2.17}$$

The post-activation stiffness and the design shear can be expressed as:

$$K_{tot} = \frac{V_d - V_\mu}{\Delta_d} \tag{2.18}$$

Where V_d=α V_μ

Combining all the equations, the area under the hysteretic curve can be rewritten as:

$$A_h = 4V_\mu\Delta_d + (\alpha V_\mu - V_\mu)\Delta_d + (V_\mu - \beta(\frac{\alpha V_\mu - V_\mu}{\Delta_d} + V_\mu))\Delta_d \tag{2.19}$$

Which can be simplified to:

$$A_h = V_\mu \Delta_d (\alpha - \alpha\beta + \beta + 3) \tag{2.20}$$

The EVD of a generic VFS can be therefore calculated as:

$$\xi_{eq} = V_\mu \Delta_d (\frac{\alpha - \beta\alpha + \beta + 3}{2\pi V_d \Delta_d}) \tag{2.21}$$

And simplified to:

$$\xi_{eq} = \frac{\alpha - \beta\alpha + \beta + 3}{2\pi\alpha} \tag{2.22}$$

Displacement Reduction Factor

It is well known that increasing the damping of a structure has the beneficial effect of reducing the overall demand on the system itself. This demand reduction is incorporated in most design frameworks (including in the DDBD) by means of a reduction factor, η. Once the equivalent properties of the system to be designed are estimated, the seismic demand on the system is calculated assuming a damping ratio of 5%. This demand is subsequently reduced (or amplified) through the reduction factor η, which is estimated as a function of the EVD computed for the system under investigation.

This idea is outlined in Figure 2.10, where it is shown that the displacement demand on a system with an estimated effective period equal to T, is first computed considering a 5% damping ratio and successively reduced to account for the higher damping ratio available in the system (deriving from the dissipated hysteretic energy).

Therefore, the damping reduction factor η, can be seen as the ratio between the displacement experienced by an over-damped system (an equivalent system with damping ratio equal to the estimated EVD) and the displacement experienced by a system with 5% damping.

$$\eta_\xi = \frac{\Delta_{ov}}{\Delta_{5\%}} \tag{2.23}$$

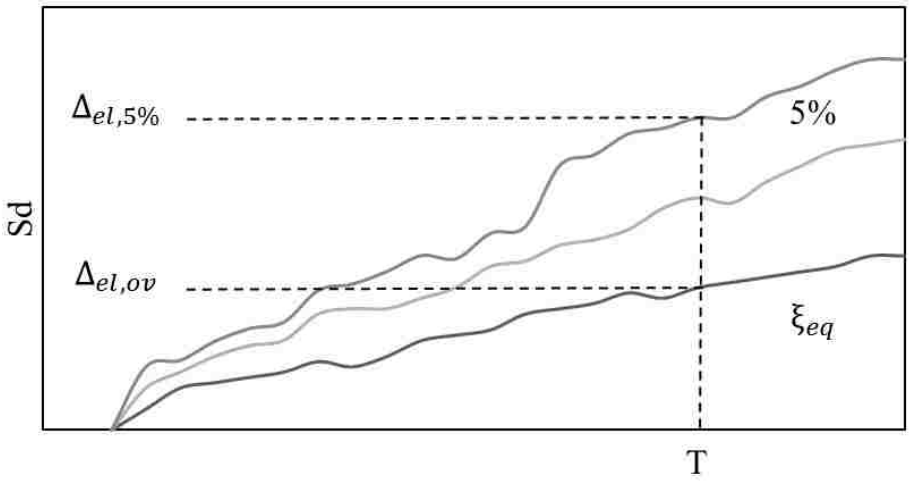

Figure 2.10: Spectral displacement reduction due to damping

The damping reduction factor is therefore smaller than 1.0 for damping ratios that are larger than 5%, while it can be greater than 1.0 if the EVD is smaller than 5% (which could be the case for a steel structure responding elastically or nearly elastically to an earthquake).

There are currently a number of design equations that are available to estimate the demand reduction factor directly from the EVD. Examples of formulations presented in literature, are the current and the previous EC8 [EC8, 1998] equations, which relate damping to the spectral reduction factor as follows:

Previous EC8

$$\eta_\xi = \sqrt{\frac{7}{2+\xi_{eq}}} \tag{2.24}$$

Current EC8

$$\eta_\xi = \sqrt{\frac{10}{5+\xi_{eq}}} \tag{2.25}$$

Equation 2.24 was recommended in a previous edition of the EC8, while equation 2.25 represents the relationship between EVD and η that the EC8 currently recommends.

Clearly, if one wishes to use an existing EVD expression for design, it is important that

they use it together with the damping reduction relationship that was characteristic of the records used to develop the EVD expression itself. To this extent, note that Priestley et al. [2007c] have been advocating the use of the old EC8 damping reduction expression (Equation 2.24) for DDBD, even though it seems that the current EC8 damping reduction expressions can better represent the effects of viscous damping on real ground motion spectra. Their motivations for doing this stemmed from the observations that inelastic displacements were best predicted when the previous EC8 damping reduction expression was used. For this reason, Calvi et al. [2016] recommended to use equation 2.24 to estimate the demand reduction factor for VFS isolated structures.

Properties of the Variable Friction System

In order to complete the desingn of a VFS, it is necessary to be able to select the physical properties of the device (e.g. radius of curvature, number of rings, frictional properties etc.), as a function of the selected design parameters (α, β, and Δ_d) and of the outcome of the DDBD procedure. These aspects are discussed in the following of this section.

A Curved VFS can be seen as a system made of a flat VFS and a frictionless pendulum working in parallel. The hysteresis of a flat VFS is outlined in figure 2.11 (a), while the hysteresis of a frictionless pendulum is shown in 2.11 (b). Combining these two force-displacement responses, the hysteresis of a curved VFS, approximated using a simple piece-wise linear response, is obtained (Figure 2.11(c)).

It can be seen that a curved VFS behaves as a rigid-elastic system under increasing or decreasing lateral loads. The lateral motion begins when the applied shear overcomes the activation shear V_μ. At this point, the lateral stiffness of the system, K_{tot}, is engaged. The post activation stiffness is partly due to the increasing friction coefficients and partly due to the radius of curvature of the sliding surface. The lateral force can be increased up to a certain maximum value referred to as V_d (or V_{max}).

As the lateral shear decreases, the system responds again rigidly until the re-centering shear, V_{d1} is overcome. At this stage, the bearing begins to move back toward the center of

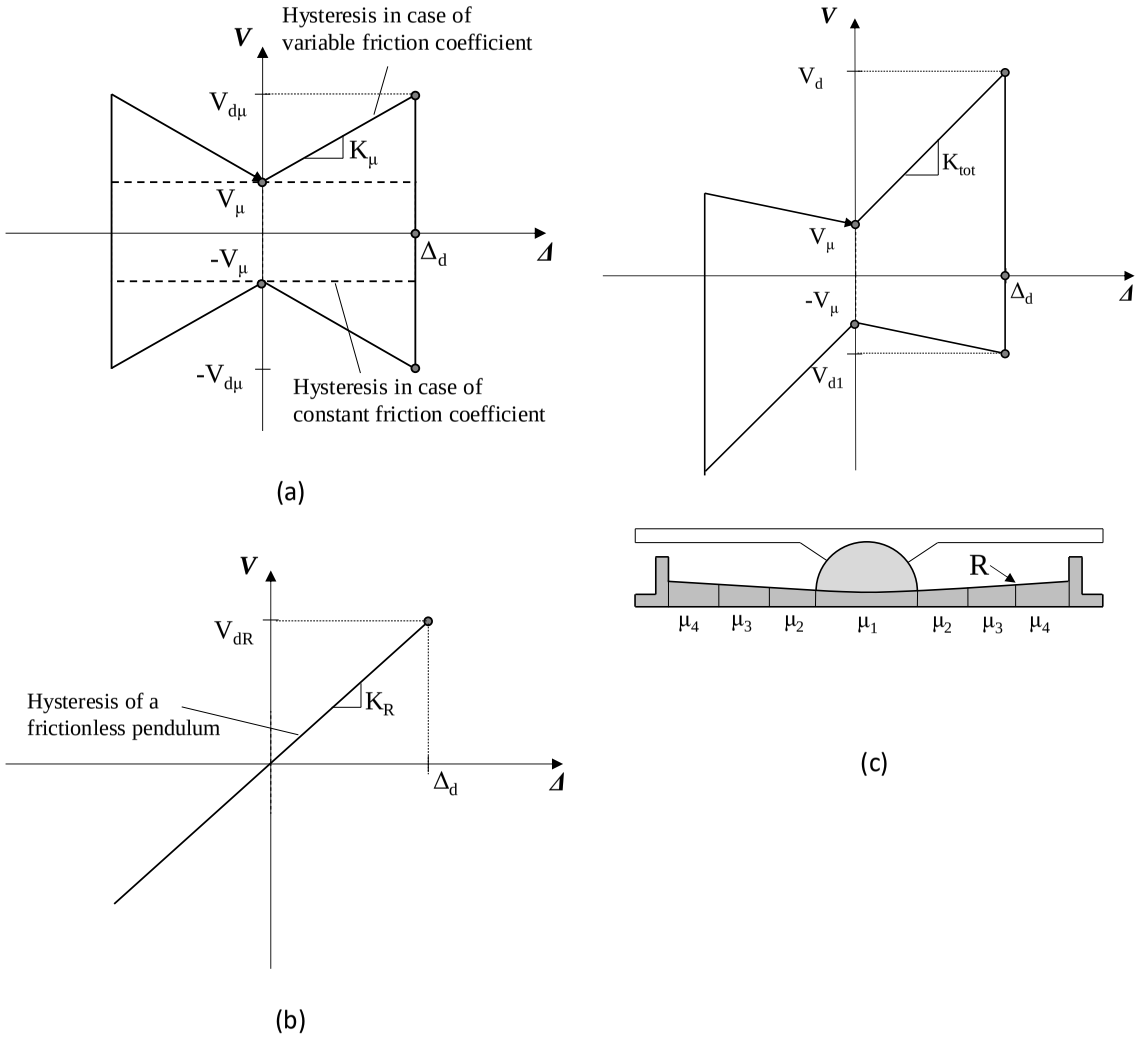

Figure 2.11: Hysterisis components of a VFS with (a) frictional component of the response, (b) component of the response due to the radius of curvature, R, and (c) global response

the sliding surface. The re-centering stiffness is a function of the frictional properties and of the radius of curvature that characterize the device and its slope could assume positive, neutral or negative sign.

It should be noted that a curved VFS converges to a traditional FP if the frictional properties of the sliding surface are maintained constant (i.e. μ is single-valued).

Considering a curved VFS, the activation shear, V_μ, can be calculated as $\mathrm{W}\mu_L$ that are the weight born by the isolation system and the lowest friction coefficient (which characterizes the central ring of the device). V_d and Δ_d (or V_{max} and Δ_{max}) are the design values of lateral shear and displacement. In this context, the post-activation stiffness of the system can be expressed as:

$$K_{tot} = \frac{V_d - V_\mu}{\Delta_d} \tag{2.26}$$

Given the re-centering shear V_{d1}, the re-centering stiffness can be expressed in an analogous manner as:

$$K_{rec} = \frac{V_{d1} - V_\mu}{\Delta_d} \tag{2.27}$$

The two key design parameters introduced earlier are the design-to-activation shear ratio α, and the re-centering-to-post-activation stiffness ratio β, mathematically defined as follows:

$$\alpha = \frac{V_d}{V_\mu} \tag{2.28}$$

$$\beta = \frac{(V_{d1} + V_\mu)/\Delta_d}{(V_d - V_\mu)/\Delta_d} = \frac{V_{d1} + V_\mu}{V_d - V_\mu} \tag{2.29}$$

With reference to the frictionless pendulum, the lateral stiffness and the lateral shear at the design displacement can be written as:

$$K_R = \frac{W}{R} \tag{2.30}$$

$$V_{dR} = \frac{W}{R}\Delta_d \tag{2.31}$$

Similarly, it is possible to derive the fundamental properties of the flat VFS:

$$V_{d\mu} = V_\mu + K_\mu \Delta_d = V_d - \frac{W}{R}\Delta_d \tag{2.32}$$

$$K_\mu = K_{tot} - K_R = \frac{V_d - V_\mu}{\Delta_d} - \frac{W}{R} \tag{2.33}$$

Since re-centering shear for flat VFS is $-V_{d\mu}$ it is possible, after substitutions, to write re-centering shear for curved VFS as:

$$V_{d1} = -V_{d\mu} + V_{dR} = -V_d + 2\frac{W}{R}\Delta_d \tag{2.34}$$

At this point, substituting V_{d1} into the β equation (Eqn. 2.29) and solving for the radius of curvature R:

$$R = \frac{W\Delta_d}{(0.5\beta + 0.5)(V_d - V_\mu)} \tag{2.35}$$

Substituting R into the frictional stiffness equation, K_μ can be conveniently re-written as:

$$K_\mu = K_{tot} - (0.5\beta + 0.5)K_{tot} \tag{2.36}$$

Equations 2.35 and 2.36 are extremely important as they allow a designer to determine all the geometrical and mechanical properties of the base isolation device right after selecting the design displacement and the coefficient β, and after having determined the magnitude of the design and the activation shear forces (this point will be discussed in more detail in later sections).

More specifically, as discussed by Calvi and Ruggiero [2016], at this point the designer

has two options:

- Select geometry of sliding surface (size of each ring) to calculate friction coefficient to be assigned to each ring as:

$$\mu_i = \mu_L + \frac{K_\mu}{W}\bar{x}_i \tag{2.37}$$

  Where $\bar{x}_i$ is center point of ring i.

- Select friction coefficients to be assigned, and calculate radius of each ring.

$$r_1 = r_0 \tag{2.38}$$

$$\bar{x}_i = \frac{\mu_i - \mu_L}{\frac{K_\mu}{W}} \tag{2.39}$$

$$r_i = \bar{x}_i + (\bar{x}_i - r_{i-1}) = 2\bar{x}_i - r_{i-1} \tag{2.40}$$

They also suggested that the smallest center ring be the size of the bearing. They also observed that the maximum number of rings needed to give an approximate linear response is given by:

$$n \geq \frac{2\Delta_D}{D_o} \tag{2.41}$$

where n is the number of concentric rings to be used for design, Δ_d is the design displacement of the isolator, and D_o is the diameter of the top plate of the isolator. They also recommended to use identical diameter for the inner circle and the bearing (the size of the bearing could be dictated by the vertical loads and by the resulting vertical pressure).

Chapter 3

VERIFICATION OF THE DAMPING PROPERTIES OF VARIABLE FRICTION SYSTEMS

As discussed in Chapter 2, the design process for VFS, at least at a preliminary level, is overall well defined. Once the designer has selected the design parameters α and β, which define the main characteristics of the desired base isolation device, the design of the optimal VFS can be completed following the straightforward steps summarized earlier.

However, it should be evident from the discussion presented in the previous chapter, that a number of relatively empirical parameters are employed within the design framework. These parameters are the EVD of the base isolator and the associated displacement reduction factor η, which is key in determining the displacement demand on the system.

As discussed, Calvi et al. [2016] and Calvi and Ruggiero [2016] have proposed to use a classic Jacobsen approach to estimate the EVD of the VFS, and have therefore derived a number of design equations to conveniently compute this parameter at the beginning of the design process. Once the EVD has been calculated, it is recommended that the displacement demand on the system be calculated as the demand on an equivalent system with a viscous damping ratio of 5%, multiplied by a reduction factor computed using Equation 2.24, which was provided in a previous edition of the EC8.

These propositions were based on the observation that the same approach has worked successfully in the past for a number of structural systems, including structures base isolated by means of Rubber Bearings and Friction Pendula. However, they have not yet been validated for the newly proposed VFS.

Thus, the main objective of this chapter is to conduct a numerical study on the damping properties of generic VFS, using the results of NLTH analysis to check the validity of the

current design assumptions and, when necessary, to improve on the existing design equations.

This chapter is therefore organized into three subsections: first, the adopted procedure, the ground motions, the numerical modeling assumptions, and the case study structures are introduced; second, the results of a very large number (more than 500,000) of NLTH analysis are processed and presented along with comparisons to existing design equations; third, the reasons for discrepancy between the existing design equations and the results of the analyses are examined, and a set of new of equations is calibrated to better estimate these parameters for design purpose.

3.1 Estimating Damping Properties from Non-Linear Time History Analysis

The process employed to estimate the EVD provided by generic VFS and the associated displacement reduction factor η is summarized in figure 3.1. The case study structures, consisting of rigid (i.e. characterized by very large lateral stiffness) or flexible SDOF systems, were first selected. These structures, were then isolated by means of VFS with various characteristics. The case study systems were fully defined in terms of seismic weight, hysteretic response, and viscous damping ratio (all this is described in more detail in section 3.1.3).

A ground motion was then selected as the input for the NLTH analysis, which was conducted using a customized computer program written in MATLAB (see section 3.1.2) and applied to the structure as shown in figure 3.1.

At the end of the analysis, the maximum displacement experienced by the SDOF system, Δ_{max}, and corresponding lateral force, V_{max}, were recorded. These parameters were used to estimate the effective stiffness, K_{ef}, of the system (the secant stiffness at peak displacement) and the effective period of vibration, T_{ef} (figure 3.1 (b)). The parameter α was also computed as V_{max}/V_{μ}.

At this point, a linear SDOF system with effective characteristics (K_{ef} and T_{ef}) was analyzed using the same input ground motion. The viscous damping ratio assigned to this system was progressively increased, until the maximum displacement of the linear "effective" system matched that of the non-linear system. This damping ratio was therefore recorded

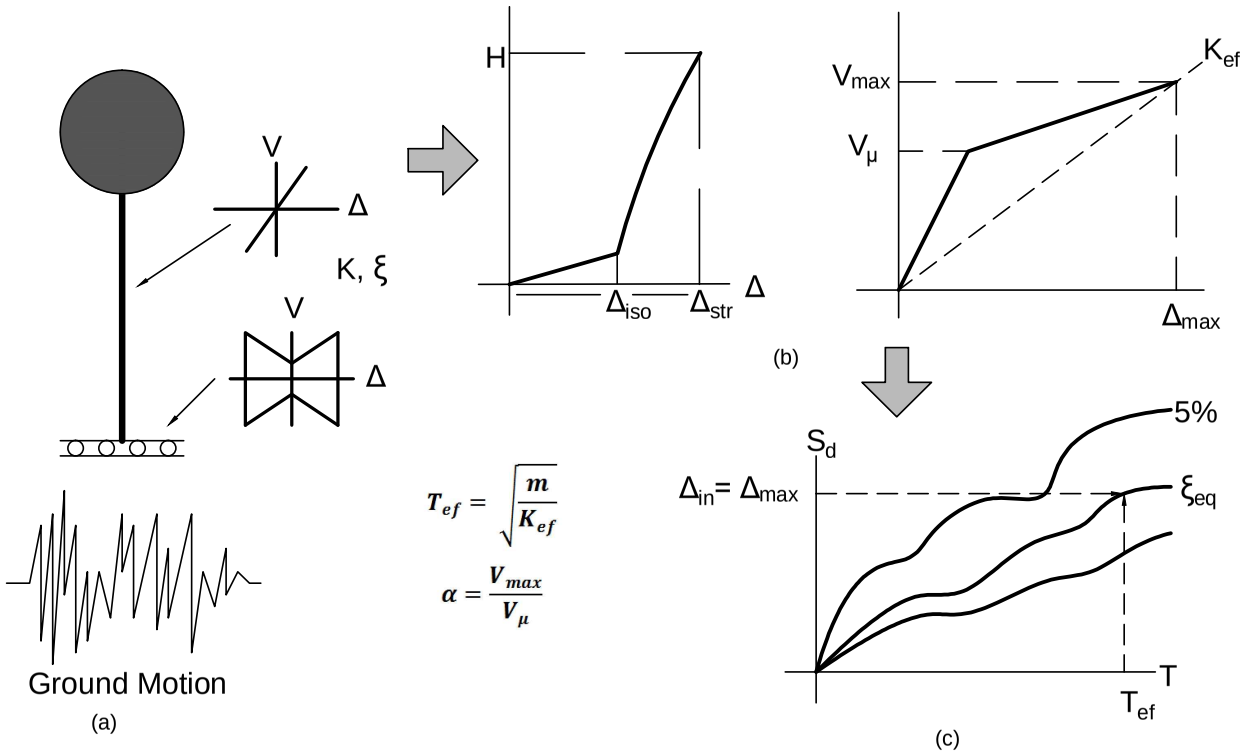

!htb

Figure 3.1: Procedure to calculate damping from non-linear analysis by (a) applying ground motion to selected structure, (b) calculating maximum non-linear and equivalent linear parameters, and (c) finding the EVD

as the EVD of the case study system (figure 3.1 (c)).

The displacement reduction factor associated to a given value of EVD was computed as the ratio between the Δ_{max} experienced by the previously analyzed non-linear system (or by the linear effective system with assigned damping ratio equal to the EVD) and the displacement of the linear effective system with assigned viscous damping ratio of 5%.

This process was repeated for 50 different ground motions scaled at different magnitudes, so to obtain a large dataset relating the EVD, η and α.

This process was employed for both rigid and flexible case study structures. However, when flexible structures that are assigned non-zero viscous damping ratio are analyzed, the EVD estimated at the end of the process includes the viscous damping of the system as well. Because the objective at this stage was to isolate the EVD provided by the VFS alone, some post processing of the results was required. More specifically, the EVD provided by the base isolator alone was calculated rearranging Equation 2.8, proposed by Priestley et al. [2007c], as:

$$\xi_{iso} = \frac{\xi_{eq}\Delta_{max} - \xi_{str}\Delta_{str}}{\Delta_{iso}} \tag{3.1}$$

Where ξ_{iso} is the EVD of the VFS alone. In equation 3.1, ξ_{eq} represents the total EVD computed from the NLTH analysis, Δ_{max} is the maximum displacement experienced by the SDOF system, Δ_{str} is the peak displacement of the flexible structure with respect to the base isolator (computed as V_{max}/K_s, K_s being the stiffness of the structure), ξ_{str} is the viscous damping ratio assigned to the structure (either 2% or 5%), and Δ_{iso} is the peak displacement of the base isolator (computed as Δ_{max}-Δ_{str}).

3.1.1 Ground Motions

A total of 50 real ground motions were selected as input for the numerical analyses conducted in this study. The records were selected from the PEER- NGA West 2 database, and the search criteria were set so that the outcome would consist of a set of accelerograms compatible with the MCE spectrum for the San Francisco area (shown in figure 3.2 for

spectral acceleration (a), and displacement (b)). When specified for a damping ratio of 5%, this target spectrum has a maximum spectral acceleration at short period (S_{MS}) of 1.5 g, a maximum spectral acceleration at 1 second (S_{M1}) of 0.871 g and a long period (T_L) of 12 seconds.

In the selection process, a preliminary screening was performed to limit the search to records pertaining to soil type C (i.e. "very dense soil and soft rock") and whose nearest rupture distance to the fault (R_{rup}) was from 0.56 km to 218 km . The wide distance range aimed to include both near-fault and far-field events. The ground motions were appropriately scaled so that the average acceleration and displacement spectra associated to the motions matched the selected design spectra.

To this end, the displacement and acceleration spectra associated with each accelerogram, along with the average spectra, are depicted in figure 3.2. It can be seen that the average curves lie reasonably close to the target (design) spectra, while the individual curves, in some instances, diverge from the average. The divergence between average and individual spectra are even more remarkable at short periods, with reference to accelerations, and at long periods, with reference to displacements. However, while in this context it is reasonable to expect a somewhat substantial dispersion within the results of the numerical analyses, the observed discrepancies between average and target curves are considered reasonable for the purpose of this study.

The key characteristics of the 50 records selected are summarized in Table 3.1. It should be noted that the scale factors listed are those required to have a match between the individual records and the target spectra. However, the magnitude of each ground motions was scaled in the analyses to simulate more or less intense earthquakes, considering factors ranging from 0.1 to 10 times the values listed in Table 3.1 for scale factors (at intervals of 0.1, so a total of 100 earthquake intensities were considered).

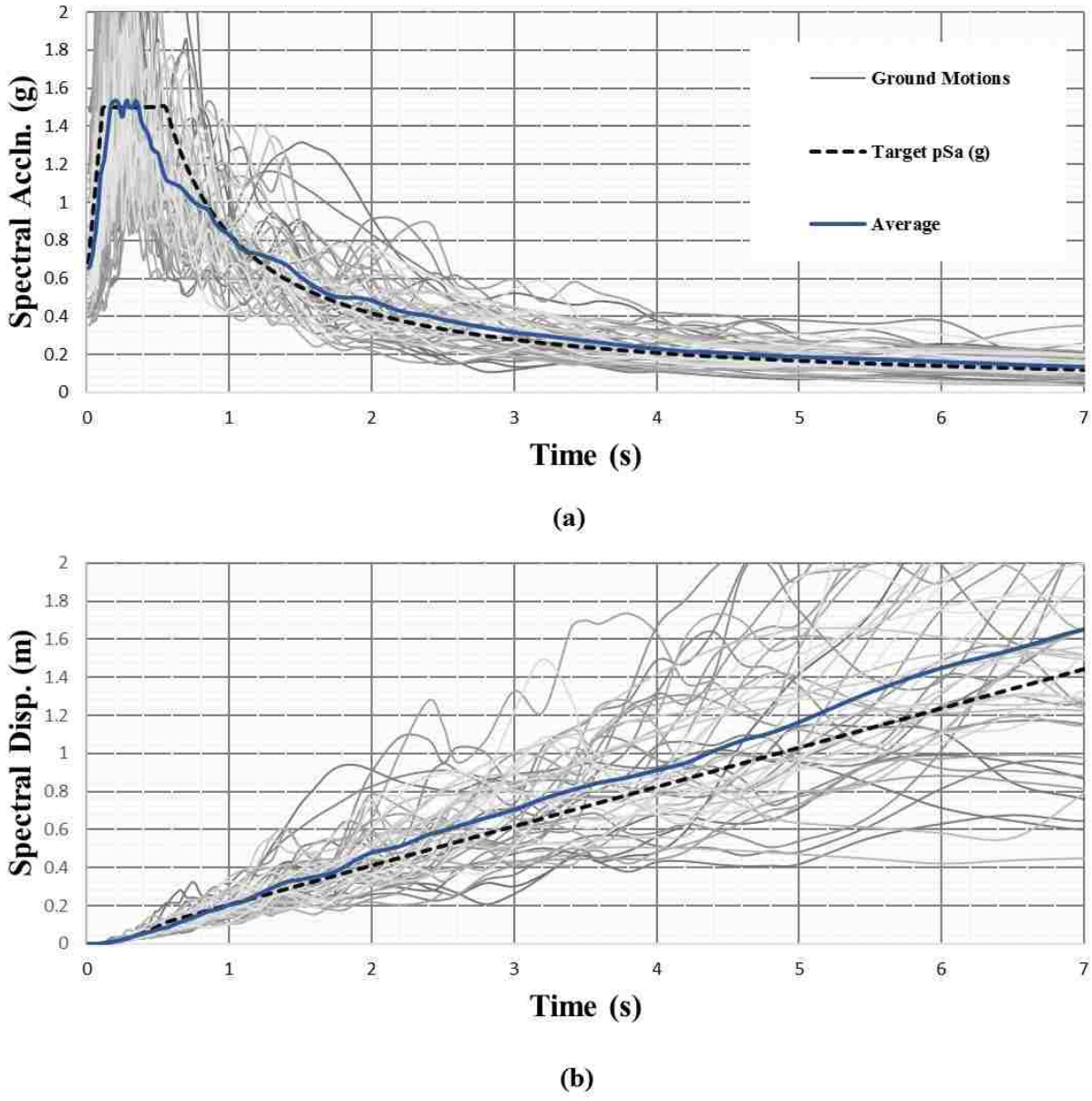

Figure 3.2: Target and average (a) acceleration spectrum and (b) displacement spectrum

Table 3.1: Table of selected ground motions

SN	RSN	Scale Factor	Earthquake Name	Year	Magnitude	R_{rup} (km)	Max PGA (g)
SN	RSN	Scale Factor	Earthquake Name	Year	Magnitude	Rrup (km)	Max PGA(g)
1	9	10.43	"Borrego"	1942	6.5	56.88	2.14
2	12	9.60	"Kern County"	1952	7.36	117.75	1.65
3	15	4.85	"Kern County"	1952	7.36	38.89	2.87
4	17	22.37	"Southern Calif"	1952	6	73.41	3.08
5	20	3.31	"Northern Calif-03"	1954	6.5	27.02	1.62
6	26	10.49	"Hollister-01"	1961	5.6	19.56	2.99
7	28	12.28	"Parkfield"	1966	6.19	17.64	2.50
8	31	5.93	"Parkfield"	1966	6.19	12.90	4.69
9	36	4.78	"Borrego Mtn"	1968	6.63	45.66	1.37
10	38	43.47	"Borrego Mtn"	1968	6.63	199.84	1.40
11	40	19.09	"Borrego Mtn"	1968	6.63	129.11	2.53
12	51	17.05	"San Fernando"	1971	6.61	55.20	1.84
13	53	63.54	"San Fernando"	1971	6.61	113.02	1.50
14	54	61.73	"San Fernando"	1971	6.61	214.32	1.60
15	55	55.06	"San Fernando"	1971	6.61	112.52	2.14
16	61	88.12	"San Fernando"	1971	6.61	218.75	1.60
17	67	77.36	"San Fernando"	1971	6.61	130.98	1.76
18	68	3.04	"San Fernando"	1971	6.61	22.77	2.29
19	74	53.91	"San Fernando"	1971	6.61	193.91	1.41
20	76	54.89	"San Fernando"	1971	6.61	110.18	1.39
21	77	0.92	"San Fernando"	1971	6.61	1.81	2.77
22	82	13.11	"San Fernando"	1971	6.61	68.84	1.84
23	83	14.99	"San Fernando"	1971	6.61	52.64	3.30
24	84	74.27	"San Fernando"	1971	6.61	205.77	1.24
25	86	37.48	"San Fernando"	1971	6.61	124.79	1.61
26	88	6.49	"San Fernando"	1971	6.61	24.87	4.79
27	90	23.46	"San Fernando"	1971	6.61	124.41	1.50
28	92	33.02	"San Fernando"	1971	6.61	70.23	3.64
29	93	7.97	"San Fernando"	1971	6.61	39.45	2.83
30	96	4.06	"Managua_ Nicaragua-02"	1972	5.2	4.98	3.00
31	170	2.64	"Imperial Valley-06"	1979	6.53	7.31	1.99
32	178	2.22	"Imperial Valley-06"	1979	6.53	12.85	2.24
33	180	1.55	"Imperial Valley-06"	1979	6.53	3.95	1.98
34	182	2.15	"Imperial Valley-06"	1979	6.53	0.56	1.70
35	184	1.69	"Imperial Valley-06"	1979	6.53	5.09	2.54
36	185	2.28	"Imperial Valley-06"	1979	6.53	7.50	2.13
37	285	4.78	"Irpinia_ Italy-01"	1980	6.9	8.18	2.09
38	316	2.44	"Westmorland"	1981	5.9	16.66	1.88
39	838	5.30	"Landers"	1992	7.28	34.86	1.87
40	1489	2.41	"Chi-Chi_ Taiwan"	1999	7.62	3.76	1.75
41	1491	2.69	"Chi-Chi_ Taiwan"	1999	7.62	7.64	1.37
42	1493	2.81	"Chi-Chi_ Taiwan"	1999	7.62	5.95	2.09
43	1511	1.93	"Chi-Chi_ Taiwan"	1999	7.62	2.74	2.25
44	4847	2.13	"Chuetsu-oki_ Japan"	2007	6.8	11.94	1.69
45	6887	3.79	"Darfield_ New Zealand"	2010	7	18.05	2.35
46	6906	0.96	"Darfield_ New Zealand"	2010	7	1.22	1.44
47	6911	1.19	"Darfield_ New Zealand"	2010	7	7.29	1.92
48	6960	3.01	"Darfield_ New Zealand"	2010	7	13.64	2.41
49	6969	3.03	"Darfield_ New Zealand"	2010	7	20.86	1.73
50	8161	1.76	"El Mayor-Cucapah_ Mexico"	2010	7.2	11.26	1.88

3.1.2 Numerical Modeling

The numerical simulations were conducted using a customized computer program coded in MATLAB [MathWorks, 2012], originally written by Calvi and Ruggiero [2016] and adapted to perform the tasks required in this study (discussed in the introduction of this chapter). The program solves the incremental equation of motion using a linear acceleration Newmark-Beta integration algorithm [Newmark and Rosenblueth, 1971] and can perform the analysis of non-linear SDOF structures, characterized by arbitrary hysteretic response. The isolation system was simulated using a non-linear translational spring characterized by an appropriate relationship between lateral force and displacement (see figure 3.1 (a)), while the supported structure was modeled using a linear spring. The hysteresis of the spring representing the base isolation system, was defined as a function of the isolator selected (key parameters are α and β). While the main aspects of the numerical modeling of VFS were discussed in section 2.2.2, the key equations employed to define the hysteretic response of each system within each routine calculations, are reported below:

$$F_r(x) = \begin{cases} max[min(F_1(x), F_2(x - x_p)), F_3(x)] & if x \geq 0 \\ max[min(F_4(x), F_2(x - x_p)), F_5(x)] & if x < 0 \end{cases}$$

Where x_p is a plastic displacement offset calculated at each converged stage of the analysis as:

$$x_p = x - x_\mu \tag{3.2}$$

and V_{act}, k_0, k_p are the activation shear, pre-activation stiffness, and post-elastic stiffness respectively of the system.

Note that the program is modified to consider any arbitrary β value in the analysis, as mentioned in section 2.2.2.

Three values of viscous damping ratio were considered and assigned to the case study systems in this phase of the work: the rigid systems were assigned a damping ratio of 0%,

while the flexible systems were assigned either 2% or 5%. Unfortunately, there is currently no agreement as to how the viscous damping of a base isolated structure should be modeled in the context of NLTH analyses [Pant et al., 2013; Petrini et al., 2008].

In this study, the damping constant "c" to be assigned to the various structures in the numerical models was computed proportionally to the post-activation stiffness, rather than to the initial stiffness (which can be very large for friction-type base isolators). This modeling choice is in line with the recommendations of Pant et al. [2013] and was driven by the desire to avoid the introduction of unrealistically high values of viscous damping in the systems [Petrini et al., 2008], which would lead to un-conservative predictions of the performance the structures [Ryan and Polanco, 2008].

Clearly, modeling the viscous damping of systems with assigned damping ratio of 0% is not a concern as, in this case, the only source of damping in the numerical models comes from the "hysteretic" component provided by the isolation system.

3.1.3 Case Study Structures

This section describes the case study structures utilized for the numerical study. The "design" of the case studies was performed by first selecting three "target" structures, isolated by means of traditional FP systems. The properties of these target FP systems were as follows:

- Lateral displacement capacity of 0.45 m
- Radii of curvature of 2.5 m, 3.1 m, and 3.7 m
- Medium friction coefficient (5.5%)
- Bearing diameter of 0.3 m (and consequently a sliding surface diameter of 1.2 m)

It was further assumed that the structures had a seismic weight of 6,000 kN and that this was also the magnitude of the total vertical load.

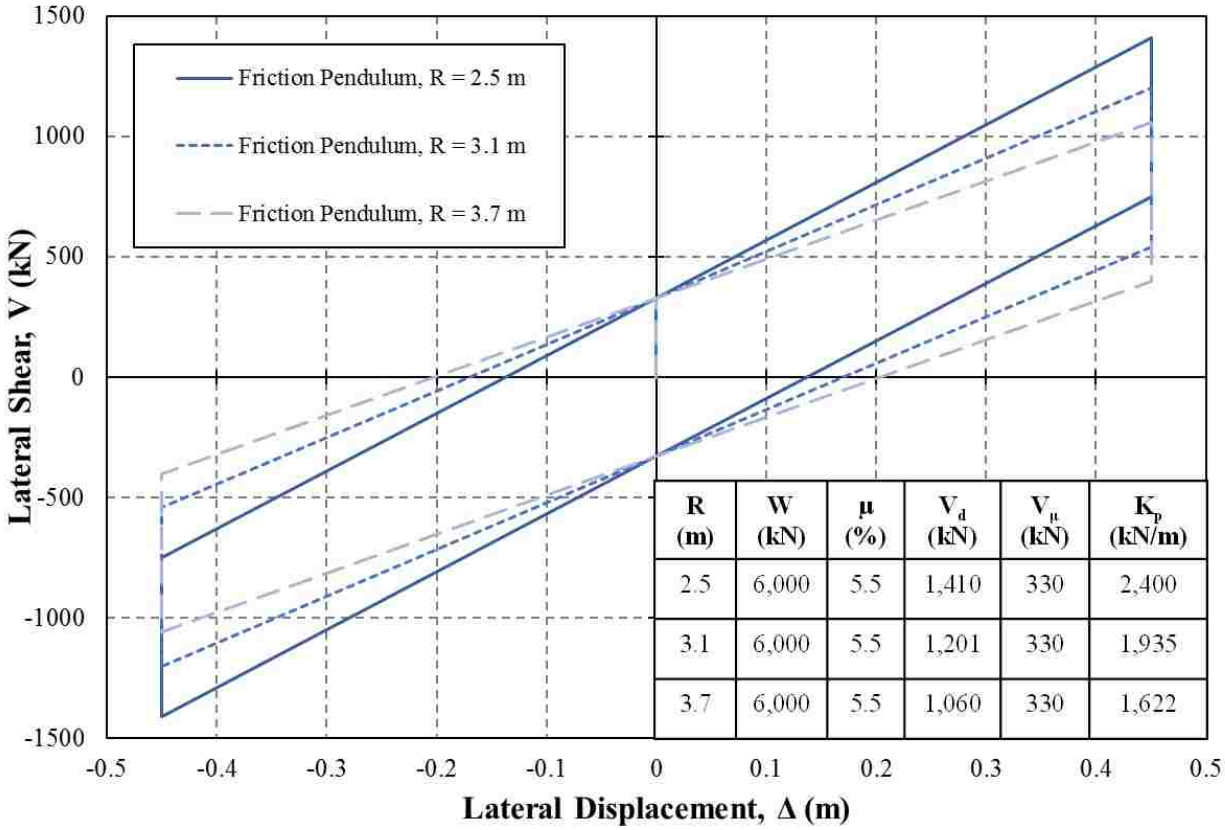

R (m)	W (kN)	μ (%)	V_d (kN)	V_μ (kN)	K_p (kN/m)
2.5	6,000	5.5	1,410	330	2,400
3.1	6,000	5.5	1,201	330	1,935
3.7	6,000	5.5	1,060	330	1,622

Figure 3.3: Force- displacement response of selected FP systems with their fundamental property values

Three FP devices with the desired characteristics were therefore selected from a manufacturer's catalog [Industriale, 2012], and all the fundamental design properties, namely the design shear V_d, the activation shear V_μ, and the post-activation stiffness K_p, were calculated. The hysteresis of the three "target" FP systems selected are summarized in figure 3.3.

At this point, a total of 24 VFS, characterized by β values ranging from -1.0 to 0.75 (at 0.25 intervals), were designed to "mimic" the response of the target FP systems described above. The properties of the VFS were therefore assigned to guarantee that the backbone of the hysteretic curve characterizing the force-displacement response of each VFS traced that of the companion FP systems.

The outcome of the design of the VFS (performed in line with the discussion presented

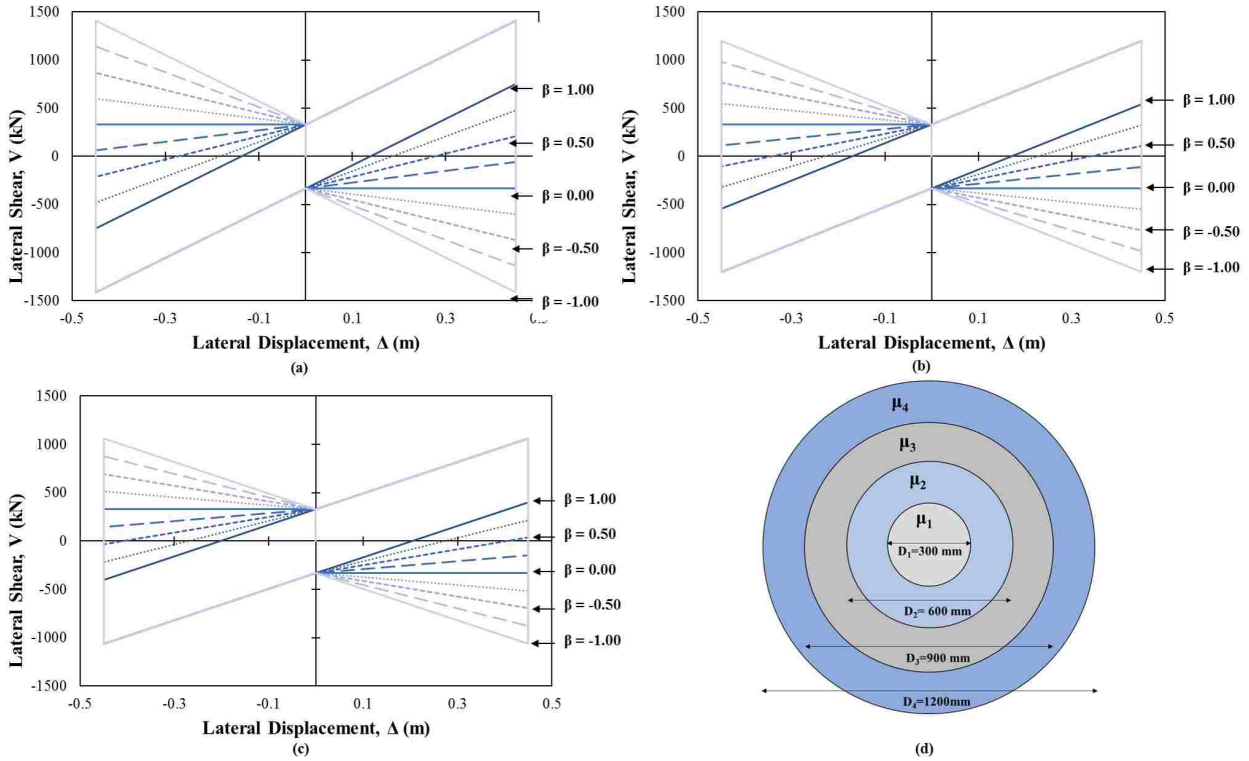

Figure 3.4: Force- response of VFS with equivalent backbones for FP with (a) R= 2.5 m (b) R= 3.1 m (c) R= 3.7 m; plan view (d) of a VFS with 4 rings

in section 2.2.1), is summarized in figure 3.4 and in Table 3.2.

It is known that different structural systems, or structures made of different materials, can rely on different amounts of viscous damping. For example, it is common practice to assign a damping ratio of 5% to reinforced concrete structures, 2% to steel buildings, and 10% to masonry structures.

In this context, it was of interest to investigate whether the viscous viscous damping specified for a base isolated structure affects the effective damping properties of the VFS and, if yes, in what ways. At the same time, it was of interest to gage if the effective damping properties of a VFS are influenced to any extent by the dynamic properties of the

Table 3.2: Case study structure frictional properties based on varying FP radius

FP R= 2.5 m; μ= 5.5%								
β	0.75	0.5	0.25	0.00	-0.25	-0.5	-0.75	-1.00
μ_1(%)	5.5	5.5	5.5	5.5	5.5	5.5	5.5	5.5
μ_2(%)	6.6	7.8	8.9	10.0	11.1	12.3	13.4	14.5
μ_3(%)	7.4	9.3	11.1	13.0	14.9	16.8	18.6	20.5
μ_4(%)	8.1	10.8	13.4	16.0	18.6	21.3	23.9	26.5
R (m)	2.86	3.33	4.00	5.00	6.67	10.00	20.00	∞
FP R= 3.1 m; μ=5.5%								
β	0.75	0.5	0.25	0.00	-0.25	-0.5	-0.75	-1.00
μ_1(%)	5.5	5.5	5.5	5.5	5.5	5.5	5.5	5.5
μ_2(%)	6.4	7.3	8.2	9.1	10.0	10.9	11.9	12.8
μ_3(%)	7.0	8.5	10.0	11.5	13.1	14.6	16.1	17.6
μ_4(%)	7.6	9.7	11.9	14.0	16.1	18.2	20.3	22.4
R (m)	3.54	4.13	4.96	6.20	8.27	12.40	24.80	∞
FP R= 2.5 m; μ= 5.5%								
β	0.75	0.5	0.25	0.00	-0.25	-0.5	-0.75	-1.00
μ_1(%)	5.5	5.5	5.5	5.5	5.5	5.5	5.5	5.5
μ_2(%)	6.3	7.0	7.8	8.5	9.3	10.1	10.8	11.6
μ_3(%)	6.8	8.0	9.3	10.6	11.8	13.1	14.4	15.6
μ_4(%)	7.3	9.0	10.8	12.6	14.4	16.1	17.9	19.7
R (m)	4.23	4.93	5.92	7.40	9.87	14.80	29.60	∞

isolated structure.

To investigate these aspects in the NLTH analyses, a set of SDOF case study structures, with different characteristics were considered. It was assumed that these case study structures had to be base isolated using the VFS described earlier. Each base isolator-super structure assembly was modeled as a SDOF system, with an hysteretic response calibrated treating the two elements as springs in series.

The structures to be isolated were either "rigid" or "flexible", with a seismic weight of 6,000 kN, and had the following characteristics:

- Rigid Structure: a very high lateral stiffness was selected (e.g. 10,000 times the post activation stiffness of the base isolator). A viscous damping ratio of 0% was assigned to the structural assembly. In this case, the energy dissipation was therefore entirely provided by the hysteretic response of the base isolator.

- Flexible Structures: three values of stiffness (35,455 kN/m, 17069 kN/m and 7,942 kN/m) and two values of damping ratio (2% and 5%) were considered. The idea was to cover a range of periods of vibration that could be representative of structures of different heights (e.g. 4 story, 8 story and 12 story), and to target the two damping ratio most widely used in practice for traditional structural systems.

The fundamental properties of the case study structures are reported in Table 3.3.

In summary, a total of 189 (the 7 structures listed in Table 3.3 times the 9 base isolator types described above, times the 3 radii of curvature selected) base isolated SDOF case study structures were selected and analyzed via NLTH analyses.

3.2 Non-Linear Time History Analysis Results

The key results of the NLTH analysis conducted in this phase of the work are summarized and presented in this chapter. Only the results of a few representative case study systems are

Table 3.3: Summary of case study structures selected

Superstructure	Storeys (approx.)	ξ (%)	Stiffness (kN/m)	Time Period (s)
Rigid	1	0	10000*W/R	0.03
Flexible 1	4	2 5	35455	0.825
Flexible 2	8	2 5	17069	1.189
Flexible 3	12	2 5	7942	1.743

included herein. Given that the main objective of the investigation discussed in this chapter is to relate the main properties of VFS (i.e. α and β) to their damping characteristics and, consequently, to appropriate values of displacement reduction factors, two types of graphs will be presented for systems identified by different values of β: EVD vs α, and EVD vs η.

3.2.1 Examination of the Results

Rigid Structures with zero viscous damping ratio

The results pertaining to the "rigid" case study structures with assigned damping ratio of 0% are presented in this subsection. The results of each single analysis are first represented by the couple α - ξ_{eq}. This outcome is outlined in Figure 3.5, for systems characterized by three values of β, namely 1.0 (representing an FP) (a), 0 (representing a BowC) (b), and -1.0 (representing a BowTie) (c) . It should be noted that the results are not separated as a function of the radius of curvature of the target FP device, in light of the observation that this parameter had virtually no effect on the damping properties of the various systems. For the three selected β values (i.e. 1.0, 0 and -1.0), Figure 3.5 (d) includes the results of all analyses, (obviously plotted separately for each β). The solid curves represent the

average trends, while the dashed curves represent the average plus or minus the computed standard deviation. Also, the average trends for all rigid systems analyzed, are reported in Figure 3.5(d).

From Figure 3.5 it can be noted that the EVD of all systems is essentially identical for low values of α (EVD for $\alpha = 1.5$). It can also be noted that the EVD decreases with increasing α. However, it can be observed that the EVD decreases more rapidly for systems characterized by higher βs. For instance, the average EVD of a system with $\beta = 1.0$ (i.e. an FP device), drops from roughly 40% to roughly 8% as α grows from 1.5 to 9.0. In contrast, the average EVD of a system with β = -1.0 (i.e. a BowTie device) goes from about 40% to roughly 27%, considering the same range of α values. It can be seen that the EVDs for all the other systems considered, follow analogous trends. This first trends observed are consistent with the expectations: smaller βs produce "fatter" hysteretic loops, which translates into a greater amount of energy dissipated, with consequent larger EVD values. At the same time, the qualitative relationship between EVD and α expressed by Equation 2.22 is confirmed by the results of the analyses (note that increasing α values correlate to increasing earthquake intensity).

While the results of Figure 3.5 confirm, to some extent, that VFS with smaller β values have a higher energy dissipation capacity, and in turn higher EVD, it can be observed, in the same Figure, that the scatter of the whole data set around the average curves is overall quite large and that it increases as β decreases. The mean coefficient of variation (defined the standard deviation divided by the mean), summarized in Figure 3.6 as a function of α, is approximately 30%, 34%, and 43% for the systems with βs of 1.0, 0, and -1.0.

The mean coefficient of variation for all the systems analyzed is summarized in Table 3.4. It can be seen that the trend shown in Figure 3.6 is confirmed. However, while the mean COV tends to increase as β decreases, its value stays roughly constant and equal to 30% for systems with positive β values. Even though the values reported in Table 3.4 are just the mean COVs, they provide a good indication of the overall trend as the COV is not greatly affected by the parameter α (i.e. it stays roughly constant throughout the whole α range).

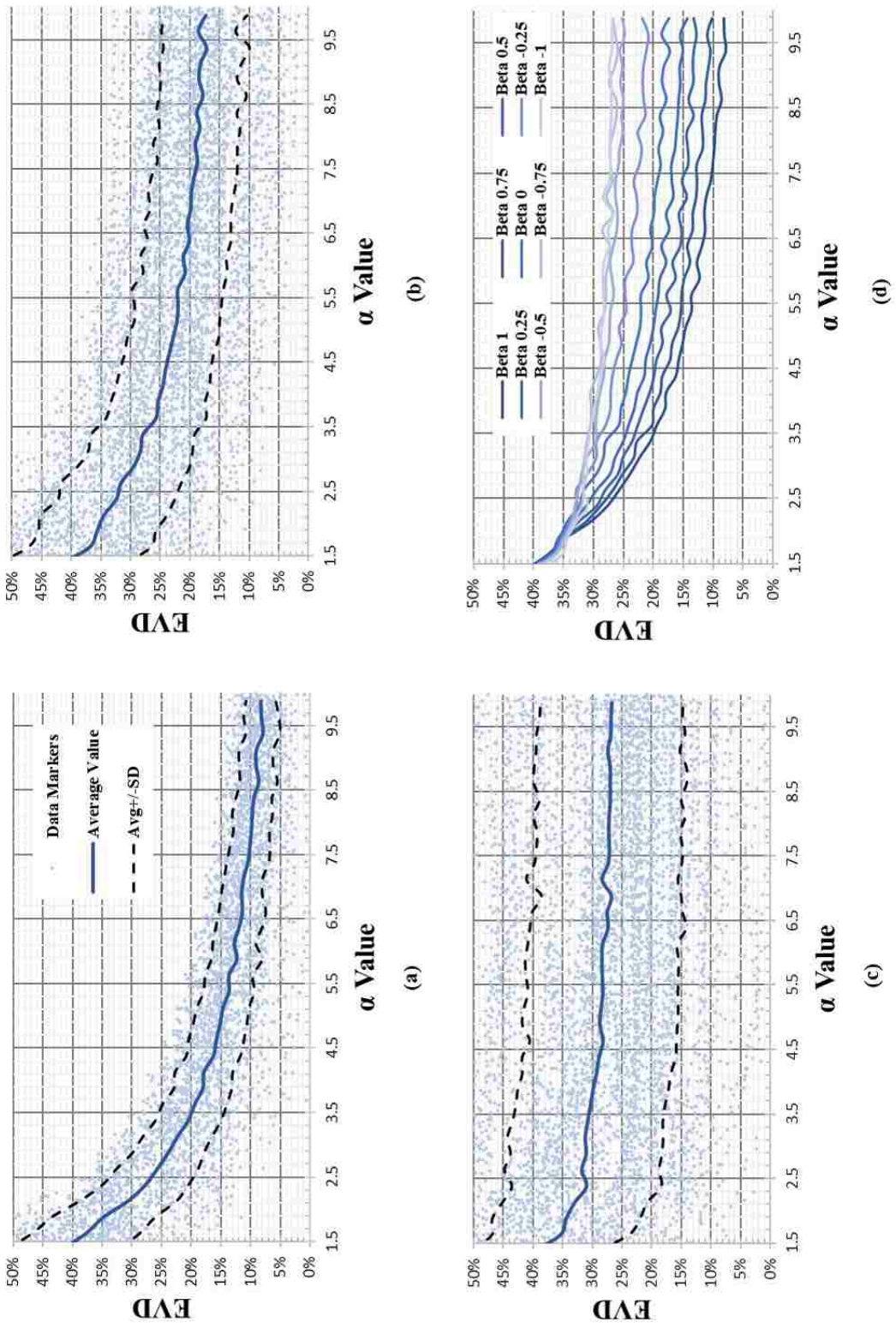

Figure 3.5: EVD vs α values for rigid SDOF isolators with (a) β= 1, (b)β= 0, (c) β= -1, and (d) average for all β values

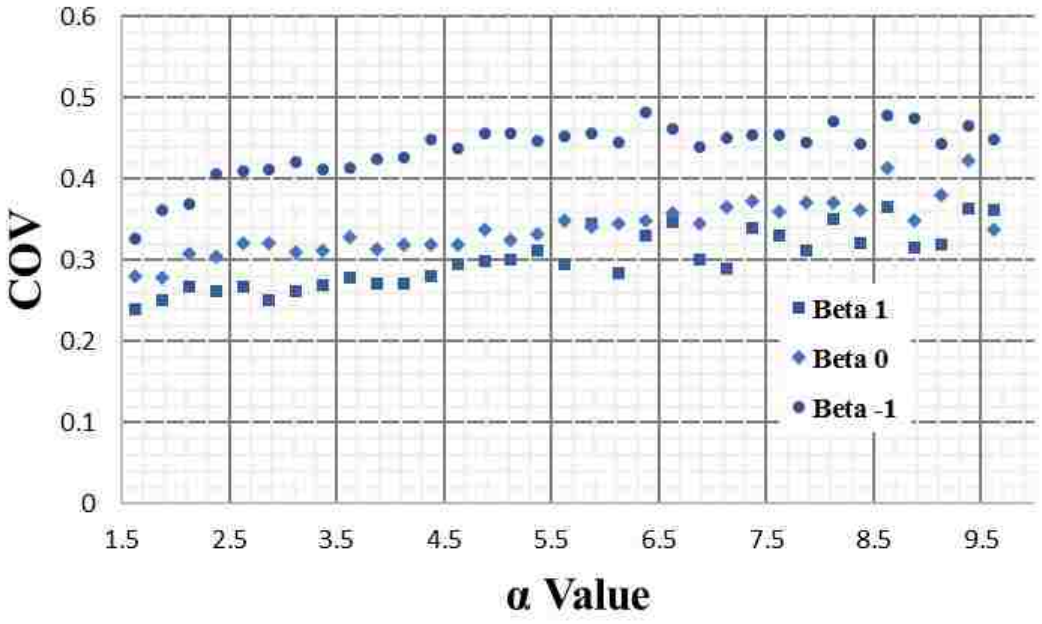

Figure 3.6: Scatter of COV vs. α for rigid SDOF

Figure 3.7 presents the results of the NLTH analyses performed on rigid case study structures in terms of η - EVD. The results of each individual analysis are outlined in Figure 3.7, for systems characterized by three values of β, namely 1.0 (representing an FP) (a) , 0 (representing a BowC) (b) and -1.0 (representing a BowTie) (c). As discussed earlier, the results are not separated as a function of the radius of curvature of the target FP device,

Table 3.4: Variation Data for EVD vs α for the rigid structure

	Beta 1	Beta 0.75	Beta 0.5	Beta 0.25	Beta 0	Beta -0.25	Beta -0.5	Beta -0.75	Beta -1
μ	0.17	0.18	0.20	0.22	0.24	0.26	0.29	0.29	0.29
σ	0.05	0.05	0.06	0.07	0.08	0.09	0.10	0.11	0.13
COV	0.30	0.31	0.30	0.31	0.34	0.35	0.36	0.37	0.43

in light of the observation that this parameter had no effect on the damping properties of the various systems. The solid curves represent the average trends, while the dashed curves represent the average plus or minus the computed standard deviation. Also, the average trends pertaining to all β values, are reported in Figure 3.7 (d). It should be noted that, in this case, the average COV is essentially constant and roughly equal to 22%.

For all systems, the most notable conclusion that can be drawn from Figure 3.7 is that the value of the demand reduction factor η, decreases as the EVD increases. This is consistent with the idea that higher energy dissipated corresponds to higher EVD and, in turn, in a lower seismic demand on the system. It is also interesting to note that, when expressed in terms of these two parameters, the results appear to be essentially independent of β, as shown in Figure 3.7 (d).

Flexible Structures with non-zero viscous damping ratio

As introduced earlier, it was of interest to examine whether the viscous damping assigned to the isolated system or its dynamic properties (i.e. its "elastic" period of vibration) had any effect on the damping properties of the VFS. To shed some lights on these matters, this section presents the NLTH analyses results pertaining to the "flexible" case study structures. Although structures characterized by three different periods of vibration and two viscous damping ratios were considered, only the results pertaining to the case study referred to as "Flexible 1", with specified damping ratio of 5%, are discussed in detail as they are considered representative of all the studied systems.

Figure 3.8 shows the results of each single analysis, again represented by the couple α - EVD. This outcome is outlined in Figure 3.8, for systems characterized by three values of β, namely 1.0 (representing an FP) (a), 0 (representing a BowC) (b) and -1.0 (representing a BowTie) (c). It should be noted that, for consistency with Figure 3.5, the EVD values summarized in Figure 3.8 are only those provided by the VFS (computed using Equation 3.1) and not those associated to the base isolator-structure assembly.

The solid curves in Figure 3.8 represent the average trends, while the dashed curves

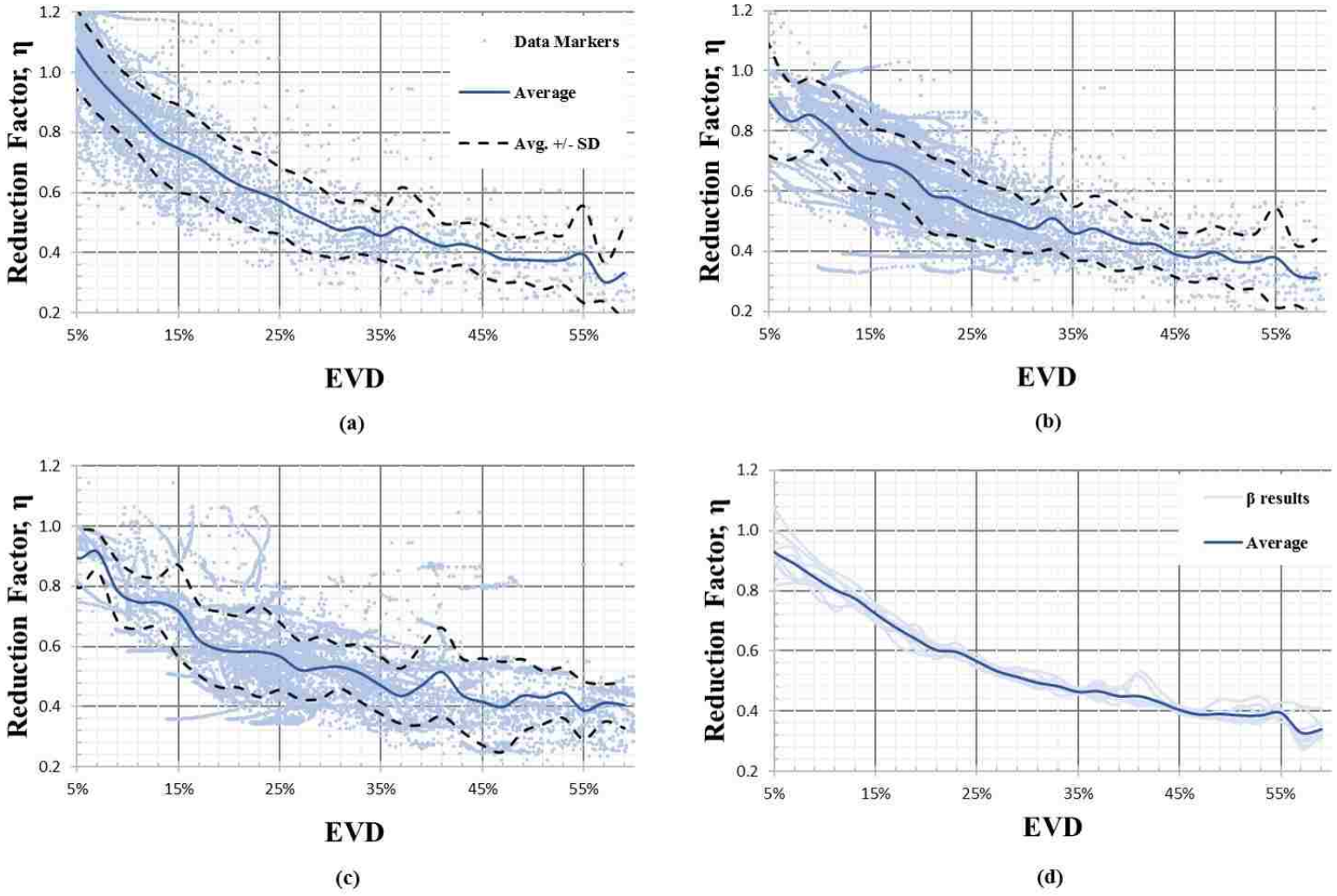

Figure 3.7: η vs. EVD values for rigid SDOF isolators with (a) β= 1, (b)β= 0, (c) β= -1, and (d) average for all β values

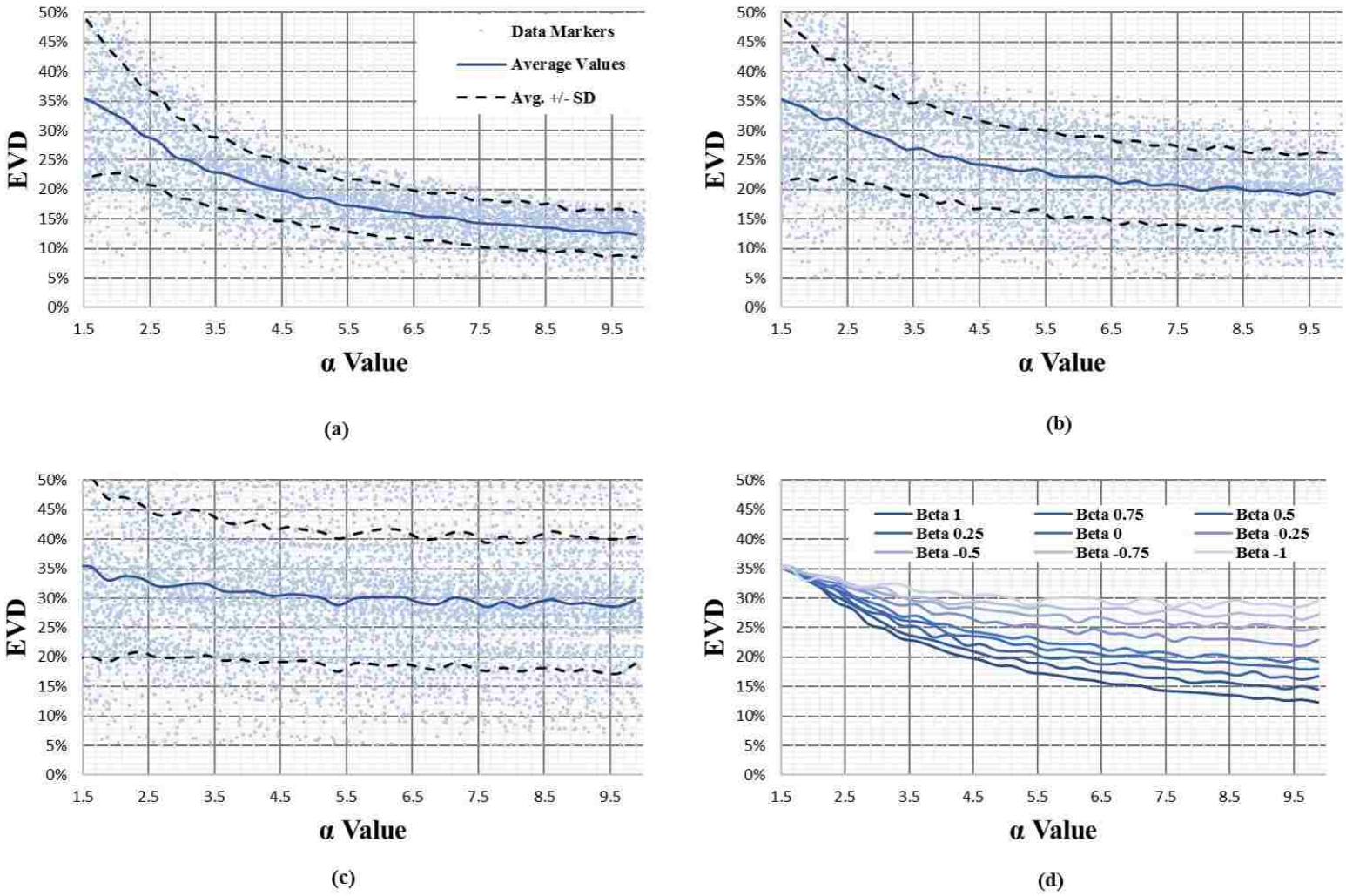

Figure 3.8: EVD vs α values for selected flexible SDOF isolators with (a) β= 1, (b)β= 0, (c) β= -1, and (d) average for all β values

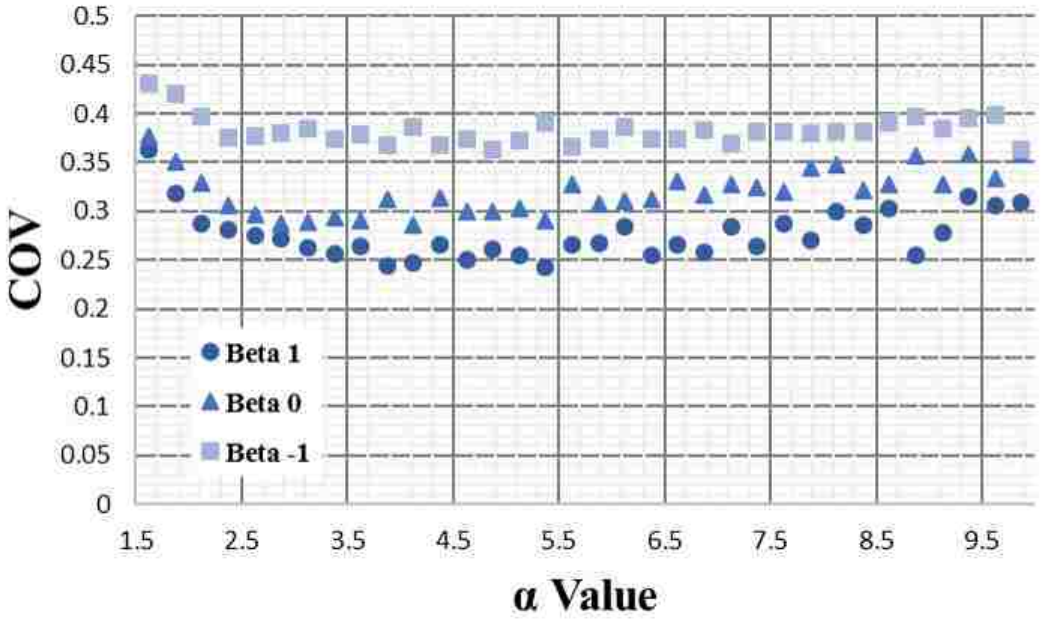

Figure 3.9: Scatter of COV vs. α for flexible 1 SDOF with 5% damping ratio

represent the average plus or minus the computed standard deviation. Also, the average trends for all "Flexible 1" with 5% visocus damping systems, are reported in Figure 3.8(d).

It can be seen that the "flexibility" of the system or the presence of a non-zero viscous damping do not really modify the outcome of the analyses. In fact, all the observations made in the previous sections hold.

The results of Figure 3.8 confirm what discussed above that is VFS with smaller β values seem to possess higher energy dissipation capacity, and in turn higher EVD. However, it is again apparent that the scatter of the whole data set around the average curves is overall quite large and that it increases as β decreases. The mean coefficient of variation (defined as the standard deviation divided by the mean), summarized in Figure 3.9 as a function of α, is approximately 28%, 32%, and 38% for the systems with βs of 1.0, 0, and -1.0, respectively.

For convenience, the mean coefficient of variation for "Flexible 1" systems with damping ratio of 5% is summarized in Table 3.5. It can be seen that the trend shown in Figure 3.9,

Table 3.5: Variation Data for EVD vs α for the selected flexible structure

	Beta 1	Beta 0.75	Beta 0.5	Beta 0.25	Beta 0	Beta -0.25	Beta -0.5	Beta -0.75	Beta -1
μ	0.20	0.21	0.22	0.23	0.24	0.26	0.28	0.29	0.31
σ	0.06	0.06	0.07	0.07	0.08	0.09	0.10	0.11	0.12
COV	0.28	0.29	0.29	0.31	0.32	0.34	0.35	0.36	0.38

and observed earlier for rigid structures, is confirmed.

It is again instructive to look at the results of the NLTH analyses in terms of η-EVD. The results of each individual analysis are outlined in Figure 3.10, for systems characterized by β values of 1.0 (a) , 0 (b) and -1.0 (c). The solid curves represent the average trends, while the dashed curves represent the average plus or minus the computed standard deviation. The average trends pertaining to all β values, are reported in Figure 3.10. Analogously to what observed for rigid structures, the average COV is essentially constant and roughly equal to 20%.

All other trends observed earlier are also confirmed: the value of the demand reduction factor, η, decreases as the EVD increases and the results appear to be essentially independent of β. To this end, Figure 3.10(d) shows that the average curves for all systems lie reasonably close to an overall mean curve.

In addition to the observed results, Figure 3.11 is provided as evidence of the fact that changing the "flexibility" of the isolated structure or modifying its viscous damping ratio do not significantly affect the EVD provided by the VFS itself. More specifically, Figure 3.11(a) summarizes the mean results (i.e. the mean EVD of the base isolator) pertaining to a system with $\beta = 1.0$, isolating structures characterized by different periods of vibration; Figure 3.11 (b) outlines the same results but pertaining to a system with $\beta = 1.0$, isolating case studies "Flexible 1" and "Rigid" with different elastic damping ratios.

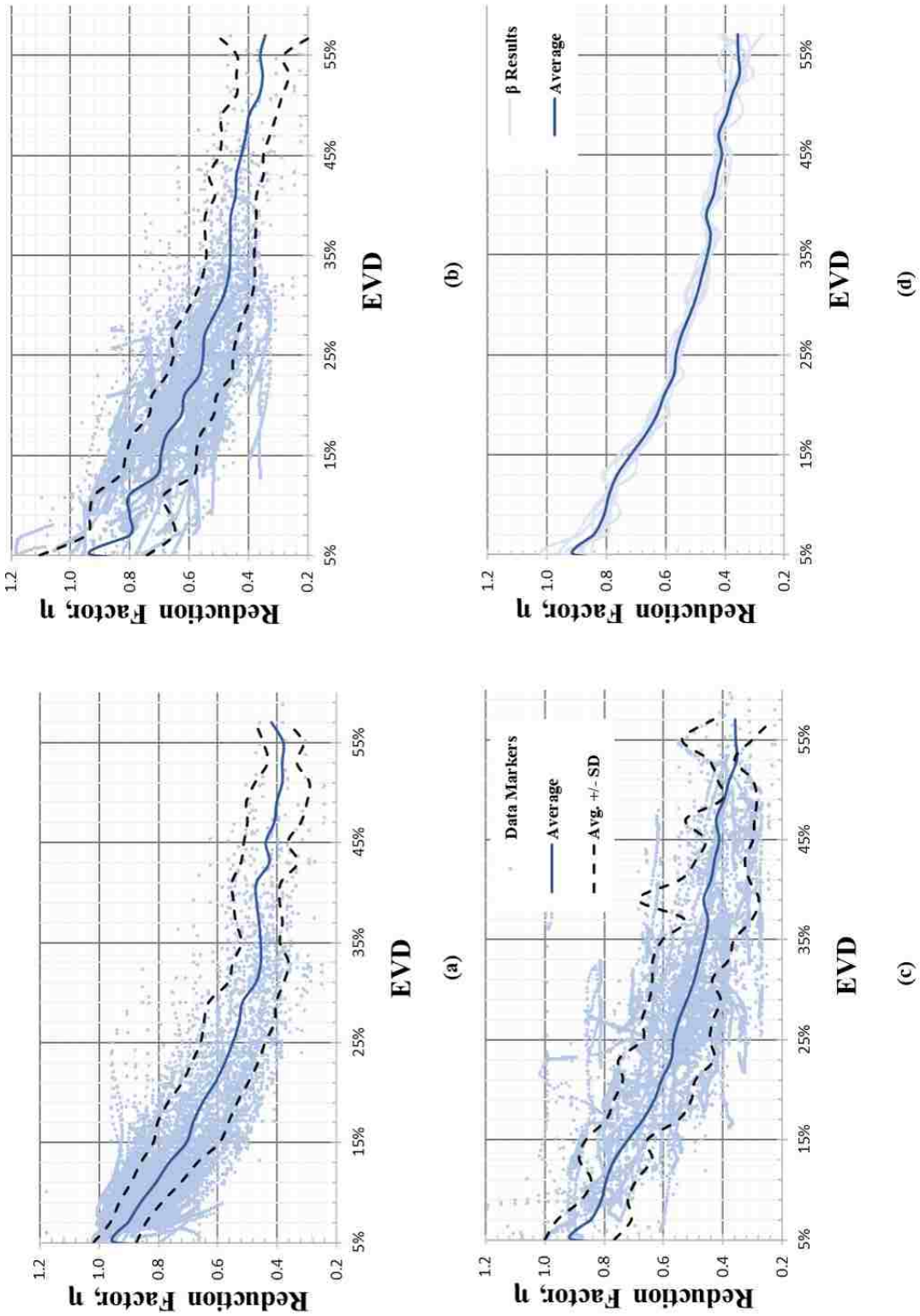

Figure 3.10: η vs. EVD values for selected flexible SDOF isolators with (a) β= 1, (b)β= 0, (c) β= -1, and (d) average for all β values

Based on the results of these sections, it is considered reasonable that, for design purposes, the EVD provided by a VFS be calculated solely as a function of parameters such as α and β, disregarding the dynamic properties of the structure to be isolated. On this account, for the remainder of this chapter, the results pertaining to the different case study structures analyzed will be combined.

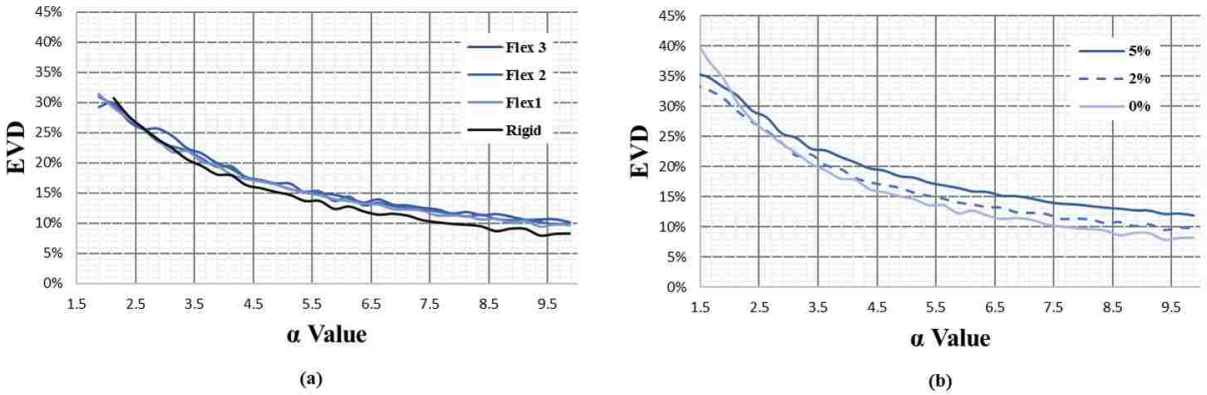

Figure 3.11: Difference in EVD response across (a) for 2% damping assigned structures and with varying flexibility (including rigid), and (b) Flexible 1 structures with different damping (including rigid) structure

3.2.2 Comparison with existing design equations

In this chapter, the results of the NLTH analyses presented and discussed thus far, are compared to the design equations outlined in Section 2.3.2 that are currently "in use" for VFS.

As discussed, one of the design steps that are necessary to design a VFS consists of estimating the EVD of the system. This is currently done using Equation 2.22, as soon as the design parameters α and β have been selected.

The EVD values obtained from the NLTH analyses, separated for different β values (all the values considered are shown, except for $\beta = 0$), are presented in Figure 3.12 versus the estimates obtained using Equation 2.22. It can be seen that Equation 2.22 does a reasonable job at capturing the trends and the qualitative relationship between EVD and

α for all cases. However, there is always some discrepancy (sometimes significant) between the mean NLTH results and the curves recommended for use within the DDBD method for VFS. It can be seen in Figure 3.12 that, for VFS with higher β, Equation 2.22 tends to be closer to the mean NLTH analyses results, and to underestimate the EVD that the system possesses. However, this trends reverses as the value of β decreases. The best overall agreement between the design equation and the NLTH results can be observed for $\beta = 0.5$, while the worst agreement occurs for systems with β = -1.0.

The discrepancy between theoretical estimates and NLTH results is quantified numerically in Figure 3.13. The "Error", is simply defined as the difference between the EVD estimated via Equation 2.22 and the corresponding value extracted from the NLTH analyses.

It can be seen that the Error is small (and on the conservative side) for systems with β ranging from 0.5 to 1.0, and it tends to grow as the value of β decreases. As mentioned, the largest error occurs for β = -1.0, for which the EVD appears to be overestimated, on average, by 10%.

Overestimating the EVD may result in an excessively low design reduction factor, and in turn, in designing the base isolation systems for excessively low seismic demands. This is apparent, referring to the discussion presented in section 2.3.2, where it was discussed that the EVD is estimated within the design process with the sole objective of calculating the demand reduction factor η. Two design equations for the calculation of this parameter were reported in section 2.3.2, where it was also suggested that Equation 2.24 should be favored over Equation 2.25.

The reduction factors η, and the EVD values obtained from the NLTH analyses, are presented in Figure 3.14 along with the estimates obtained using Equations 2.24 and 2.25. The mean analyses results and the mean plus and minus one standard deviation are also included in the graphs. It should be noted that, following the discussion presented in previous chapters, the η - EVD results are no longer grouped as a function of the various parameters. This is done on account of the apparent in-dependency of the relationship between these two parameters with respect to any other variables considered in the parametric study conducted.

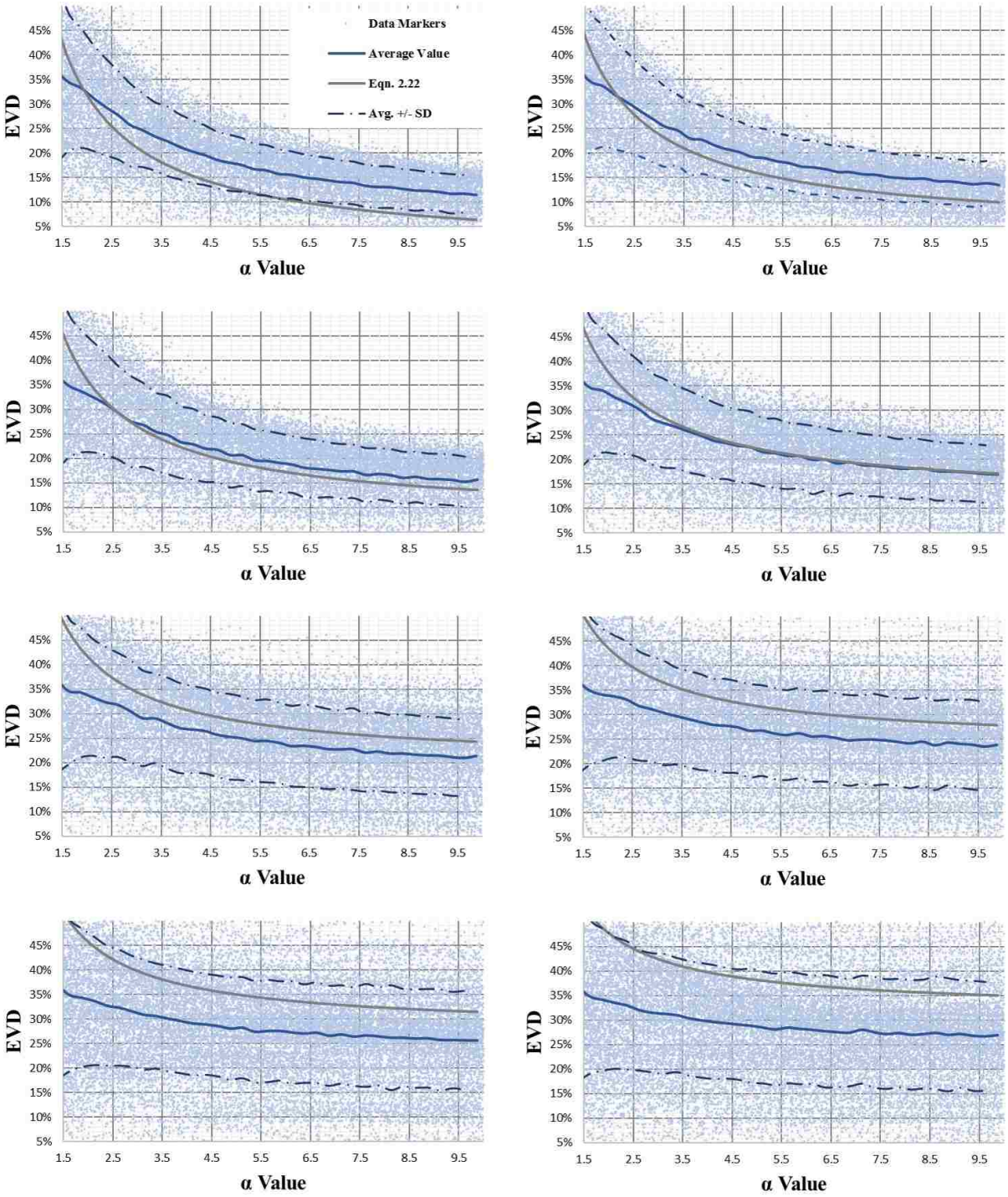

Figure 3.12: EVD (from isolator) vs α results for all structures combined, for β= 1,0.75,0.5,0.25,-0.25,-0.5,-0.75,-1 (top to bottom)

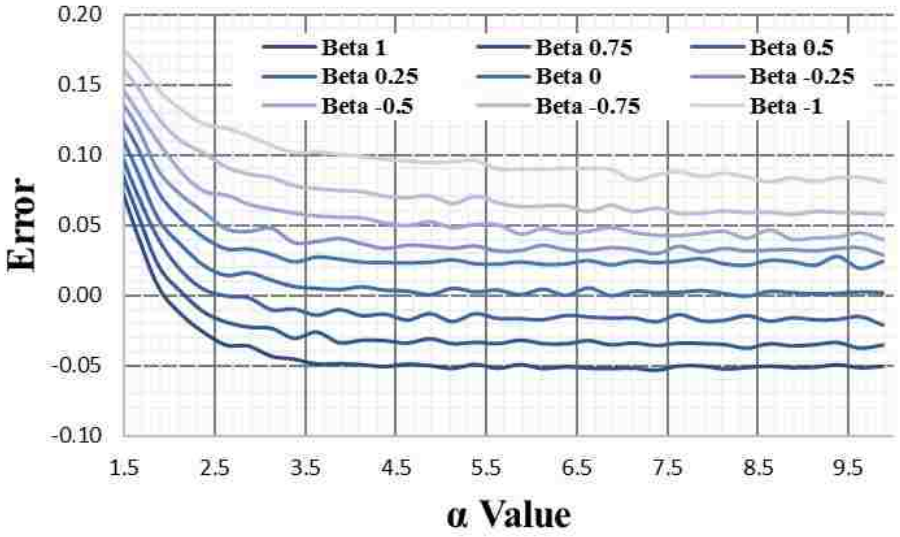

Beta	Average Error
1.00	-0.04
0.75	-0.02
0.50	-0.01
0.25	0.01
0.00	0.03
-0.25	0.04
-0.50	0.06
-0.75	0.08
-1.00	0.10

Figure 3.13: Error values from equation 2.22 and experimental data for different β systems

It can be seen in Figure 3.14 that both Equations 2.24 and 2.25 do a pretty good job at capturing the average relationship between η and EVD. Obviously, some discrepancy exists between the design equations and the results of the NLTH analyses. In particular, it appears that the mean NLTH analyses results fall in between the two design curves, with Equation 2.25 overall on the conservative side and Equation 2.24 slightly un-conservative.

The discrepancy between theoretical estimates and NLTH results is quantified numerically in Figure 3.15. The "Error", is defined as the difference between the η estimated via design equations 2.24, and 2.25 and the corresponding value extracted from the NLTH analyses, for different EVDs.

All the trends and the reasons for the discrepancies presented in this Chapter are further discussed in section 3.3, where alternative design equations are developed and proposed.

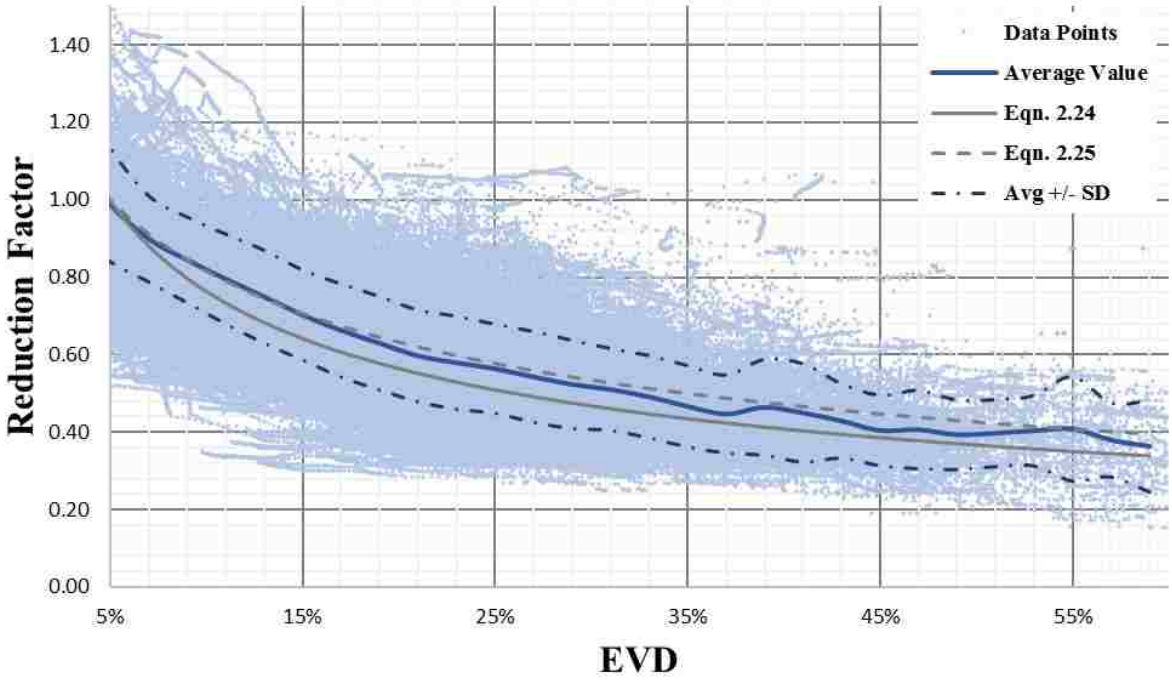

Figure 3.14: η vs EVD for all systems combined, compared to existing equations

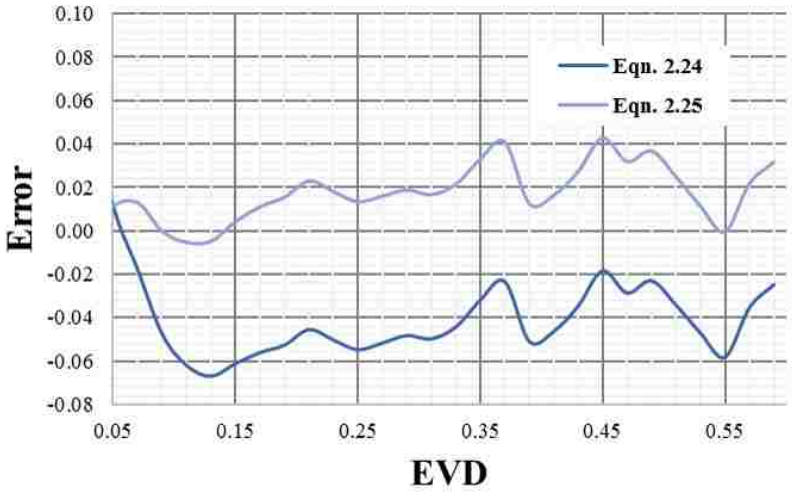

EVD	Eqn. 2.24	Eqn. 2.25
5%	0.011469	0.011469
11%	-0.06202	-0.00525
15%	-0.06108	0.004336
21%	-0.04548	0.023015
25%	-0.0547	0.013473
31%	-0.04973	0.016751
35%	-0.03195	0.03309
41%	-0.04635	0.016426
45%	-0.01849	0.042803
51%	-0.03422	0.024938
55%	-0.05823	-0.00042

Figure 3.15: Error values for η vs EVD calculated as difference between equation 2.24, 2.25 and average of experimental data for different β systems

3.3 Design Parameters Calibration

The previous chapter has emphasized that the EVD design equations recommended for use within the DDBD process for VFS have merit, in that they provide some means of capturing the relationship trends between the EVD, and the design parameters α and β.

However, it has also been shown that some discrepancies exist between the NLTH analysis results and the outcome provided by the design equations. In particular, while the estimates provided for systems characterized by positive β values may be acceptable from both a qualitative and quantitative perspective, this is not necessarily the case for systems with low βs.

Because the available design equations seemed to be more suitable for systems with higher β, while losing accuracy as β decreases, it was believed that the best way to explain this trend was to look closely at the dynamic response of all the systems analyzed, and to find something that was fundamentally different in the response of systems with different βs.

A thorough post-processing of the results of the NLTH analyses showed something very interesting: VFS characterized by positive βs tend to produce a quite symmetric response (i.e. the recordedpositive peak displacements roughly correspond to the negative peak displacements), while VFS with negative βs are prone to a non-symmetric response. This is shown in Figure 3.16, in which the force-displacement response of systems with different values of β (namely: 1.0, 0.25, -0.25 and -1.0) to one of the input ground motions is outlined. With reference to the same figure, it can be further seen that the asymmetry is more pronounced as the value of β decreases. While these are only the results of one of the analyses, it should be noted that they are representative of the whole numerical campaign and that this trend is observed, to different extents, for all input ground motions at all intensities. While there are other aspects of the response of the different systems as a function of the design parameter β that may be of interest, the focus of this chapter is exclusively on the damping properties. However, the overall performance of VFS (considering all relevant aspects) will be further discussed in Chapter 4.

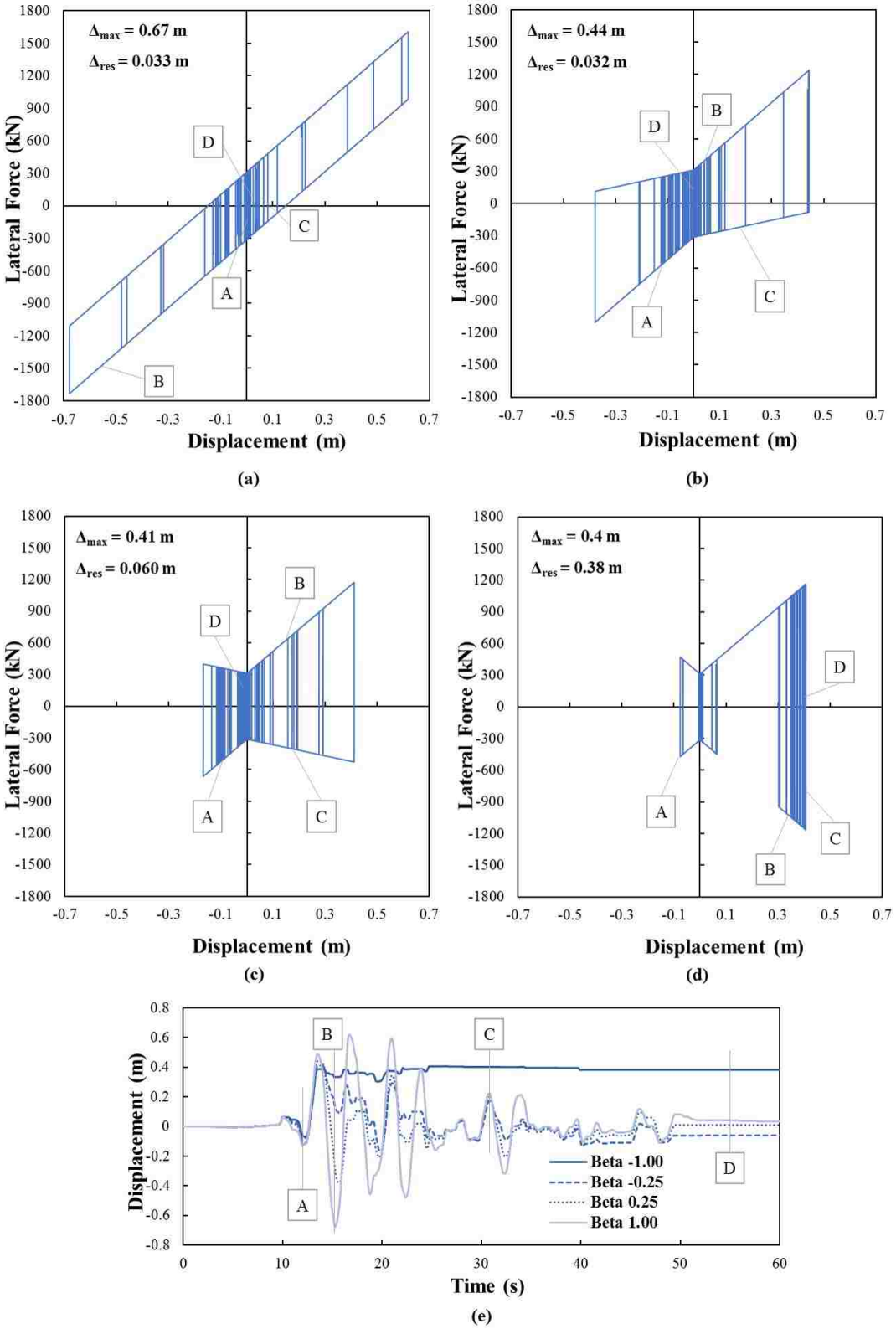

Figure 3.16: Force-displacement behavior of (a) Friction Pendulum (β=1.0), (b) β =0.25, (c) β=-0.25, and (d) β= -1.0; displacement history for these systems (e)

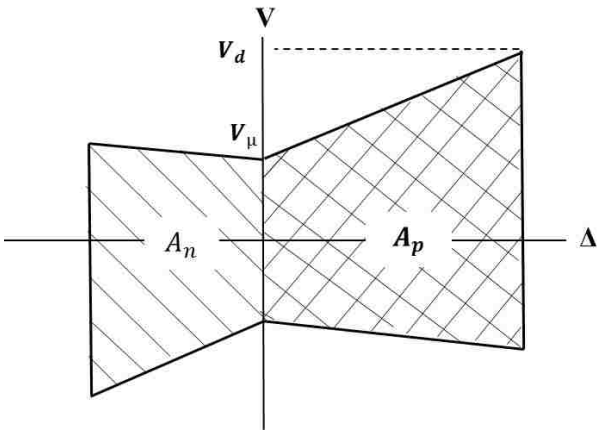

Figure 3.17: Force-Δ response of un-symmetrical arbitrary VFS

The symmetry or asymmetry of the force-displacement response of a system is extremely relevant with respect to the EVD that a system possesses, as current design equations were derived relying on the assumption that all systems manifest a symmetrical hysteretic response. However, as the results of the NLTH analyses have shown, the response of a VFS may be highly non-symmetrical, particularly for decreasing values of β. Treating a non-symmetrical hysteresis as symmetrical, leads to overestimating the area under the force-displacement curve and, in turn, the available EVD (since the EVD is directly related to the hysteretic area).

The general "idealized" hysteretic response of a VFS is outlined in Figure 3.17. It is shown that the "positive" area (the area under the curve to the right of the vertical axis) may be larger than the "negative" area (the area under the curve to the left of the vertical axis). Clearly, the "negative" area could be greater than the "positive" area, but this eventuality does not defeat the point of the discussion that follows.

With reference to Figure 3.17, the total area under the hysteretic curve, A_h, should be computed as the sum of the two areas, as follows:

$$A_h = A_p + A_n \tag{3.3}$$

To express the "negative" area as a function of the "positive" area, a corrective parameter, γ, is introduced so that:

$$A_h = A_p + A_n = A_p + \gamma A_p \tag{3.4}$$

It was derived in section 2.3.2 , that the EVD term associated to A_p can be computed solely as a function of the design parameters α and β as:

$$\xi_{eq,p} = \frac{\alpha - \alpha\beta + \beta + 3}{4\pi\alpha} \tag{3.5}$$

Therefore, combining Equation 3.4 and Equation 3.5, the total EVD of the system can be calculated as:

$$\xi_{eq} = \frac{\alpha - \alpha\beta + \beta + 3}{4\pi\alpha} + \gamma\frac{\alpha - \alpha\beta + \beta + 3}{4\pi\alpha} \tag{3.6}$$

The corrective coefficient γ is meant to quantify the asymmetry in the hysteretic response and, in turn, to quantify the reduced EVD available. This coefficient was calibrated directly from the results of the NLTH analyses, trying to maximize the reduction of the "Error" inherent in Equation 2.22. In particular, the error is defined as the difference between the EVD computed via Equation 2.22 and the mean EVD extracted from the NLTH analyses. This can be expressed as:

$$Error(E) = EVD_{Eqn.2.22} - EVD_{NLTH} \tag{3.7}$$

If it is assumed that the newly proposed Equation perfectly matches the mean results of the NLTH analyses, the error can be rewritten as:

$$E = \frac{\alpha - \alpha\beta + \beta + 3}{2\pi\alpha} - (\frac{\alpha - \alpha\beta + \beta + 3}{4\pi\alpha} + \gamma\frac{\alpha - \alpha\beta + \beta + 3}{4\pi\alpha}) \tag{3.8}$$

Which can be rearranged to obtain:

$$\gamma = 1 - E\frac{4\pi\alpha}{\alpha - \alpha\beta + \beta + 3} \tag{3.9}$$

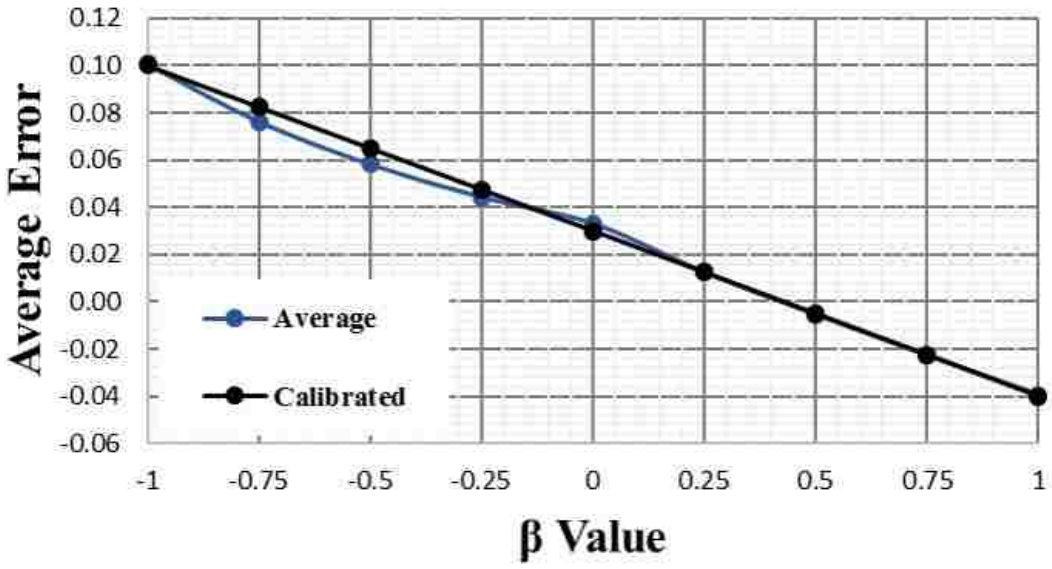

Figure 3.18: Calibration of error for varying β value as a linear approximation

The mean Error E, obtained directly from the results of the NLTH analyses is presented in Figure 3.18 as a function of the design parameter β.

It can be seen (Figure 3.18) that there is a roughly linear trend between the Error and β. This allows for the calibration of a simple equation to relate the two parameters:

$$Error = -0.07\beta + 0.03 \tag{3.10}$$

Which leads to an expression for the corrective parameter γ of the form:

$$\gamma = 1 - (-0.07\beta + 0.03)\frac{4\pi\alpha}{\alpha - \beta\alpha + \beta + 3} \tag{3.11}$$

Combining Equation 3.10 and Equation 3.11, the following relationship can be found:

$$\xi_{eq} = \frac{\alpha - \alpha\beta + \beta + 3}{4\pi\alpha} + (1 - (-0.07\beta + 0.03)\frac{\alpha - \alpha\beta + \beta + 3}{4\pi\alpha}) \tag{3.12}$$

Which can be simplified to:

$$\xi_{eq} = \frac{\alpha - \alpha\beta + \beta + 3}{2\pi\alpha} + (0.07\beta - 0.03) \tag{3.13}$$

Equation 3.13 represents a general design equation to calculate the EVD of a generic VFS. Its performance can be appreciated in Figure 3.19. As expected, the new equation matches the mean results of the analyses well for all β values. In the future, it should be tested for VFS with different characteristics and considering different sets of input ground motions.

It was shown in section 2.3.2 that the relationship between the EVD and the reduction, is overall well captured by both Equations 2.24 and 2.25. As such, there is no real need for any substantial modifications of the available design equations. However, it was shown that the mean NLTH analyses results fell in between the two design curves and that, as a consequence, Equation 2.24 tends to provide slightly more conservative estimates than Equation 2.25, despite Equation 2.25 is still recommended when using DDBD procedures. In any case, in the attempt of minimizing the discrepancy between design equations and the NLTH analyses results, a new equation is introduced, that better fits the results of the current study:

$$\eta_\xi = \sqrt{\frac{9}{5 + \xi_{eq}}} \tag{3.14}$$

It can be seen that Equation 3.14 represents a minor modification of the existing functions and that the "structure" of all three equations reported in this study is identical. Moreover, it should be noted that even though Equation 3.14 lies closer to the mean results of the analyses, it hardly represents an improvement over the existing equations, which are still considered satisfactory and possibly better, when employed with a different set of ground motions.

The discrepancy between the three design equations and the results of the NLTH analyses

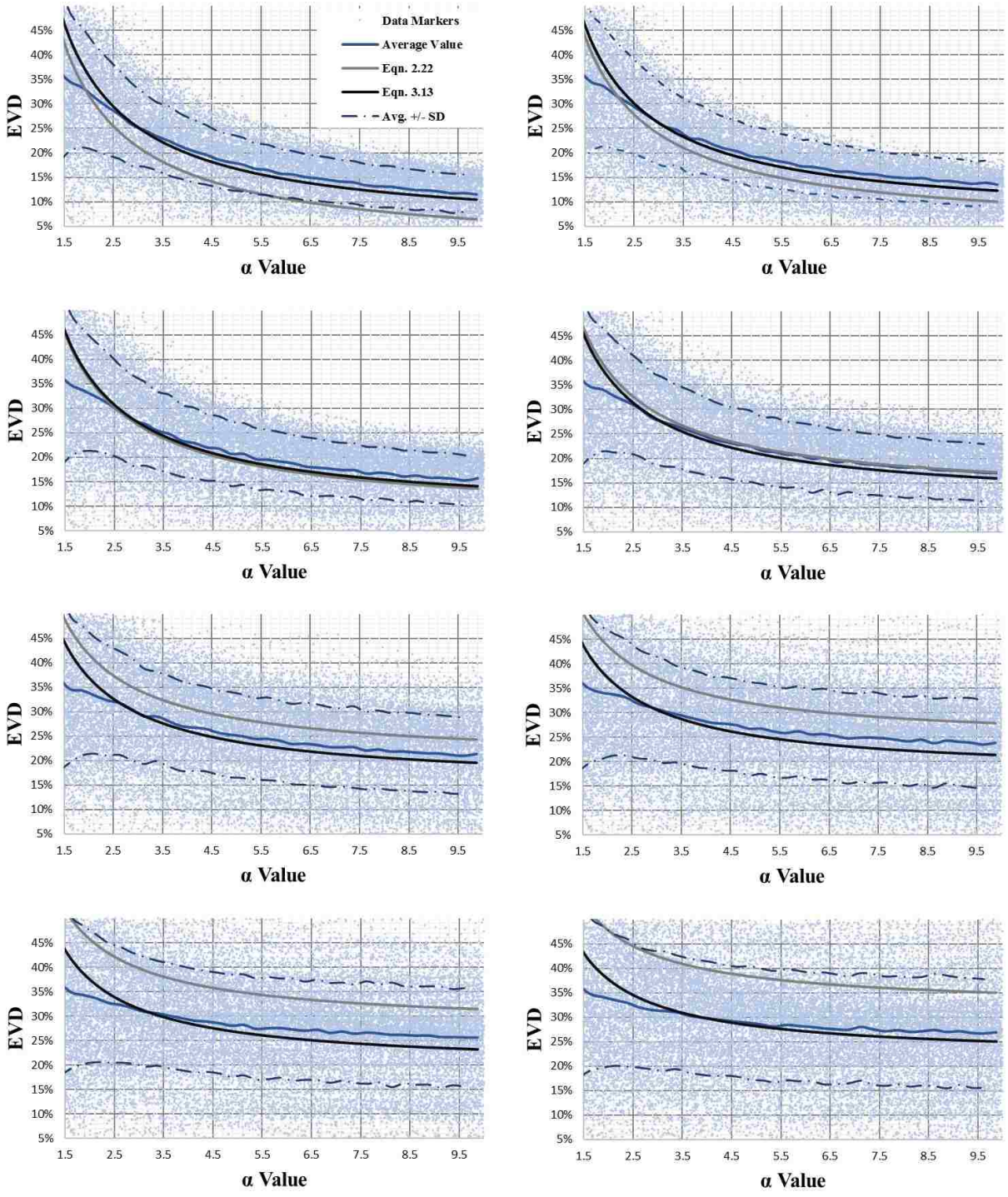

Figure 3.19: EVD (from isolator) vs α results for all structures combined, for β= 1,0.75,0.5,0.25,-0.25,-0.5,-0.75,-1 (top to bottom) compared with results from equations 2.22 and 3.13

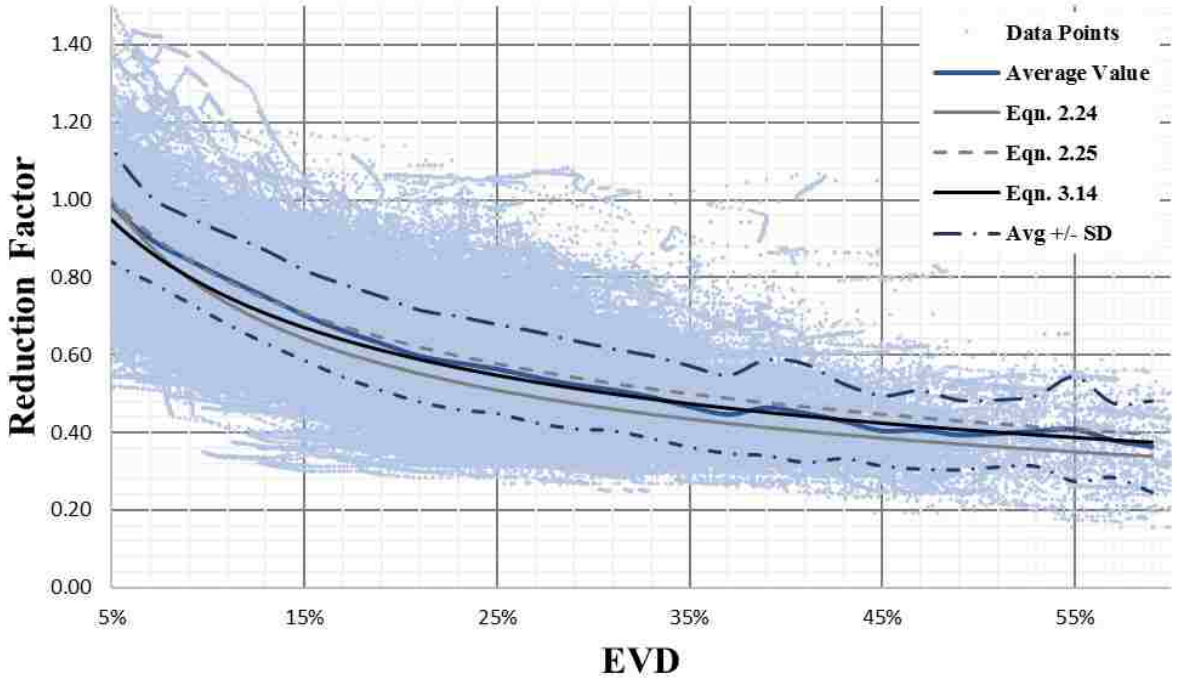

Figure 3.20: η vs EVD for all systems combined, compared to existing and proposed equations

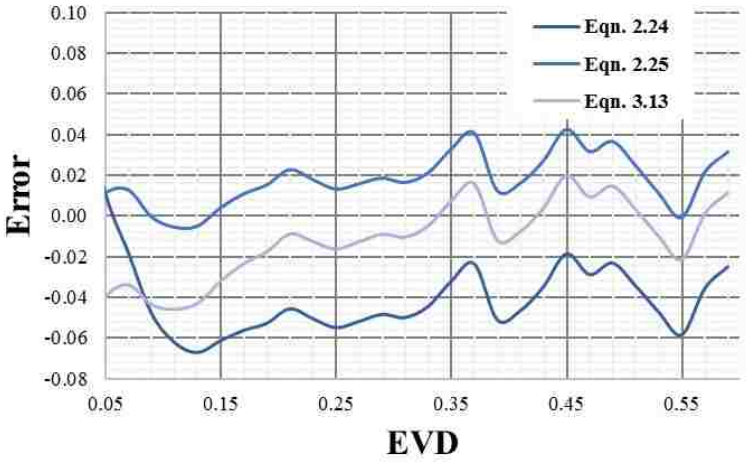

EVD	Eqn. 2.24	Eqn. 2.25	Eqn. 3.13
5%	0.011469	0.011469	-0.03985
11%	-0.06202	-0.00525	-0.04582
15%	-0.06108	0.004336	-0.03195
21%	-0.04548	0.023015	-0.00881
25%	-0.0547	0.013473	-0.01615
31%	-0.04973	0.016751	-0.01029
35%	-0.03195	0.03309	0.007432
41%	-0.04635	0.016426	-0.0075
45%	-0.01849	0.042803	0.019854
51%	-0.03422	0.024938	0.003252
55%	-0.05823	-0.00042	-0.02137

Figure 3.21: Error values for η vs EVD for equations 2.24, 2.25, and 3.13 for different β systems

are quantified mathematically by calculating an "Error" (defined earlier), which is shown graphically in Figure 3.21.

3.4 Conclusions

This chapter has presented the results of an extensive numerical study aimed at investigating the damping properties of the recently proposed VFS. Of particular interest, were the relationship between the design parameters α and β, the EVD that a device can rely on, and the relationship between the EVD and the design demand reduction factor, η.

The results of the analyses have demonstrated that VFS may rely on high energy absorption and, in turn, on higher EVD coefficients. This is particularly true as the systems are hit by stronger ground motions and are therefore characterized by high values of α. Decreasing the value of the design parameter β has the effect of creating devices with fatter hysteretic loops and high damping. However, it was discussed that decreasing β has also the effect of causing a greater scatter in the results, and of enhancing the probability of non-symmetrical response.

It was also shown that the EVD that a VFS possesses, is not affected by fundamental characteristics of the isolated structures, such as their viscous damping ratio or their period of vibration. It was observed that current design equations for VFS that relate the design parameters α and β to the EVD of the device, are fairly accurate for systems with positive βs but they lose in accuracy as the value of β decreases. This trend was attributed to the non-symmetrical response that VFS, and particularly those characterize by low values of β, tend to experience and by the fact that current deign equations were derived assuming perfectly symmetrical response. For these reasons, a new general design equation capable of accounting for the asymmetry in the response of a VFS was derived and proposed.

Finally, it was discussed how available design equations relating the EVD to the design demand reduction factor do a reasonably good job at approximating the mean results of the NLTH analyses, however a new equation was proposed that gives the best results.

Chapter 4

PERFORMANCE OF VARIABLE FRICTION BASE ISOLATED SDOF SYSTEMS

This chapter presents a numerical investigation on the performance of SDOF case study structures isolated with VFS. The dual aim of this chapter is to provide some insight into the dynamic behavior of these systems, providing some information on how to select the device parameters to maximize the systems' response, and to validate the design process presented in the previous chapters. These objectives were achieved by conducting a large number of NLTH analysis on a comprehensive set of case study structures. To this end, two sets of structures were considered:

- Set A included all the case study structures described in Chapter 3.1.3;
- Set B consisted a new group of case studies, discussed in more detail in later sections.

The analyses were performed using the customized computer program described in section 3.1.2, and the numerical models assembled as discussed earlier. The input ground motions considered are those described in section 3.1.1 and summarized in Table 3.1, scaled at different intensities.

The results of the analyses are presented and discussed in detail. Interesting aspects of the behavior of VFS are emphasized and some preliminary conclusions on the advantages and drawbacks of the various systems are drawn.

The Chapter is broken into two main subsections: first, the results of the analyses pertaining to the case study structures of Set A are presented; second, the case study structures pertaining to Set B are described and the results of the analyses discussed in detail.

4.1 NLTH Analysis Results: Set A

The case study structures of Set A have been extensively described in section 3.1.3. However, in section 3.1.3, the results of the NLTH analyses conducted on this set of structures were mainly discussed from a damping properties standpoint. In this chapter, the results of the numerical analyses are processed in terms of overall performance of the VFS analyzed. Chapter 3 has outlined how 189 case study structures were tested numerically under a suite of 50 spectrum compatible ground motions, scaled at a number of intensities (the scale factors were varied from 0.1 to 10, at 0.1 increments). This wide range of scale factors were considered with the intent to study the response of the structures under relatively small to very large earthquakes, and to examine the systems response in a variety of scenarios. However, this led to consider earthquakes characterized by unrealistically high or excessively low peak ground accelerations (PGAs). For this reason, only selected ground motion intensities (i.e. with realistic values of PGA) are studied closely herein (scale factors of 0.5, 1.0, 1.5 and 2.0 are considered).

Even though the base isolators were designed for a peak lateral displacement of 0.45 m (see 3.1.3), it was assumed herein that their displacement capacity was in fact larger and the analyses were not terminated if the isolators reached the design displacement. This was done in the interest of studying the system performance under ground motions with large magnitude (i.e. greater than the design earthquake magnitude).

4.1.1 Rigid SDOF Structures

Figure 4.1 shows the design level (i.e. EQ multiplier equal to 1.0, PGA = 0.591g) results, pertaining to the Rigid case study structures, in terms of the four main parameters of interest. The results are separated as a function of the radius of curvature characterizing the target FP systems considered. It can be seen that lowering β has beneficial effects with respect to lateral forces (figure 4.1(c)) and accelerations (d), but tends to produce systems with lower re-centering capabilities (figure 4.1 (b)).

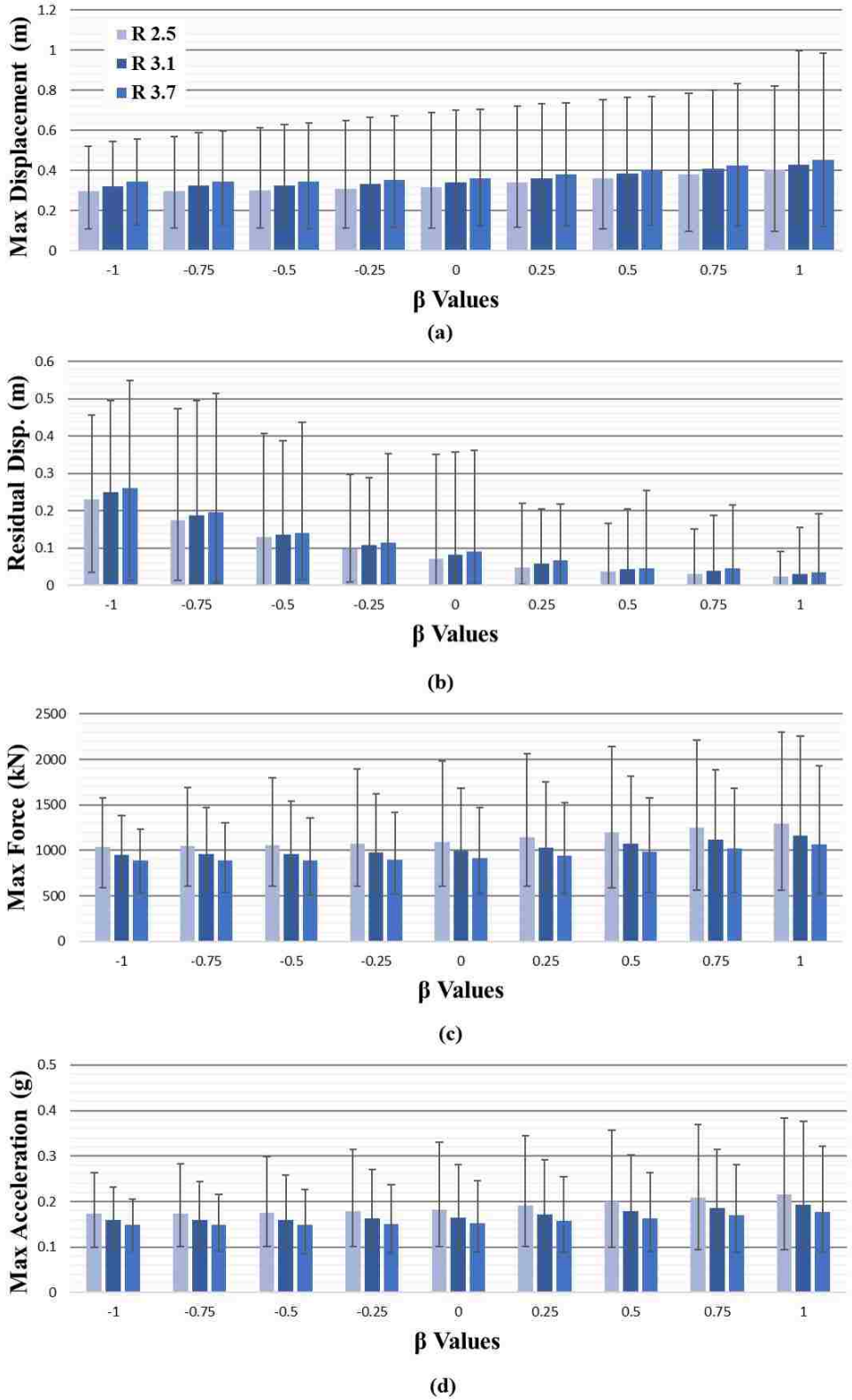

Figure 4.1: Case study B structures results of NLTHA in terms of (a) maximum displacements, (b) residual displacements, (c) maximum lateral forces, and (d) maximum accelerations

It should also be observed that the lower the value of β, the lower the displacement demand on the system (Figure 4.1 (a)). It is interesting to point out that, pertaining to parameters such as displacements, forces, and accelerations, the scatter of the results is lower for systems with low β. However, this trend is reversed when considering residual displacements.

The effects of using different radius of curvature R can also be observed. Basically, using smaller radius (i.e. higher post activation stiffness) is beneficial with respect to parameters such as maximum and residual displacements but tends to induce greater lateral forces and accelerations in the system.

Important topics of discussion are the effect of the earthquake magnitude, and the performance of the systems when hit by rare and frequent events (i.e. of higher and lower magnitude with respect to the design earthquake). The effects of the earthquake intensity on the structures are shown in Figure 4.2. As mentioned, four scale factors (0.5, 1, 1.5 and 2, corresponding to PGAs = 0.296g, 0.591g, 0.89g, and 1.18g, respectively) are considered. Since the role played by the radius of curvature R appeared to be minor, this parameter is eliminated by computing the average results, with respect to R.

For convenience, the peak displacements extracted from the analyses are normalized with respect to a nominal displacement of 0.45 m. For a hypothetical frequent earthquake (SF=0.5), all systems experienced similar maximum displacements, about 25% of the nominal capacity (Figure 4.2 (a)). As the earthquake intensity increased, systems with different βs manifested different responses. At scale factor of 2.0, the displacement demand on the FP appears to be much higher (2.9 times the nominal capacity) compared to the demand on a BowTie (1.75 times nominal capacity). Other devices have demands in between these two bounds. It can also be seen that the demand on the FP increases more rapidly than for a BowTie. The mean results, the standard deviation, and the coefficient of variation (μ, σ, and COV respectively) have also been included in Table 4.1. With respect to peak displacements, these parameters grow as the values of β decrease. This suggests that systems with higher β are somewhat less reliable, at least with respect to this response parameter

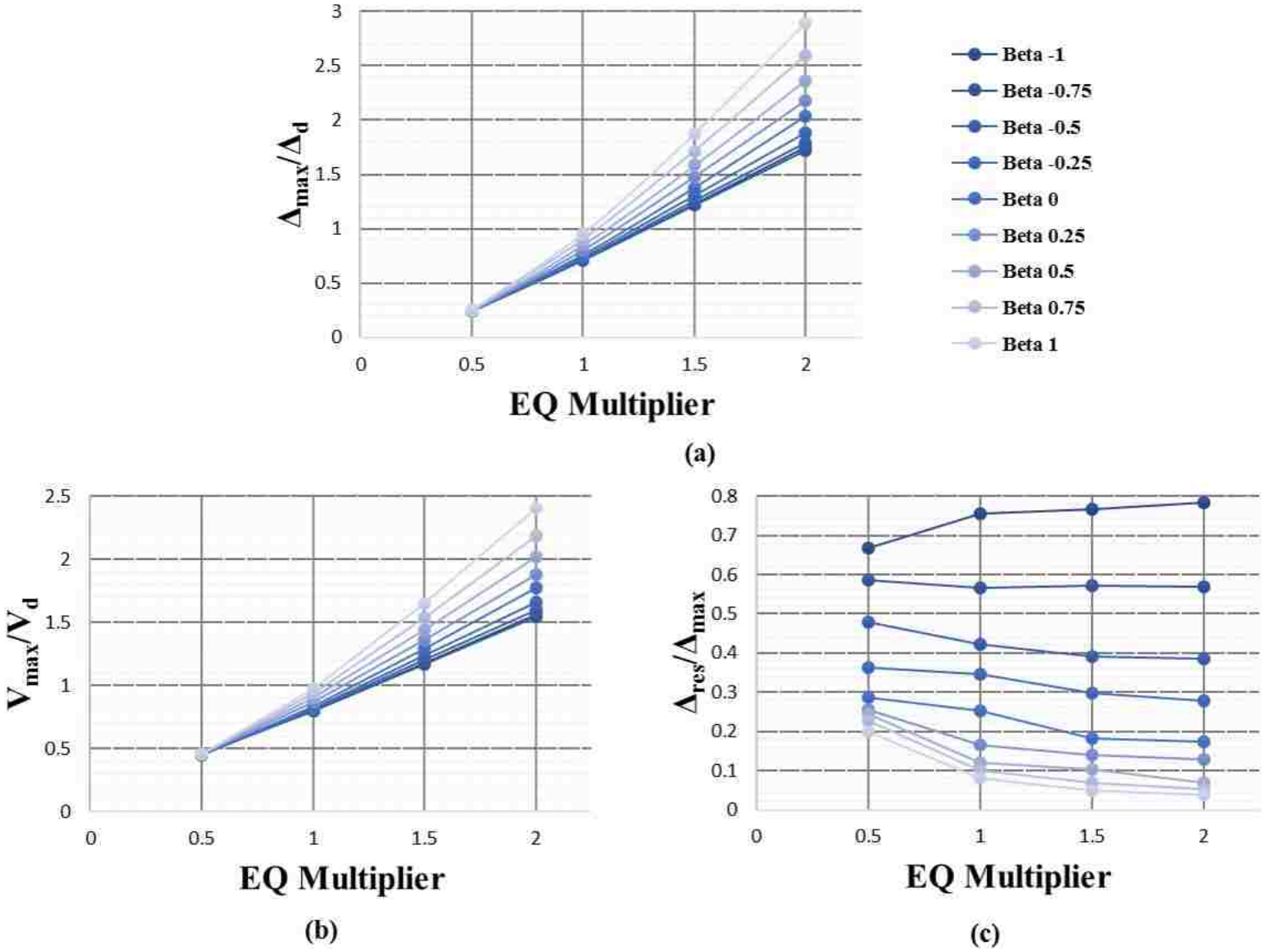

Figure 4.2: Normalized results for Case B structures for different EQ intensities in terms of (a) displacements (b) lateral force, (c) residual displacement

(the peak displacement). A similar trend is observed with respect to the peak lateral forces, while the trend reverses if the residual displacement is taken as the response parameter of interest.

Analogously to the peak displacements, the peak lateral forces have been normalized with respect to the nominal strength of the system, 1200 kN (for FP R=3.1), and plotted against the earthquake multipliers (Figure 4.2(b)). Again, it is seen that at small earthquake intensity, all the systems experience analogous response, and that this trend changes at larger earthquake intensity. It can also be seen that lower the value of β, lower is the lateral force that the isolator attracts. Since forces and accelerations are closely related, analogous conclusions can be drawn for both parameters.

The residual displacements have been normalized with respect to the corresponding maximum displacements, and plotted against earthquake intensity multipliers (Figure 4.2 (c)). It can be seen that, at all intensity levels, the residual displacement is higher for systems with low βs and vice versa.

However, the issue of the residual displacement is not as simple as measuring its magnitude following a seismic event and should be further examined.

To this end, consider a scenario in which an FP with the characteristics of the target system (R = 3.1 m, μ = 5.5%) is used to protect a rigid 6,000 kN structure against a rare event (e.g. EQ Multiplier = 1.5). In this context, the maximum displacement demand on the system would be 0.84 m (1.87 times 0.45 m, the capacity of the reference device). Neglecting the size of the slider, this performance could be achieved by employing an FP with a diameter of 1.7 m. Alternatively, the FP system could be replaced by a less costly 1.7 diameter β= -1.0 VFS, with identical backbone response. If this was the case, the maximum demand on the VFS would be 0.55 m.

Based on the results reported in Figure 4.2 (d), the expected residual displacements for the two systems would be 0.042 m and 0.42 m, respectively. It is evident that in case of an

Table 4.1: Results obtained for case B structures for different earthquake intensities

Normalized Displacement (Δ_{max}/Δ_d)												
	EQ Multiplier 0.5			EQ Multiplier 1			EQ Multiplier1.5			EQ Multiplier 2		
β	μ	σ	COV	μ	σ	COV	μ	σ	COV	μ	σ	COV
-1.00	0.25	0.12	0.48	0.72	0.25	0.35	1.23	0.40	0.33	1.75	0.54	0.31
-0.75	0.25	0.12	0.49	0.72	0.26	0.36	1.22	0.42	0.34	1.73	0.57	0.33
-0.50	0.25	0.12	0.50	0.73	0.28	0.38	1.26	0.44	0.35	1.8	0.58	0.33
-0.25	0.24	0.13	0.51	0.74	0.29	0.39	1.31	0.45	0.35	1.89	0.61	0.33
0.00	0.25	0.13	0.52	0.76	0.30	0.40	1.38	0.49	0.35	2.04	0.68	0.34
0.25	0.25	0.13	0.52	0.81	0.33	0.40	1.48	0.54	0.37	2.18	0.76	0.35
0.50	0.25	0.13	0.53	0.86	0.36	0.42	1.59	0.62	0.39	2.37	0.88	0.38
0.75	0.25	0.14	0.53	0.91	0.41	0.45	1.72	0.72	0.42	2.60	1.04	0.40
1.00	0.26	0.14	0.54	0.96	0.46	0.48	1.87	0.85	0.45	2.89	1.31	0.46
Normalized Maximum Force (V_{max}/V_d)												
	EQ Multiplier 0.5			EQ Multiplier 1			EQ Multiplier1.5			EQ Multiplier 2		
β	μ	σ	COV	μ	σ	COV	μ	σ	COV	μ	σ	COV
-1.00	0.46	0.09	0.19	0.80	0.19	0.23	1.18	0.30	0.25	1.56	0.40	0.26
-0.75	0.45	0.09	0.20	0.80	0.19	0.24	1.17	0.31	0.26	1.54	0.42	0.27
-0.50	0.45	0.09	0.20	0.81	0.21	0.26	1.20	0.33	0.27	1.60	0.44	0.27
-0.25	0.45	0.09	0.20	0.82	0.22	0.26	1.24	0.34	0.27	1.66	0.46	0.28
0.00	0.45	0.09	0.21	0.83	0.23	0.27	1.29	0.37	0.29	1.77	0.51	0.29
0.25	0.45	0.10	0.21	0.87	0.25	0.28	1.36	0.41	0.30	1.88	0.57	0.31
0.50	0.46	0.10	0.21	0.90	0.28	0.30	1.44	0.47	0.33	2.02	0.67	0.33
0.75	0.46	0.10	0.22	0.94	0.31	0.33	1.54	0.55	0.35	2.19	0.79	0.36
1.00	0.46	0.10	0.22	0.98	0.35	0.35	1.65	0.63	0.38	2.40	0.98	0.41
Normalized Residual Displacement (Δ_{res}/Δ_d)												
	EQ Multiplier 0.5			EQ Multiplier 1			EQ Multiplier1.5			EQ Multiplier 2		
β	μ	σ	COV	μ	σ	COV	μ	σ	COV	μ	σ	COV
-1.00	0.67	0.29	0.43	0.76	0.22	0.30	0.77	0.22	0.29	0.78	0.21	0.27
-0.75	0.59	0.28	0.48	0.57	0.29	0.52	0.57	0.28	0.50	0.57	0.28	0.50
-0.50	0.48	0.27	0.56	0.42	0.26	0.61	0.39	0.28	0.72	0.39	0.28	0.72
-0.25	0.36	0.26	0.72	0.35	0.23	0.67	0.30	0.23	0.77	0.28	0.22	0.80
0.00	0.29	0.24	0.84	0.25	0.20	0.81	0.18	0.17	0.94	0.18	0.17	0.98
0.25	0.26	0.22	0.86	0.17	0.13	0.79	0.14	0.17	1.21	0.13	0.14	1.13
0.50	0.25	0.21	0.84	0.12	0.14	1.18	0.10	0.11	1.07	0.07	0.08	1.16
0.75	0.23	0.20	0.88	0.10	0.11	1.07	0.07	0.09	1.26	0.05	0.06	1.11
1.00	0.20	0.18	0.91	0.08	0.08	1.02	0.05	0.05	1.05	0.04	0.05	1.18

aftershock the FP could rely on its full displacement capacity. However, the β = -1.0 VFS could also rely on nontrivial residual capacity, namely 0.43 m, which may be sufficient to absorb the effects of potential aftershocks.

It is now assumed that the same two systems are hit by a more intense event. Considering an EQ Multiplier equal to 2.0, the displacement demand on the FP would grow to 1.3 m which is well beyond the maximum capacity of the device, designed for a more frequent event (Δ_{max} = 0.85 m). In contrast, the demand on the β = -1.0 VFS would only correspond to 0.7 m, which could be easily absorbed by the device. The VFS would also be left with a 0.3 m displacement capacity following the event, which may be sufficient to protect the structure against secondary events.

This example was presented with the intent of pointing out that the real issue that should be addressed is being able to predict what residual displacement should be expected for the various base isolation systems, rather than blindly trying to limit its value sacrificing the overall performance in terms of other parameters.

To this end, it is interesting to note that the normalized residual displacement appears to be somewhat independent of the earthquake intensity, particularly for EQ multipliers greater or equal to 1.0 (Figure 4.2 (c)). The normalized residual displacement can then be represented in a more convenient way solely as a function of β, as shown in Figure 4.3. This kind of graphs could be used to link the design displacement to the residual displacement so as to explicitly consider this important parameter over the course of the design phases.

This information, in combination with the knowledge of the demand imposed by potential aftershocks and secondary events, would permit to establish whether a certain value of residual displacement is acceptable. Designing for a target residual displacement in addition to maximum displacement, force, and acceleration would consent a more rational design and a more complete control over the response of the systems, ultimately leading to the possibility of selecting the optimal device for the desired performance.

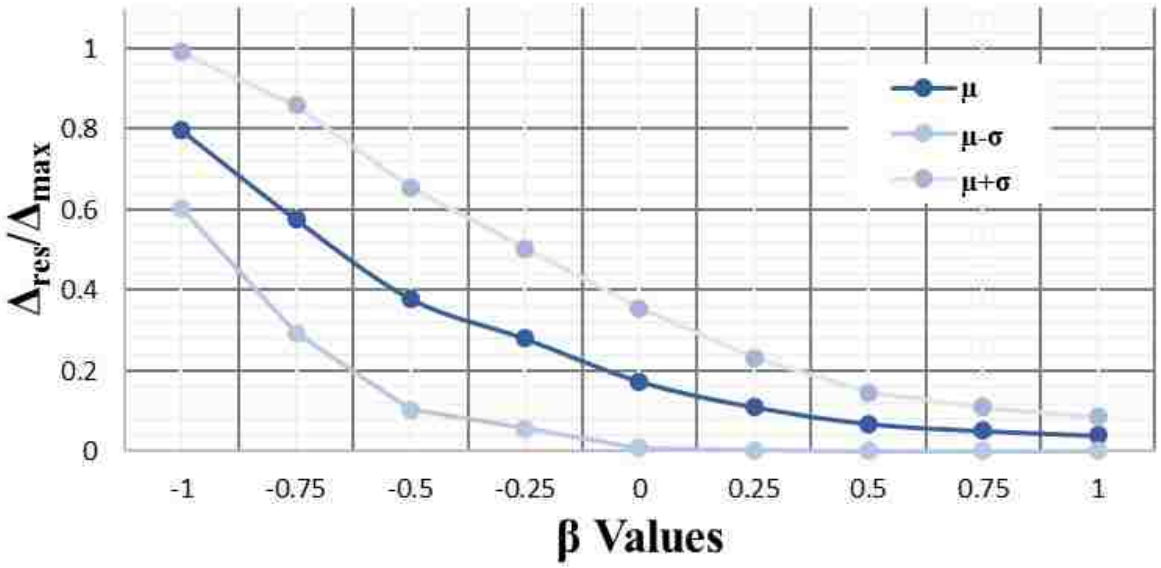

Figure 4.3: normalized residual displacement for EQ intensity =1

4.1.2 Flexible SDOF Structures

The response of the "flexible" case study structures (see section 3.1.3) under the design earthquake (PGA of 0.591g) is examined in this section. Figure 4.4 shows the response of all systems in terms of peak accelerations (representative of peak lateral forces as well), peak displacements, and residual displacements. Figure 4.4 (a) shows the results pertaining to case study "Flexible 3" with damping ratio of 5%, keeping the results separated as a function of the radius of curvature of the "target" FP systems (2.5 m, 3.1 m, and 3.7 m).

Analogously to what observed for "Rigid" SDOF structures, a larger value of R (which corresponds to a flatter device) makes for systems that attract lower accelerations and forces, but higher peak and residual displacements. For instance, considering the FP system, the displacement demand grows by approximately 15% going from a system with R =3.7 m to a system with R = 2.5 m. However, considering the same two systems, the acceleration varies only by about 0.05%. This suggests that R has a greater influence on displacements than on forces and accelerations.

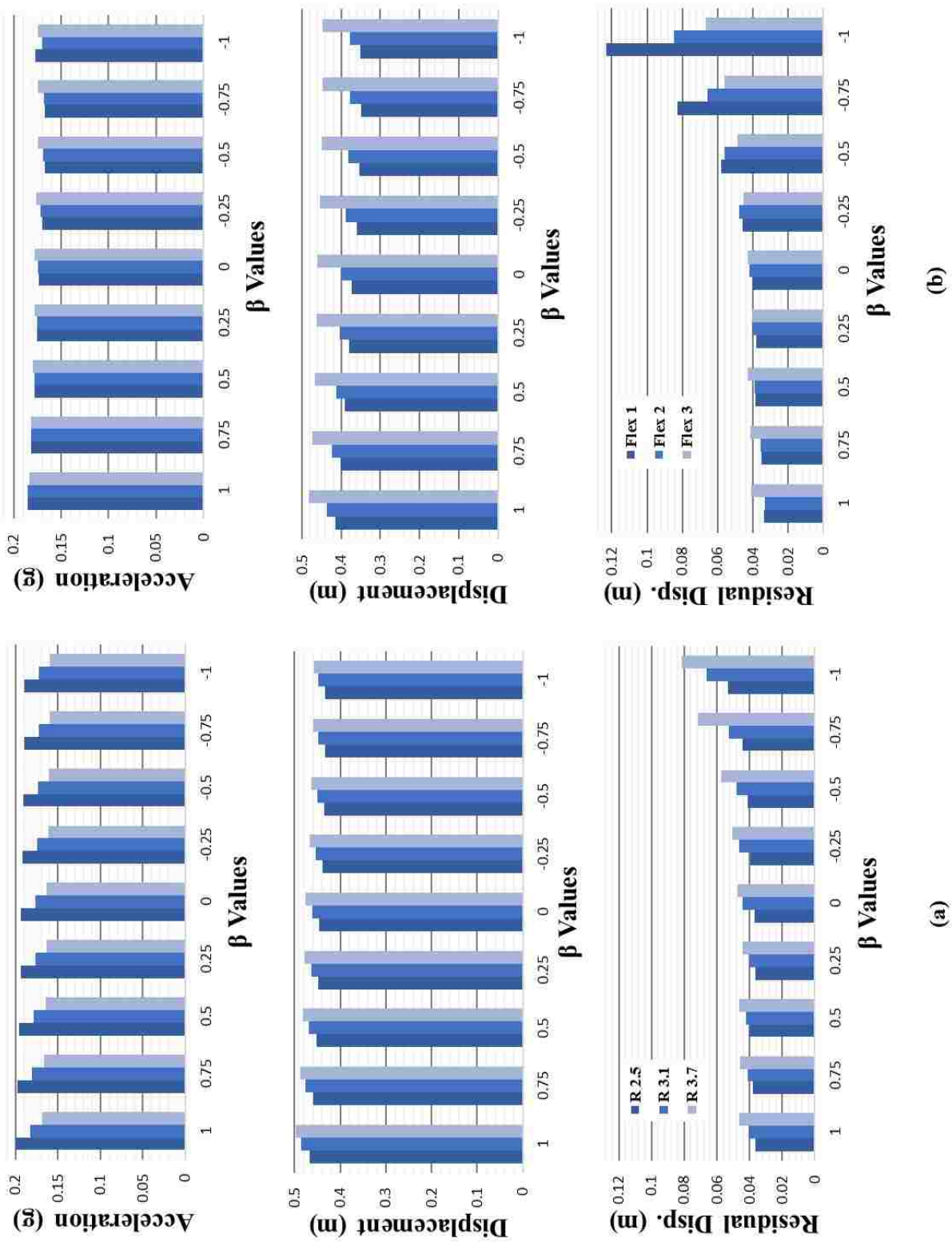

Figure 4.4: Response of different β systems: (a) for different R values for Flexible 3 structures with 5% damping ratio, (b) for all flexible structures with 5% damping

Figure 4.4 (b) shows response of all structures in terms of the key parameters, separating the results in terms of the superstructures flexibility. Only structures with a 5% damping ratio are considered, since the trend is similar for structures with 2%. In this case, the variable R is eliminated by averaging the results pertaining to the different R values. The structures' flexibility does not appear to have a significant influence on peak displacements. Overall, case study "Flexible 3" experiences the highest displacements across all β values, while "Flexible 1" experiences the lowest displacements. This trend is somewhat different with respect to residual displacements. More specifically, "Flexible 3" structures are characterized by the highest residual displacements at positive β values, while "Flexible 1" have higher residual displacements at negative β values. This may suggest that, in these respects, softer structures work better with VFS with negative β, and vice versa. This trends appear reversed, if accelerations are considered.

The effects of assigning different viscous damping ratios to the case study structures can be examined closely from Figure 4.5. As expected, the overall seismic demand is lower on the structures with higher damping ratio. With reference to case study "Flexible 3", it can be seen in Figure 4.5 that increasing the damping ratio by 3% reduces the acceleration demand by approximately 5%, and the peak displacement by about 8%. The residual displacement is reduced by approximately 15%.

Analogously to what done for "Rigid" SDOF structures, the effect of varying earthquake intensity was studied for flexible structures and summarized in Figure 4.6. The results are separated as a function of the assigned viscous damping ratio. The results have been normalized as discussed earlier for "Rigid" systems.

It can be seen that, in general, the normalized lateral force and the normalized displacement follow analogous trends that is they steadily increase with increasing earthquake intensity. The demands tend to grow as the value of β grows. Similar results were seen earlier for the "Rigid" SDOF systems, but the demands appear to be lower this time. As expected, the seismic demand decreases if the damping ratio is increased, while the demand increases if the earthquake intensity is increased.

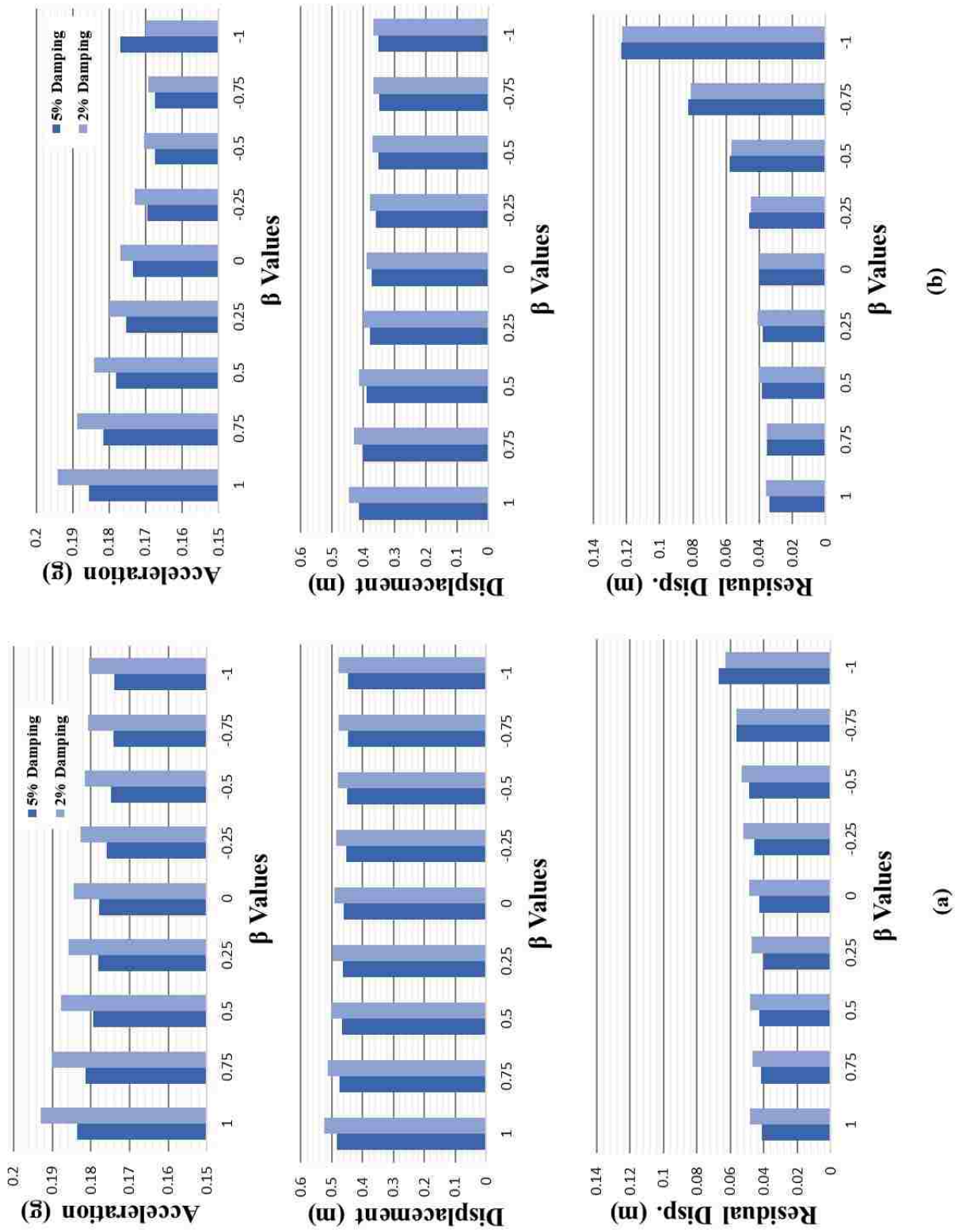

Figure 4.5: Response of different β systems for different damping ratios for (a) flexible 3 and (b) flexible 1 structures

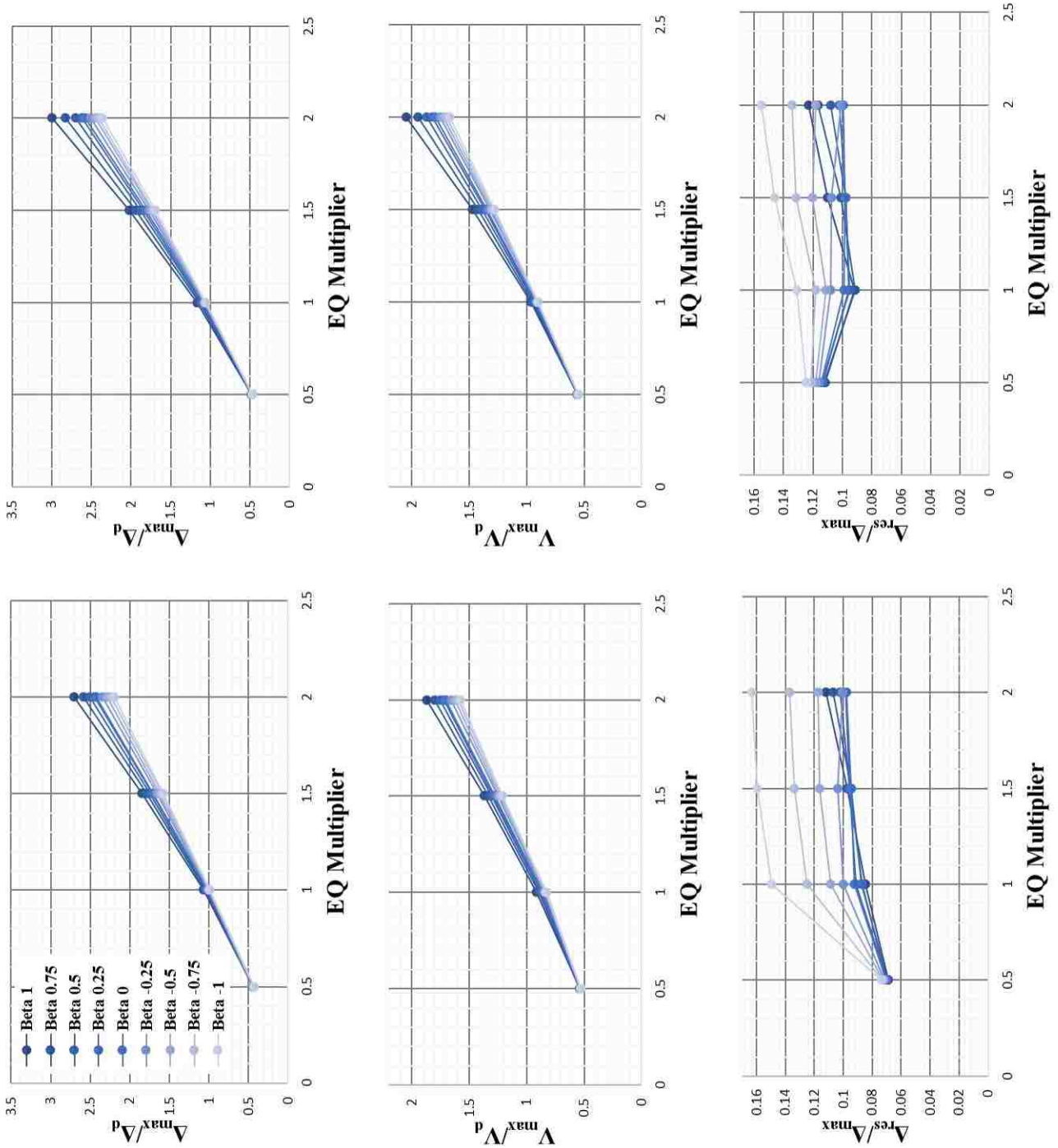

Figure 4.6: Normalized results for flexible structures for different EQ intensities in terms of displacements, lateral force, and residual displacement for (a) 5% aand (b) 2% damping ratio assigned respectively

It can further be noted that, at small earthquake intensities, the normalized residual displacement values for all β systems, are approximately the same, and is very low for 5% damped systems, while tends to spread out as damping is lower (figure 4.6 (a) and (b)). This may be attributed to the fact that VFS tends not to activate at small earthquake intensities, particularly if the systems possess high damping. As the earthquake intensity increases, the systems see an increase in the normalized residual displacement values (highest for β= -1 systems). As the intensity increases further, the data tends to stabilize at similar values for both the 2% and 5% damped systems. This implies that, for high intensity earthquakes, the beneficial effects that come from possessing higher viscous damping vanish, as the hysteretic damping term becomes predominant.

4.2 NLTH Analysis of Case Study Structures: Set B

As introduced, in addition to the case study structures presented in section 3.1.3, NLTH analyses are carried out in this phase of the work considering a new set of SDOF case study structures (Set B), whose design and fundamental properties are discussed below. The main objective of this chapter it to validate the design process for VFS, discussed in earlier chapters, while providing further insight into the dynamic behavior of VFS.

4.2.1 Case Study Structures (Set B)

The case study structures pertaining to set B were designed following the DDBD step by step procedure described in section 2.3.2. The newly proposed equation for calculating the EVD (Equation 3.13) was integrated in the design framework, while Equation 3.14 was used to estimate the design demand reduction factor η. All structures were designed under the following assumptions:

- The structures to be isolated are considered rigid, and characterized by a 0% damping ratio

- A constant vertical load of 6000 kN is applied on the isolators, and all load is taken by one isolator
- The bearing diameter is taken as 0.3 m for all systems
- The target displacement is taken as 0.3 m at the isolation layer
- The seismic input is represented by a linear displacement spectrum that is specified for 5% damping, that has a displacement of 1.45 m at period of 6 seconds (consistent with the spectrum shown earlier in Figure 3.2)
- The design-to-activation shear ratio (the coefficient α) for all devices is equal to 3 (which is a reasonable value for FP systems that are currently produced)
- The loading-to-re-centering stiffness of the devices (the coefficient β) is varied between -1.0 and 1.0 at intervals of 0.25.

Based on the outlined assumptions, 9 different base isolators were designed. The isolators have different hysteresis, but are expected to meet the same maximum displacement at the isolation layer. The design outcome is summarize in Tables 4.2 and 4.3, while the force-displacement curves associated with the various systems are shown in Figure 4.7. It can be seen that given a certain displacement demand, devices with lower β are characterized by greater equivalent damping, lower design and activation shear forces and larger radius of curvature. The implications of these aspects will be discussed later, with the results of the numerical analyses.

From a practical standpoint, to accommodate the displacement demand and taking into account the size of the bearing, the FP system ($\beta = 1.0$) was made of a single sliding surface with a diameter of 0.9 m. For the VFS, the design requirements listed in Table 4.2 can

Table 4.2: Structural design properties from DDBD (Set B)

β	ξ_{eq}	η	Δ at 6s (m)	T_{eff} (s)	K_{eff} (kN/m)	V_d (kN)	V_μ (kN)	μ_1 (%)	K_p (kN/m)	K_μ (kN/m)	R (m)
1	25.22%	0.51	0.74	2.45	4029.33	1208.80	402.93	6.7	2686.22	0.00	2.23
0.75	26.12%	0.50	0.72	2.49	3900.01	1170.00	390.00	6.5	2600.01	325.00	2.64
0.5	27.03%	0.49	0.71	2.53	3778.74	1133.62	377.87	6.3	2519.16	629.79	3.18
0.25	27.93%	0.48	0.70	2.57	3664.78	1099.43	366.48	6.1	2443.18	916.19	3.93
0	28.83%	0.48	0.69	2.61	3557.49	1067.25	355.75	5.9	2371.66	1185.83	5.06
-0.25	29.73%	0.47	0.68	2.64	3456.31	1036.89	345.63	5.8	2304.20	1440.13	6.94
-0.5	30.64%	0.46	0.67	2.68	3360.72	1008.22	336.07	5.6	2240.48	1680.36	10.71
-0.75	31.54%	0.46	0.66	2.72	3270.28	981.08	327.03	5.5	2180.18	1907.66	22.02
-1	32.44%	0.45	0.65	2.75	3184.57	955.37	318.46	5.3	2123.05	2123.05	∞

Table 4.3: Example design of set B structures

β	0.75	0.5	0.25	0.00	-0.25	-0.5	-0.75	-1.00
μ_1	6.5%	6.3%	6.1%	5.9%	5.8%	5.6%	5.5%	5.3%
μ_2	8.1%	9.4%	10.7%	11.9%	13.0%	14.0%	15.0%	15.9%

be met by arranging a series of sliding surfaces with 2 rings and diameters equal to 0.3 m and 0.9 m, respectively. In this geometric configuration, each ring needs to be assigned the friction coefficient values listed in Table 4.3. The constant radius of curvature to be assigned to the various systems is reported in the last column of Table 4.2.

It should be noted that constructibility or other practical considerations may limit the freedom in selecting a specific value of friction coefficient or radius of curvature. With this in mind, it was nonetheless assumed that systems characterized by the exact values that came out of the design process can in fact be realized, and were considered for the analyses.

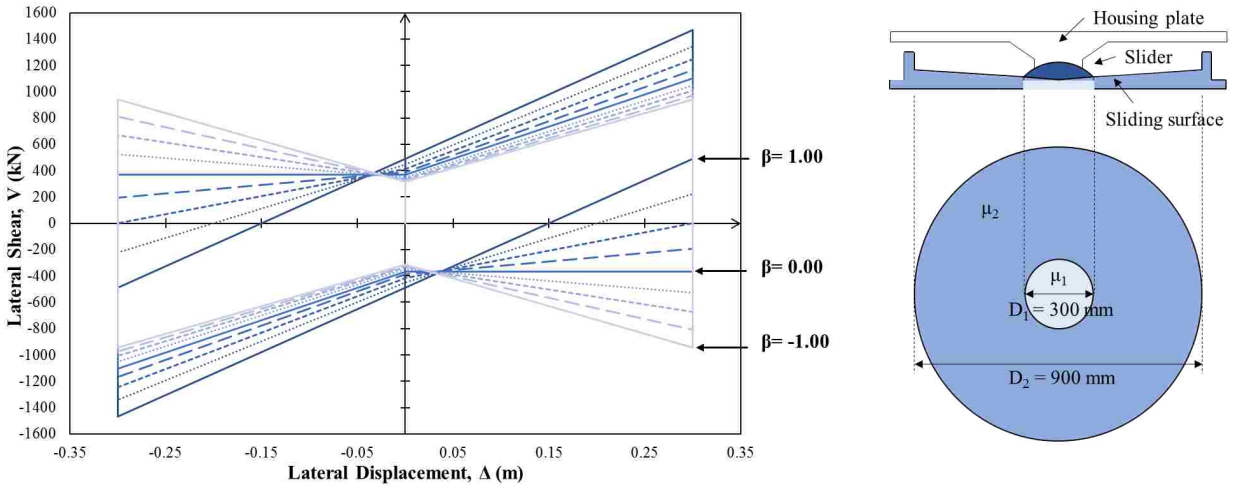

Figure 4.7: Force- displacement response of case study structure (left) and typical VFS isolator (right)

Note that the friction coefficient for the FP was found to be 6.7% across the sliding surface and a radius of curvature of 2.23 m (see Table 4.2), which is smaller than the radius of curvature of all the systems with smaller β values. It can be seen in Figure 4.7 that the VFS systems have an increasingly larger hysteresis for decreasing β value.

4.2.2 NLTH Analyses Results : Set B

The case study structures part of Set B were tested numerically, under the selected suite of ground motions, scaled to match the intensity of the design spectrum. The key results of the NLTHAs are summarized in Figure 4.8. Four parameters of interest are compared: maximum displacement, residual displacement, maximum lateral force and maximum acceleration, As a result of the application of 50 distinct ground motions, a range of outputs are obtained for each case study system. The bar graphs show the average value over all 50 time histories, while the error bars show the maximum and minimum values.

The first observation that can be made is that, on average, the maximum displacement experienced by the isolators is reasonably close to the design displacement (i.e. 0.3 m),

suggesting that the design method outlined in section 2.2.2 represents a reasonable design approach. It can be seen in Figure 4.8(a) that the average maximum displacement reached by the system characterized by β = -1.0 is about 5% higher than the target displacement while the FP system (β = 1.0) undergoes a displacement of 0.28 m, which is about 7% lower than the target value. These discrepancies are considered reasonable on account of the uncertainties related to the input, represented by 50 ground motions that impose very different demands on the systems and mimic the target spectrum only on average.

It is interesting to notice that even though the maximum displacement reached by the various systems is uniform on average, there seems to be a greater spread of results as the value of β turns from negative to positive. For instance, while the maximum displacement achieved by a system with β = -1.0 ranges from 0.13 m to 0.53 m, an FP system (β = 1.0) spans displacements from 0.07 to 0.67 m.

It is evident from Figure 4.8 (b) that the systems residual displacement tends to decrease as the value of β turns from negative to positive, with the system characterized by β = -1.0 being the worst and the FP being the best performing system. This suggests that systems with a low value of β may have problems in case of strong aftershocks as their displacement capacity may be significantly reduced at the end of the main event. The scatter of the results also tends to be greater for systems with negative β. Further discussion on the systems performance in terms of residual displacement will be provided below.

Figures 4.8 (c) and (d) show that lateral forces and accelerations attracted by the systems grow with the magnitude of β. As expected, lowering β provides better protection in terms of these two parameters. As β decreases, the average demand as well as the scatter of the results tend to decrease. For instance, the maximum lateral force on a flat VFS is 980 kN while an FP system is subjected to 1,400 kN. In this context, a hypothetical structure protected by means of an FP system would need to be 40% stronger than what would be necessary in the case of a flat VFS. The lateral accelerations follow an analogous trend (Forces and accelerations are closely related via the mass of the system), which means that a flat VFS could be more effective at protecting non-structural elements and contents.

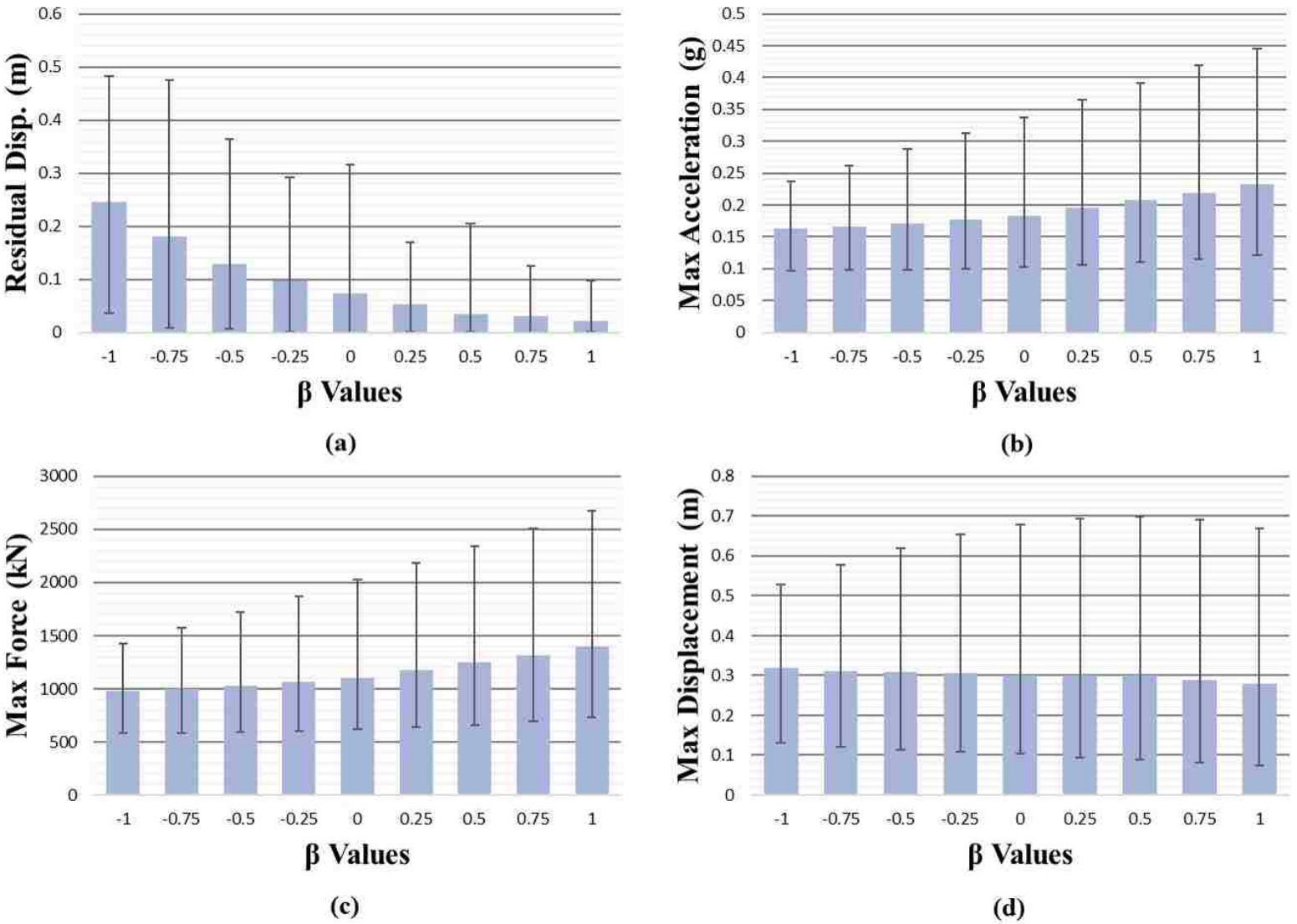

Figure 4.8: Case study B structures results of NLTHA in terms of (a) maximum displacements, (b) residual displacements, (c) maximum lateral forces, and (d) maximum accelerations

Overall, the results outlined in Figure 4.8 confirm that VFS may have the potential to outperform single-valued friction systems designed for the same target displacement with respect to certain response parameters, and that increasing the energy absorption capabilities of the devices (by lowering the value of β), has beneficial effects as it limits the forces and the accelerations transferred to the superstructure.

The price for this enhanced protection is paid in terms of residual displacement, which, as already discussed, tends to be greater for systems with low β values. This may jeopardize the response of the systems in case of severe aftershocks. However, suitable solutions may be found adopting systems with intermediate values of β. For instance, for the case analyzed, a system with β= 0 may provide adequate protection of the isolated structure while simultaneously limiting the residual displacement to acceptable values, leaving room to absorb the effects of potential secondary events (see the discussion presented in Section 4.1).

In addition to the issue of the residual displacement, there is another important aspect of the response of VFS that has been already pointed out, but needs to be further emphasized, that is the tendency of systems characterized by low values of β to experience a non-symmetric response. This can be seen in Figure 3.16, which shows the force-displacement response of some of the systems analyzed to one of the ground motions. While the systems with positive β undergo analogous maximum and minimum displacements, completing a large number of vibration cycles, the systems with negative β, and particularly the system with β = -1.0, tend to drift mainly toward the positive side of the graph. However, despite its non-symmetric response, the system with β = -0.25 behaves substantially better than its β= -1.0 counterpart as, while the latter gradually drifts away from the zero position, the former ultimately returns to the center, limiting the residual displacement to 0.06 m.

Furthermore, likewise its positive β counterparts, the system with β = -0.25 undergoes a large number of vibration cycles. In contrast, the system with β = -1.0 essentially stops vibrating after completing a few cycles. The reason for this undesirable response lies in the fact that the lower the value of β, the greater is the lateral force that needs to be generated in order to initiate the reversed motion of the system.

4.3 Conclusions

This section has studied response of rigid and flexible SDOF structures that use VFS characterized by a wide range of values. Based on the results of the analyses, a number of conclusions can be drawn about the performance of VFS as a function of a number of parameters.

For example, it was shown that decreasing the value of the design parameter β may have beneficial effects and reduce the seismic demand on the system in terms of peak displacement, acceleration, and lateral force. However, it was also shown that decreasing the value of β tends to produce systems characterized by higher residual displacement, at the end of an earthquake. Particularly critical in this regard are systems with β = -1.0, for which the residual displacement is on average around 80% of the maximum displacement reached.

Although this may represent a significant drawback, pertaining to certain situations, it has been discussed that systems with poor re-centering capabilities may still be employed to achieve high overall seismic performance.

Analogously, increasing the radius of curvature of the sliding surface contributes to bringing down the overall demands on the structures, while decreasing the re-centering capacity. However, the observed changes are not significant across the three realistic values of R considered.

Effects of the flexibility and of the damping values of the superstructures on the isolators performance were also examined. As expected, increasing the viscous damping ratio assigned to the structure decreases the overall demand on the structure-isolator assembly, without really affecting the performance of the isolator in any way. Analogously, the performance of the base isolators is not affected by the dynamic properties of the supported structure (while the performance of the overall system is obviously influenced by this parameter).

Chapter 5

PERFORMANCE OF VARIABLE FRICTION BASE ISOLATED MDOF SYSTEMS

Chapter 3 and 4 have studied some important aspects of the behavior of VFS, providing insight into their damping properties and seismic performance for SDOF structures. However, only SDOF case study structures have been considered thus far. While studying this type of systems is very useful in that a number of key aspects of the response of the base isolation devices can be isolated and studied, there are some key parameters that are neglected, and their effects are inevitably missed. For instance, real structures are characterized by a number of degrees of freedom that may be high or low, but certainly greater than one. Transitioning from SDOF to MDOF (Multiple-Degree of Freedom) structures clearly adds some complications to the problem in terms of design, modeling, analysis, and interpretation of the results. However, it also contributes to providing a more realistic expectation of the performance of the base isolation systems, and in particular, of the newly proposed VFS. While a thorough investigation on the response of "real structures" base isolated via VFS is beyond the scope of the present study, some preliminary steps are made in this sense in this chapter.

To this end 3 MDOF case study structures are designed, modeled and analyzed in the following section. While the numerical models of the structures were kept very simple, and the number of analyses conducted was somewhat limited, the results presented in this chapter provide some preliminary understanding of the implications of employing VFS to base isolate MDOF systems, particularly with respect to the effects of the higher modes of vibration.

5.1 Case Study Structures

This section describes the case study structures utilized for the numerical study. The first step of the process, consisted in designing three "target" MDOF structures, base isolated by means of traditional FP systems. The design of these structures was performed using the DDBD process, as described in 2.3. Structures with 4, 8, and 12 stories were considered. The fundamental properties of the structures and the design parameters were as follows:

- The mass of each floor was 880 tonnes (this was computed assuming buildings with a symmetrical 30 x 30 m plan). The mass was assumed to be the same for all floors (including the roof)
- A 0.2% design drift ratio was selected for all structures (the low value was selected to guarantee that all systems would respond elastically to the design earthquake)
- A viscous damping ratio of 5% was assumed for all structures
- The design displacement spectrum specified was represented by the curve reported in Figure 5.1

The fundamental design properties selected for the FP systems were as follows:

- The design displacement of all isolators was 0.45 m
- The design parameter α was taken as 3.0
- The target pressure on each bearing was 70 MPa
- As a consequence of the target pressure, the bearing radii were: 0.15 m (for the 4 story structure), 0.175 m (for the 8 story structure) and 0.2 m (for the 12 story structure)
- A total of 13 bearings were used to isolate each case study structure.

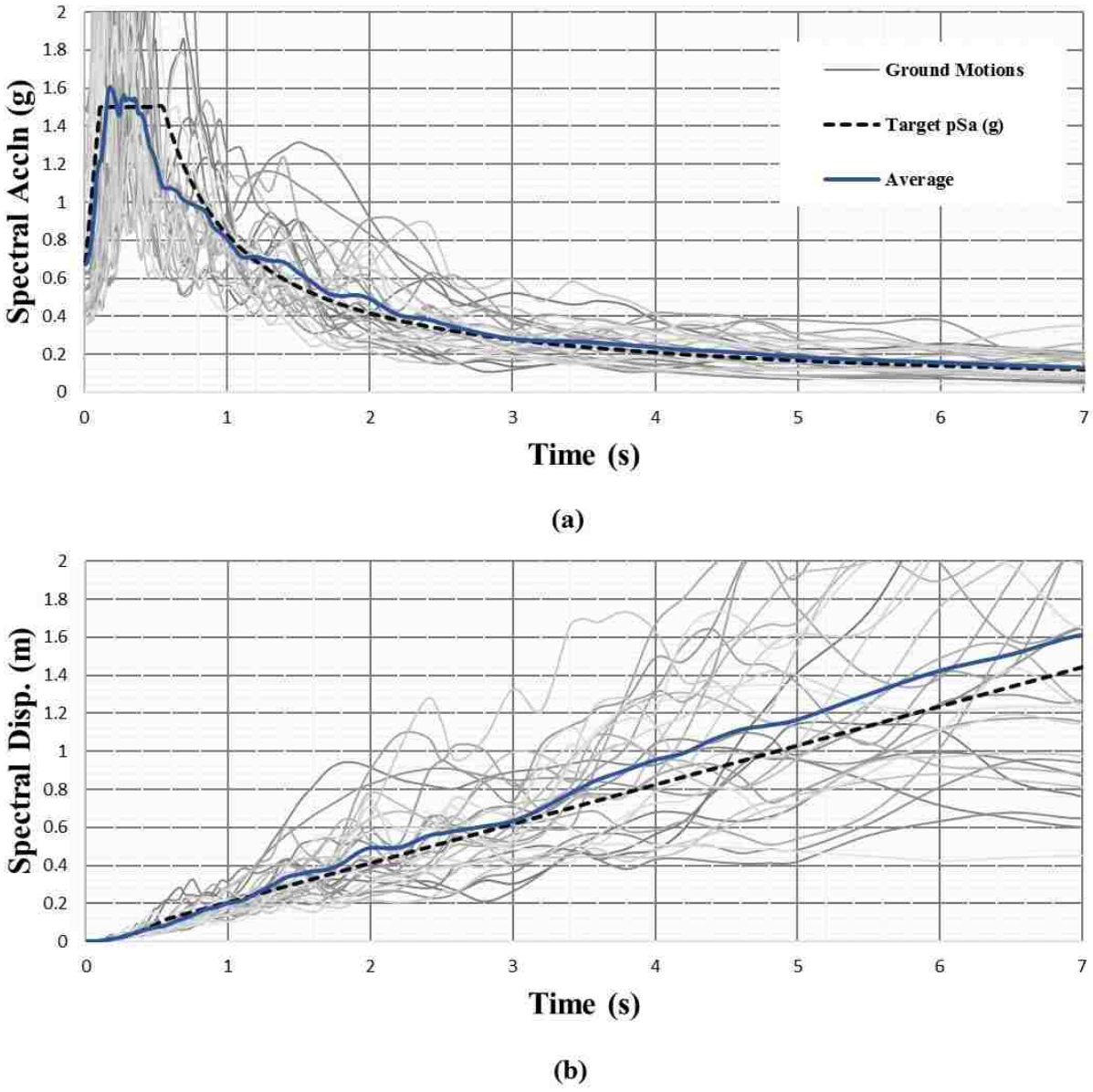

Figure 5.1: Acceleration (a) and displacement (b) spectra for 30 selected ground motions

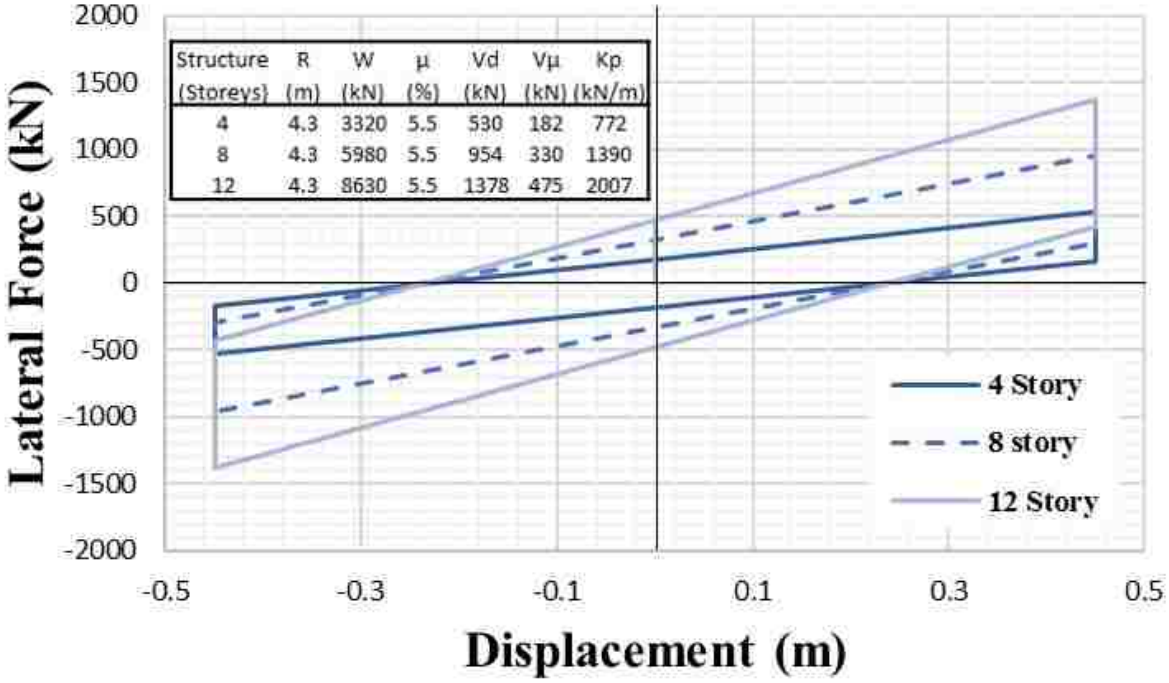

Figure 5.2: Force-displacement response of selected FP systems with fundamental property values

The step by step design process for base isolated structures described in section 2.3.2, combined with the design parameters listed above, led to the design of FP devices with characteristics summarized in Figure 5.2 (with R = 4.3 m and $\mu = 0.055$), and to the case study structures with the floor stiffness values listed in Table 5.1. Note, that the case study buildings were modeled as "shear-type" systems: the masses, allowed exclusively to translate in the x-direction, were lumped at each floor, and were connected through linear springs (with stiffness calibrated to represent all the elements contributing to resisting the applied lateral loads at a given level).

At this point, a total of 12 VFS, characterized by β values ranging from -1.0 to 0.5 (at 0.5 intervals), were designed to mimic the response of the target FP systems described

Table 5.1: MDOF structures: stiffness properties

Story	Stiffness of each story (kN/m)											
	1	2	3	4	5	6	7	8	9	10	11	12
4	902089	680932	456864	229887								
8	1787383	1573796	1357399	1138192	916174	691346	463707	233259				
12	2655114	2448786	2239743	2027968	1813513	1596326	1376424	1153807	928475	700428	469667	236191

Table 5.2: MDOF structures frictional properties

β	0.5	0	-0.5	-1
μ_1	5.50%	5.50%	5.50%	5.50%
μ_2	6.74%	7.97%	9.21%	10.44%
μ_3	7.46%	9.42%	11.39%	13.35%
μ_4	8.26%	11.02%	13.78%	16.55%
R	5.73	8.60	17.20	∞

above (analogously to what done in section 4.1 for SDOF case study structures). Thus, the properties of the VFS were computed to guarantee that the backbone of the hysteretic curve characterizing the force-displacement response of each VFS traced that of the FP system companions shown in Figure 5.3 for (a) 4, (b) 8, and (c) 12 story designed structures. For all VFS, the properties of the isolated structures are those discussed pertaining to the FP systems. The outcome of the design of the VFS (performed in line with the discussion presented in section 2.3.2), is summarized in Figure 5.3 and in Table 5.2. Note that only friction design for a 4 story structure is included, since it is similar to design of 8 and 12 story structures.

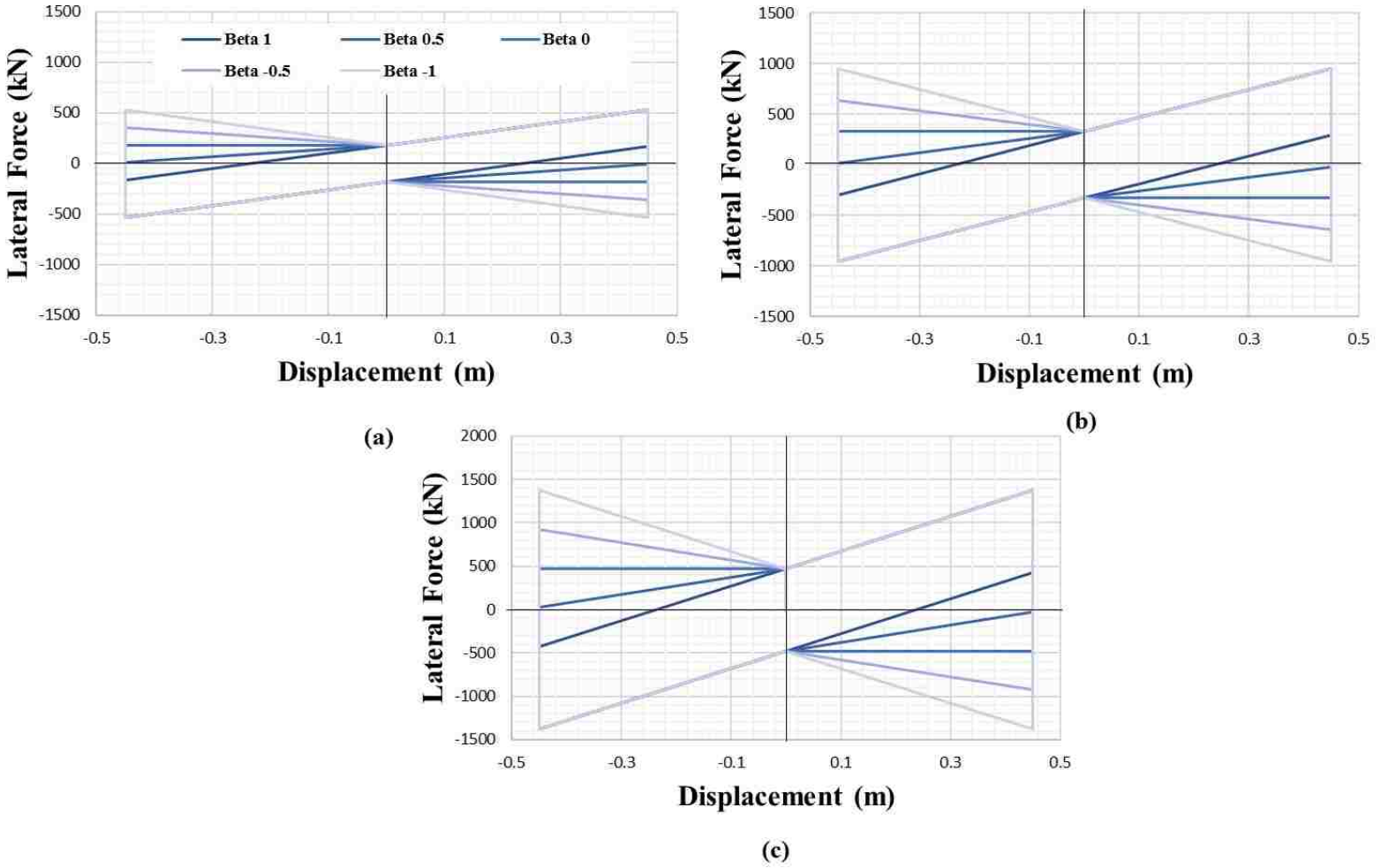

Figure 5.3: Force-displacement response of selected β systems for (a) 4 story, (b) 8 story, and (c) 12 story structures

5.2 Numerical Modeling

In order to conduct numerical testing of the base isolated structures described in the previous section, a customized computer program, coded in MATLAB [MathWorks, 2012] by Calvi and Ruggiero [2016] and adapted for this project, was employed. This program can compute the non-linear dynamic response of base isolated structures to base excitations by solving the incremental equation of motion using a linear acceleration Newmark-Beta integration algorithm [Newmark and Rosenblueth, 1971]. The program is ideal to perform the analysis of non-linear multiple degree of freedom "shear-type" structures, such as that idealized in Figure 5.4. The isolation system is simulated using a non-linear translational spring characterized by the appropriate relationship between lateral force and displacement. The hysteresis of this spring is defined as a function of the isolator selected, as discussed in chapter 2.2.2. The structure is idealized through a series of masses connected by translational springs that can be assigned linear or non-linear (elasto-plastic, with or without hardening) hysteretic behavior. In this context, the masses are lumped at the floor levels and are allowed to translate exclusively in the x-direction.

The damping matrix is obtained as a function of the tangent stiffness, assigning a low damping ratio to modes 1 and (n - 1), where n is the number of stories. This modeling choice is in line with the recommendations of Pant et al. [2013] and was driven by the fact that a traditional Rayleigh's model tends to produce unrealistically high damping of lower frequencies [Petrini et al., 2008] leading to overly optimistic predictions of the performance of base isolated structures [Ryan and Polanco, 2008].

The numerical simulations were run using a set of 30 real ground motions as input, scaled to match the design earthquake. The characteristics of all records were listed earlier in section 3.1.1, Table 3.1. the response spectra associated with each individual ground motion are shown in Figure 5.1, above. Note that only the first 30 ground motions from table 3.1 were considered for this study, and hence the spectral displacement was 1.43 m at 6 seconds.

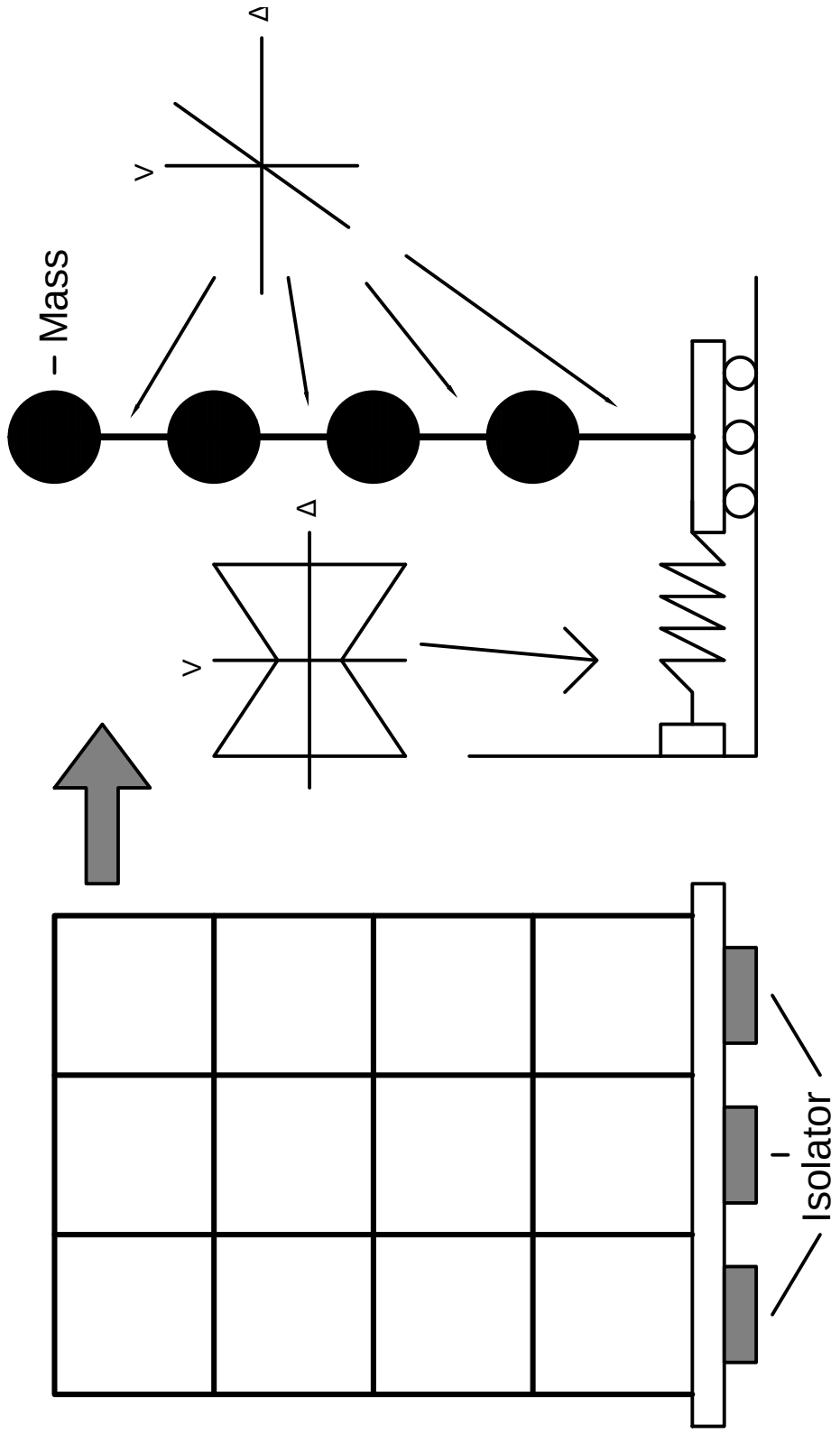

Figure 5.4: Schematic of structural model considered by NLTH program

5.3 NLTH Analysis Results

5.3.1 Verification of the MATLAB Code

To check the reliability of the customized program at simulating the response of MDOF base isolated structures, the 4-story case study structure, isolated via FP system, was modeled using the software RUAUMOKO 2-D and subjected to the set of input ground motions selected for the analyses. The same case study structure was analyzed through the customized program, and the outcomes of the two programs were collected and compared. The results of the analyses, expressed in terms of story shears and lateral displacements, are shown in Figure 5.5.

Comparisons of time history results for a selected ground motion (RSN 74) are also provided in Figure 5.6.

It can be seen that the results obtained from the two programs lie reasonably close, particularly with respect to lateral floor displacements (figure 5.6 (a)) compared to accelerations (b). However, despite the attempt of maintaining identical assumptions and similar modeling approaches across the two programs, minor discrepancies exist. These may be partly attributed to slightly different damping models used within the two programs, partly to the slightly different solving algorithms and partly to the somewhat different ways the base isolator response is simulated (figure 5.7). Obviously, the observed differences may be due to other issues, perhaps more relevant that those just pointed out, and this should be further investigated in the future.

However, the overall performance of the customized MATLAB program was deemed acceptable, particularly given the preliminary nature of the numerical study proposed in this chapter, and it was decided to go ahead with the analyses of all case study structures.

5.3.2 Discussion of the NLTH Analysis Resuts

As discussed with reference to SDOF systems, the key outcome parameters of interest are the maximum displacements, the peak accelerations, the inter-story shears and drifts and

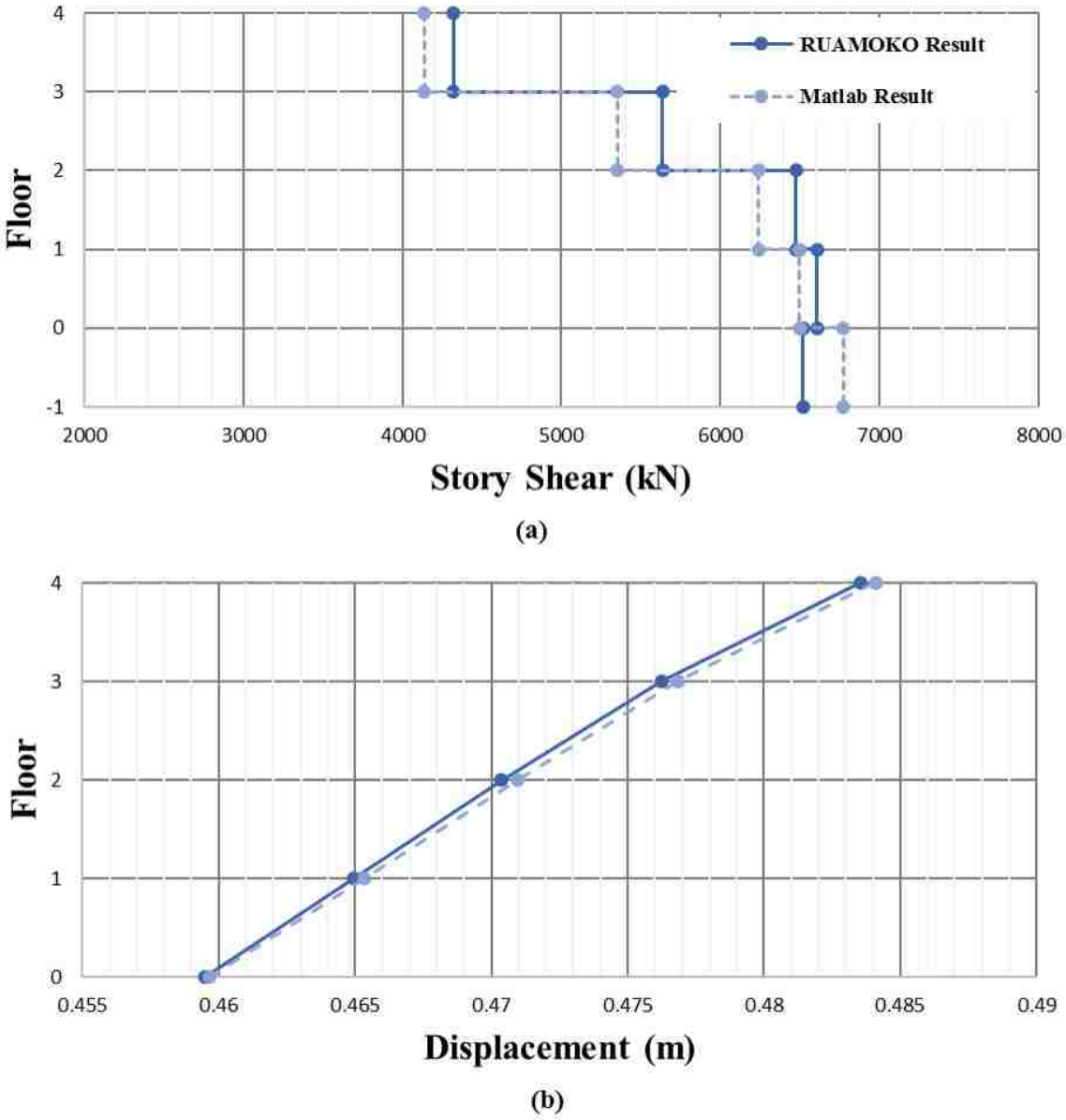

Figure 5.5: Story shear (a) and displacement (b) comparison from Ruaumoko and Matlab results

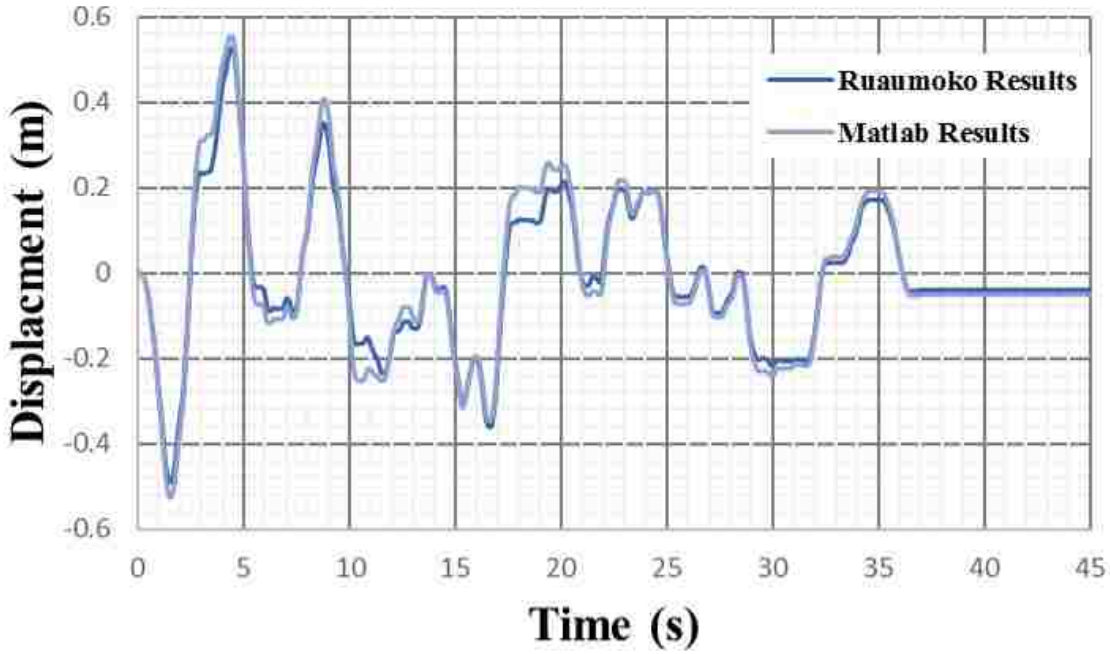

(a)

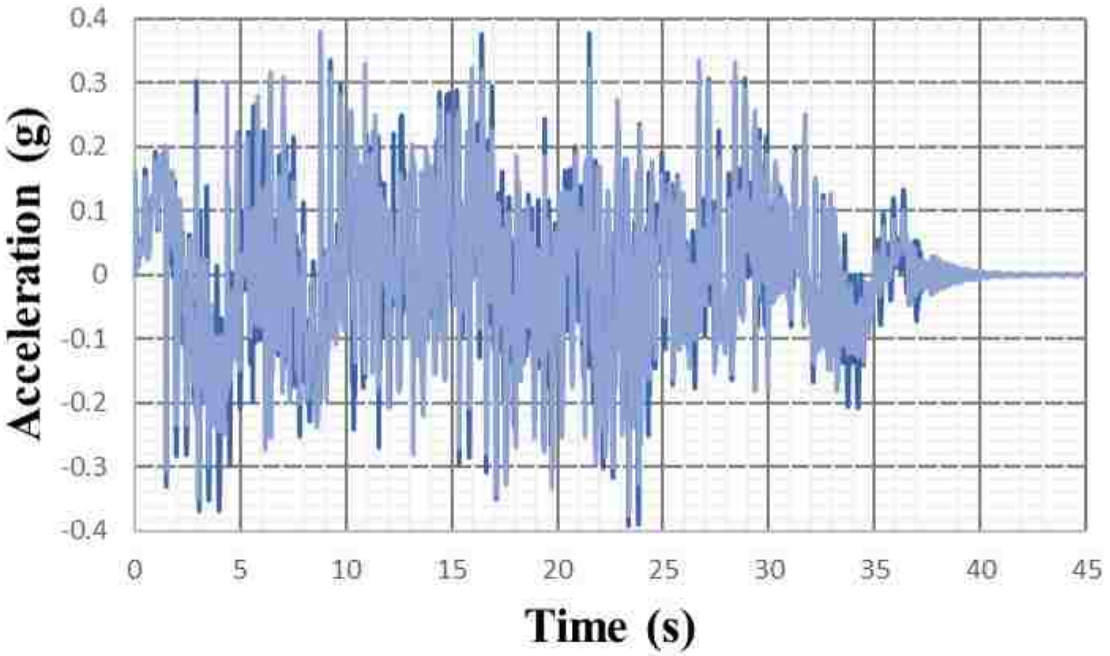

(b)

Figure 5.6: Displacement (a) and acceleration (b) time history for story 1 of a 4 story structure

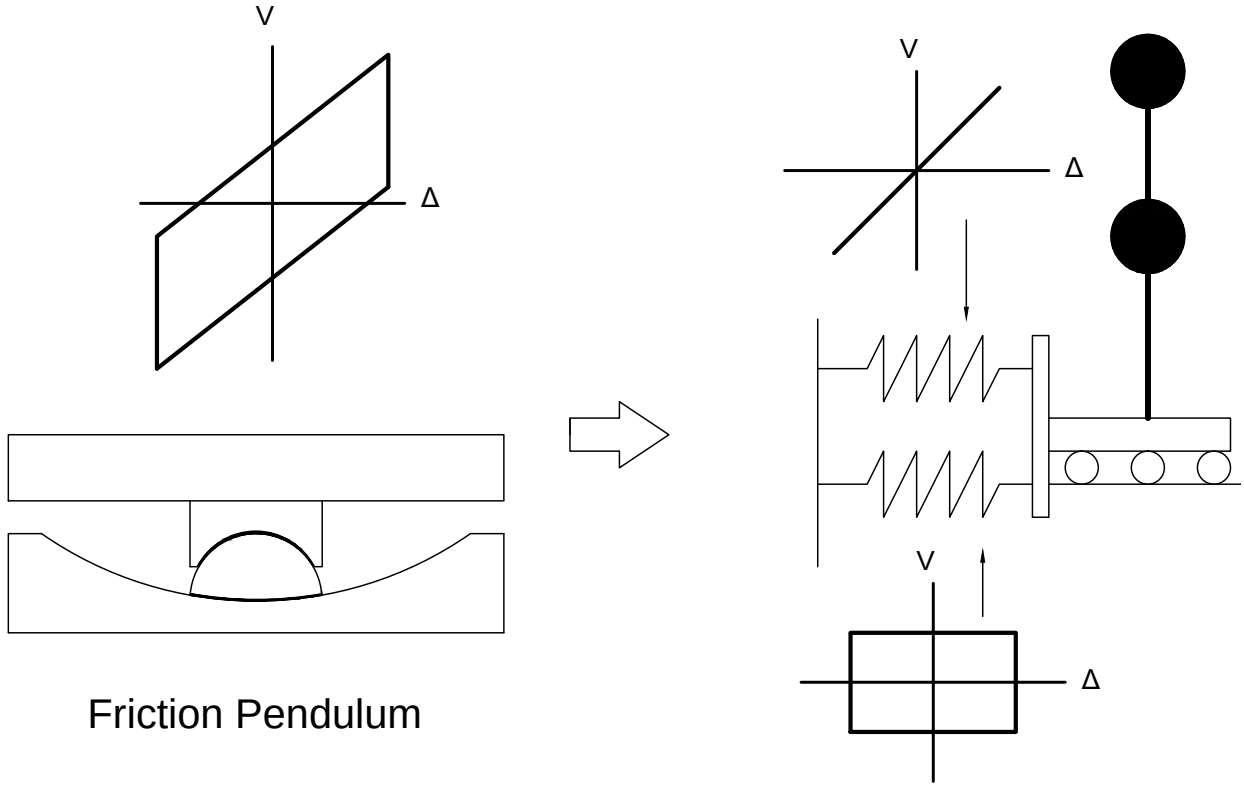

Figure 5.7: Simulation of FP for Ruaumoko

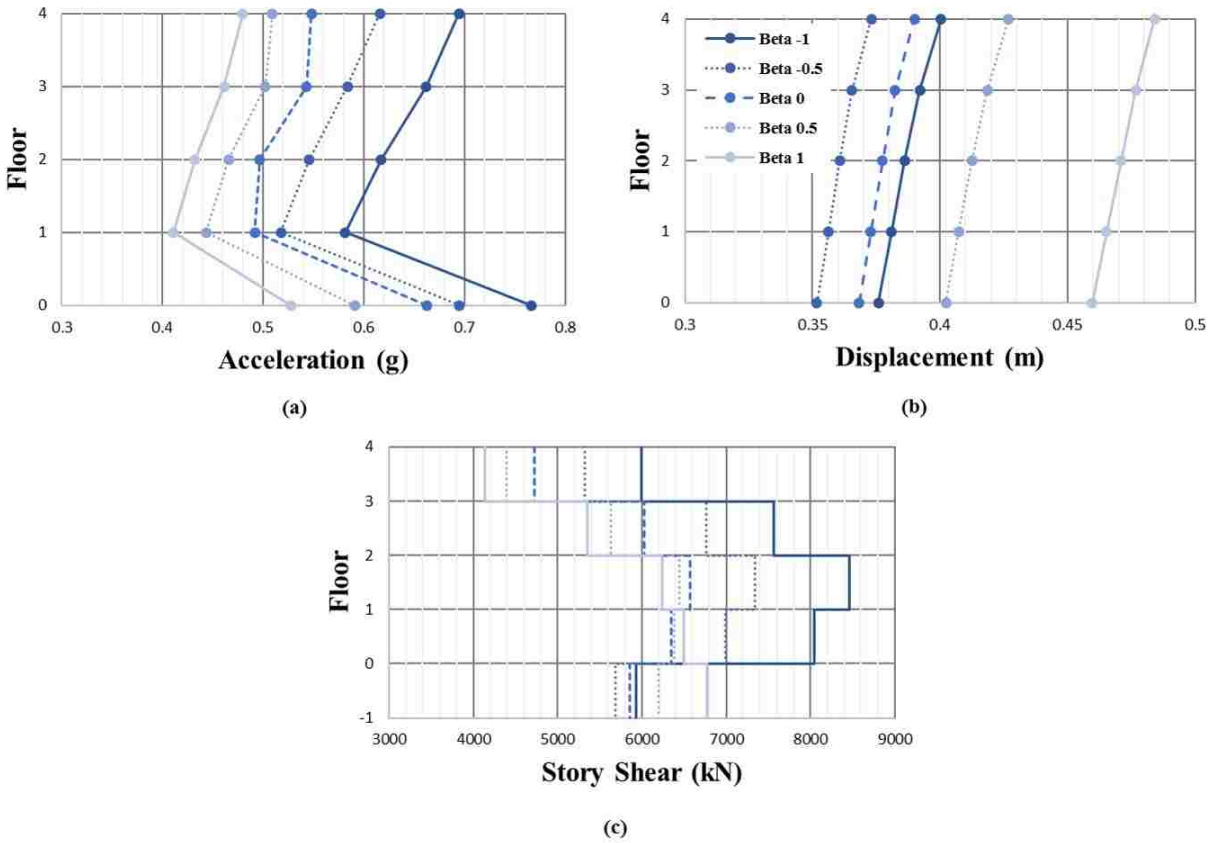

Figure 5.8: Response of a 4 story structure in terms of (a) acceleration, (b) maximum displacement, and (c) story shear

the residual displacements at the isolation layer. The NLTH analyses results pertaining to these parameters, are shown in Figure 5.8 , for the 4-story case study structure and all the base isolators considered.

Different conclusions can be drawn, with respect to different performance parameters. For instance, it can be seen in Figure 5.8 (a) that the peak floor accelerations (PFA) are higher at the ground level for all the devices considered. The PFAs drop in value at the first floor, and then increase, somewhat linearly, moving to the upper stories. It is interesting to note that, somewhat unexpectedly, the PFAs are lower for systems with higher β and vice versa. For instance, in a system with β = -1.0, the PFAs grow roughly by a factor of 1.5 with

respect to a system with $\beta = 1.0$. The higher than expected PFAs recorded can be attributed to the effects of the higher modes, which are clearly more pronounced for systems with low βs. This can be seen in Figure 5.8 (c), with reference to the inter-story shear profiles. While the systems with positive βs experience analogous response, and shear diagrams that are compatible (to different extents) with a linear distribution of lateral forces, the system with negative βs are characterized by shear force diagrams which clearly show the contribution of the higher modes of vibration. To this end, particularly critical is the system with β = -1.0, which experiences the highest shear forces. It should be noted that this observed trend is consistent with the mechanics of the different isolation devices. It was shown earlier (section 3.16), that a VFS with β = -1.0 tends to complete a low number of vibration cycles, responding to a seismic event, for the most part, in a locked position. When the base isolator locks, the base isolated structure no longer benefits of the presence of the device and feels the effects of the earthquake in full.

The benefit of lowering the value of β can be seen with reference to the displacement profiles shown in Figure 5.8 (b). While the displacements profile grows roughly linearly along the height of the structures, following analogous trends with respect to their base displacement, it can be seen that lowering the value of β has the beneficial effect of lowering the displacement demand at the isolation layer. However, it is interesting to notice that the lowest demand in this sense is on the systems with β = -0.5 and not on the VFS with β of -1.0, as one might expect.

Figure 5.9 (a) and (b) summarize the key results pertaining to the 8 and the 12 story structures. The trends are similar to those observed for the 4-story structure analyzed above. As reasonable to expect, the effects of the higher modes appear to be more pronounced as the case study structures grow in height. To this end, the performance of systems with β= -1.0 is further compromised, with the structures not only attracting high accelerations and inter-story shears, but also high displacements both along the height of the structure and at the isolation layer.

All the other systems, appear to provide analogous performance, doing slightly better or

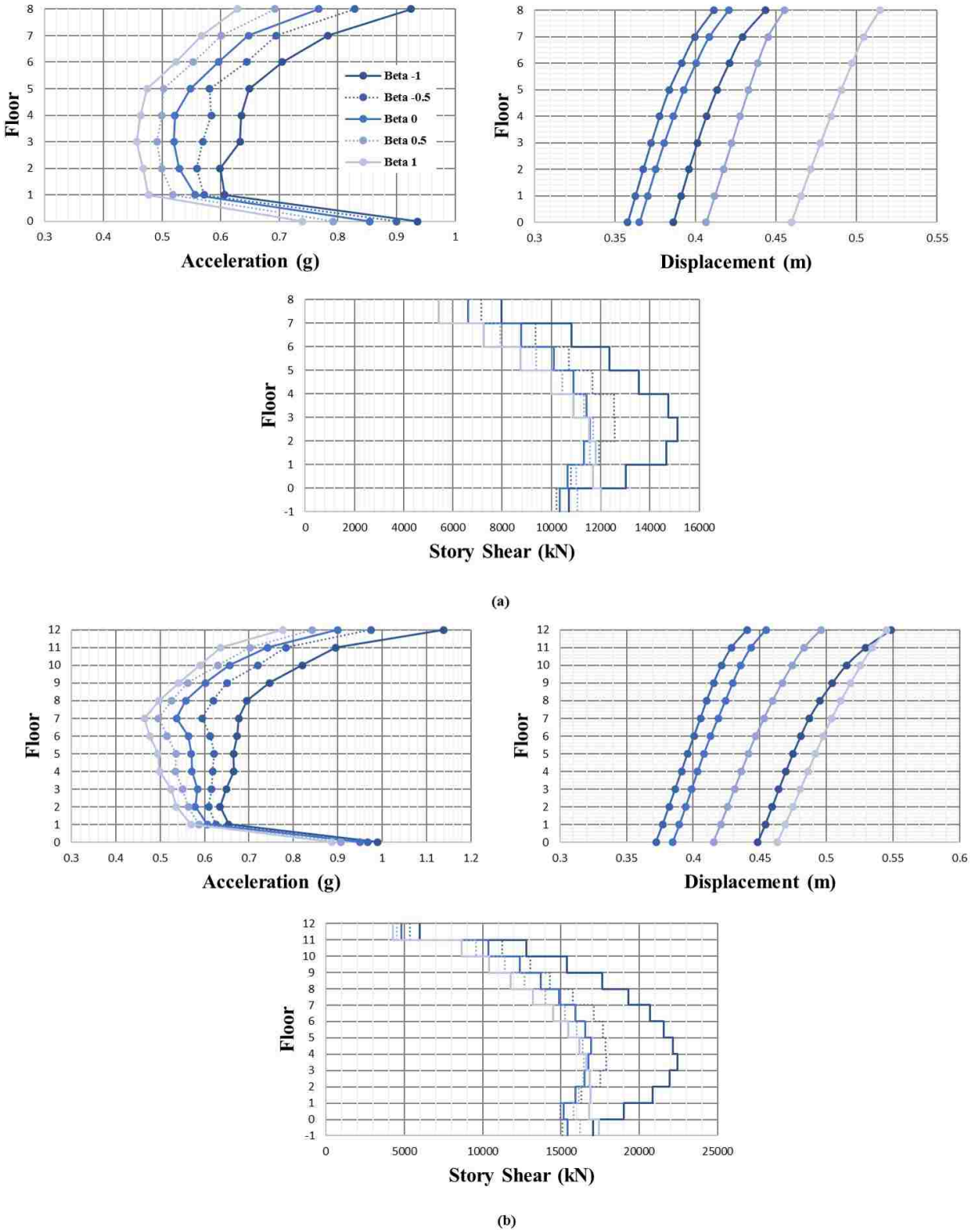

Figure 5.9: Response of (a) 8 and (b) 12 story structures in terms of acceleration, maximum displacement, and story shear

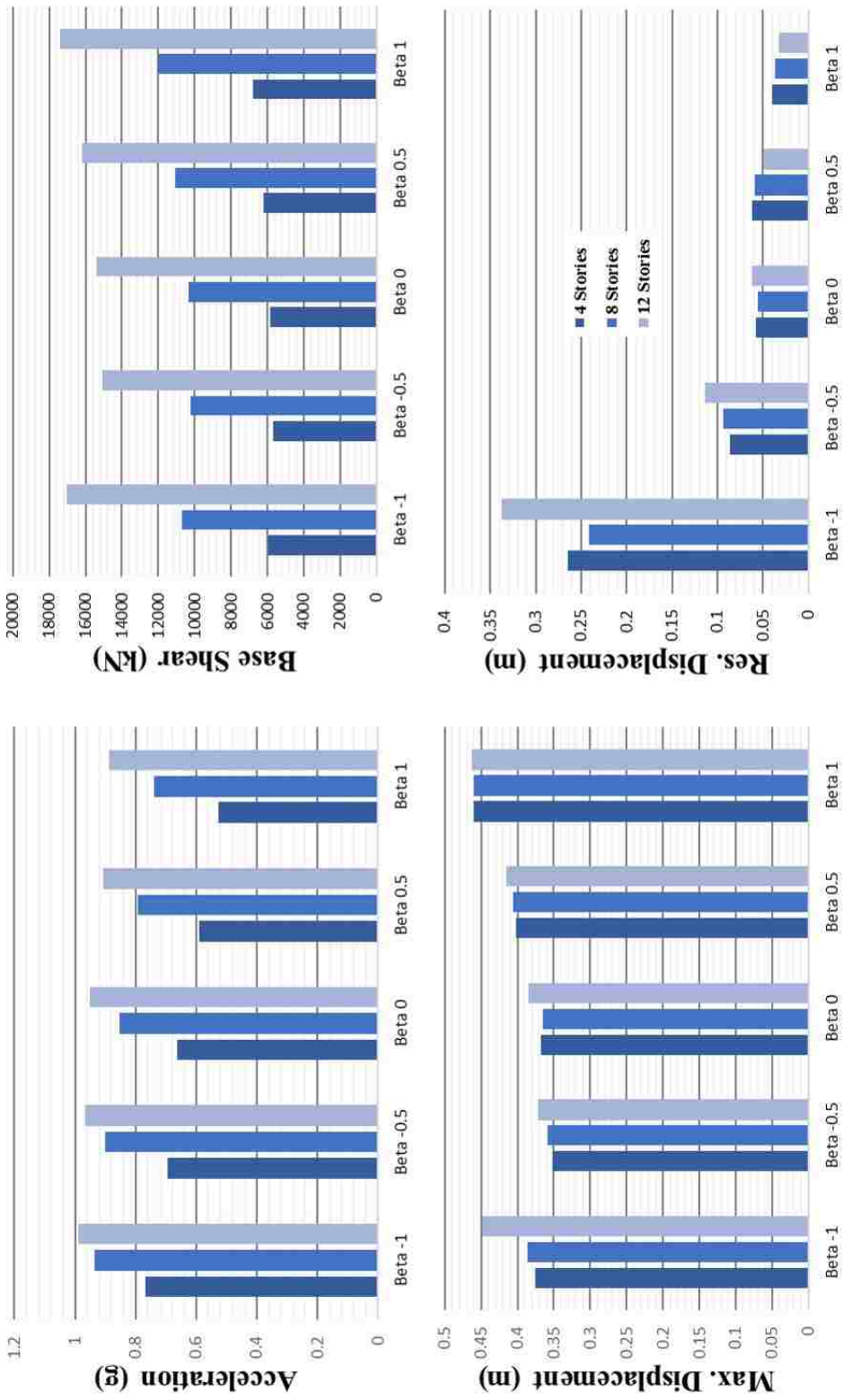

Figure 5.10: Response of a 4,8, and 12 structures in terms of base acceleration, base shear, base maximum displacement and residual displacement

slightly worse, depending on the parameters of interest.

To fully characterize the performance of VFS employed to protect MDOF structures, it is necessary to look closely at the seismic demand on the isolators. To this end, important parameters include peak acceleration (at the ground level), peak base shear, peak displacement and residual displacements. These results are shown in Figure 5.10 for all systems analyzed. It can be seen that the ground level accelerations tend to decrease with increasing βs, with peak values dropping from roughly 1.0 g, for the 12 story system with β = -1.0, to about 0.84 g, for the same structure with β = 1.0. Neglecting the VFS with β = -1.0, which provides the poorest performance with respect to all parameters, it can be seen that the base shear attracted by the various systems increases with β. The same trend can be observed with respect to peak displacements, while the residual displacements follow the opposite trend. However, it can be seen that the three systems with β= 0, β = 0.5 and β= 1.0, can all rely on good re-centering properties as analogous (low) values of peak residual displacements were recorded at the end of the analyses.

5.4 Conclusions

While the results presented in this chapter are of very preliminary nature, a number of interesting observations can be made. First, the results presented herein have pointed out a number of issues pertaining to flat VFS (β = -1.0) that were not evident following the analysis of SDOF case studies. In contrast, it emerged that VFS with intermediate values of β may bring some advantages, at least pertaining to certain performance parameters such as peak lateral displacements.

While there is not a single VFS that has performed consistently better than the others, one may cautiously conclude that a system with β = 0 may represent the optimal base isolation solution for the structures analyzed, as it behaves consistently well, with respect to all the parameters considered.

Overall, it is believed that the results discussed in this chapter are encouraging, particularly considering that the case study structures were designed considering a base isolation

system made of a series of FP, and not targeting the optimal VFS characteristics.

Chapter 6

CONCLUSIONS AND FUTURE WORK

A new family of friction bearings, referred to as Variable Friction Systems, have recently been introduced as earthquake protection devices potentially capable of achieving high performance. It is believed that the extra degree of freedom, introduced in the form of a sliding surface characterized by variable friction properties, allows the designer to obtain high-performing base isolators. This thesis has presented an extensive discussion on VFS, going over the mechanics, the numerical modeling and the design processes currently available for these systems. In this context, this research work has attempted to make some contributions towards a better understanding of the seismic behavior and performance of these new systems, in the hope of furthering their development and practical implementation.

A number of tasks have been undertaken over the course of this project: first, the damping properties of VFS have been studied and characterized; second, the performance of these new devices has been studied through an extensive numerical campaign, conducted on SDOF case study structures; third, a preliminary investigation on the effectiveness of VFS at protecting MDOF structures has been carried out.

In the process, design equations to calculate the effective damping pertaining to VFS with different characteristics, as well as equations to calculate design demand reductions, have been validated and/or developed.

One important outcome of this project is that a generalized design approach for VFS characterized by arbitrary combinations of radius of curvature and frictional properties, is now available. To this end, the results of more than 500,000 nonlinear time history analyses, conducted with a customized computer program, have been used to provide evidence of the reliability of Direct Displacement Based Design approach (DDBD) proposed.

The performance of different VFS (classified as a function of the parameterβ, the ratio between the re-centering stiffness and the post-activation stiffness) has also been extensively investigated. Studies on SDOF case study structures of various characteristics showed that, in general, lowering the value of β tends to produce devices capable of higher performance with respect to parameters such as maximum displacement, maximum forces, and maximum accelerations. However, lowering the value of β tends to reduce the re-centering properties of the systems. To this end, the re-centering properties of the systems remain high for all positive values of β and acceptable for negative values of β greater than -0.5. Particularly critical in this regard are systems with β = -1.0, for which the residual displacement is on average around 80% of the maximum displacement reached.

Having base isolators with good re-centering properties is of relevance mainly with respect to contingent aftershocks, which may induce further motion before the system has been forcedly returned to its original position. This issue should be explicitly taken into account during the design phases, and informed decisions should be made not only with respect to the peak response of the systems, but incorporating the residual displacement, along with aftershock induced demands, into a rational design framework. In fact, it has been discussed that systems with poor re-centering capabilities may still be employed to achieve high overall seismic performance. In general, different base isolation devices may have benefits and drawbacks, depending on specific situations and particular needs. It should also be noted that even though not addressed in this work, there may be practical constraints that may limit the freedom to select certain values of friction coefficients or radii of curvature.

Preliminary analyses performed on MDOF case study structures have pointed out a number of interesting aspects of the behavior of VFS that could not be observed while studying SDOF systems. For instance, it was shown in Chapter 5 that flat VFS (β = -1.0), when used in combination with MDOF structures, do not perform as well as expected and that they may not be ideal solutions after all. However, the results of Chapter 5 have also shown that VFS with intermediate values of β bring a number of advantages pertaining to certain performance parameters, such as peak lateral displacements, and that may indeed

offer enhanced seismic protection in certain situations. For example, while none of the VFS studied performed consistently better than the others, it seems that the highest overall performance of the MDOF structures studied may be theoretically achieved using a VFS with $\beta = 0$. This system, appeared to behave consistently well, with respect to all the parameters considered.

Although the variable friction concept is still preliminary and requires further practical development, the potential capability to improve the seismic performance of structures with relatively minor effort, and the encouraging results of this study, suggest that VFS may be a viable and effective alternative to more "traditional" methods of isolation.

Further research including numerical simulations and laboratory experiments is obviously required, to verify the behavior of the devices under more complex conditions (e.g. velocity and pressure dependency, bi-directional loading). Future research projects could also look into the possibility of extending the variable friction idea to multiple curvature base isolators, such as double and triple pendula.

REFERENCES

ASCE (2013). *Minimum Design Loads for Buildings and Other Structures : ASCE7- 10*. American Society of Civil Engineers/ Structural Engineering Institute (oct).

Bollard, A. and Ranchhod, S. (2011). "Economic impacts of seismic risk: lessons for wellington, <rbnz.govt.nz>.

Calvi, G., Ceresa, P., Casarotti, C., Bolognini, D., and Auricchio, F. (2004). "Effects of axial force variation in the seismic response of bridges isolated with friction pendulum systems." *Journal of Earthquake Engineering*, 8(spec01), 187–224.

Calvi, P. M., Moratti, M., and Calvi, G. M. (2016). "Seismic isolation devices based on sliding between surfaces with variable friction coefficient." *Earthquake Spectra*, 32(4), 2291–2315.

Calvi, P. M. and Ruggiero, D. M. (2016). "Numerical modelling of variable friction sliding base isolators." *Bulletin of Earthquake Engineering*, 14(2), 549.

Casarotti, C. and Pavese, A. (2014). "Statistical results of a wide experimental campaign on full scale curved surface sliders." *Proceedings of the 2nd ECEE&S, Istanbul*.

Center, P. E. E. R. (2013). *PEER - NGA database*.

Charles Roeder, John Stanton, A. T. (1990). "Fatigue of steel-reinforced elastomeric bearings." *Journal of Structural Engineering*.

Chopra, A. K. (2014). *Dynamics of Structures: Theory and Applications to Earthquake Engineering*. Pearson.

Chopra, A. K. and Chintanapakdee, C. (2001). "Comparing response of sdf systems to near-fault and far-fault earthquake motions in the context of spectral regions." *Earthquake engineering & structural dynamics*, 30(12), 1769–1789.

Constantinou, M., Mokha, A., and Reinhorn, A. (1990). "Teflon bearings in base isolation ii: modeling." *Journal of Structural Engineering*, 116(2), 455–474.

Dhakal, R. (2010). "Damage to non-structural components and contents in the 2010 darfield earthquake." *Bulletin of the New Zealand Society for Earthquake Engineering*, 43(4), 404.

EC8 (1998). "Eurocode 8: Design of structures for earthquake resistance." British Standard.

Emilio Rosenbleuth, I. H. (1964). "On a kind of hysteretic damping." *Journal of the Engineering Mechanics Division*.

FEMA (1999). "Earthquake loss estimation methodology." *HAZUS Technical Manual*.

Fenz, D. M. and Constantinou, M. C. (2006). "Behaviour of the double concave friction pendulum bearing." *Earthquake Engineering & Structural Dynamics*, 35(11), 1403–1424.

Fenz, D. M. and Constantinou, M. C. (2008). "Modeling triple friction pendulum bearings for response-history analysis." *Earthquake Spectra*, 24(4), 1011–1028.

Filiatrault, A. (2003). "Performance of non-structural components during the february 28, 2001 nisqually (seattle-olympia) earthquake." *Proceedings of the Structures Congress and Exposition*, 763–774, <www.scopus.com>.

Girish, M. and Pranesh, M. (2013). "Sliding isolation systems: state-of-the-art review." *J. Mech. Civil Eng*, 2278(1684), 30–35.

Industriale, F. (2012). *FIP catalogue*. FIP Industriale, Italy.

Kasalanati, A. and Constantinou, M. C. (2005). "Testing and modeling of prestressed isolators." *Journal of Structural Engineering*, 131(6), 857–866.

Kelly, J. M. (1982). "The influence of base isolation on the seismic response of light secondary equipment." *Report no.*, California Univ., Berkeley (USA). Earthquake Engineering Research Center.

Kelly, J. M. (1993). "The implementation of base isolation in the united states." *ASME-PUBLICATIONS-PVP*, 256, 159–159.

Kelly, J. M. and Tsai, H.-C. (1985). "Seismic response of light internal equipment in base-isolated structures." *Earthquake Engineering & Structural Dynamics*, 13(6), 711–732.

MathWorks (2012). "Matlab and statics toolbox release." The MathWorks Inc.

Mokha, A., Constantinou, M., and Reinhorn, A. (1990). "Teflon bearings in base isolation i: testing." *Journal of Structural Engineering*, 116(2), 438–454.

Mokha, A., Constantinou, M., Reinhorn, A., and Zayas, V. A. (1991). "Experimental study of friction-pendulum isolation system." *Journal of Structural Engineering*, 117(4), 1201–1217.

Morgan, T. A. (2007). *The use of innovative base isolation systems to achieve complex seismic performance objectives*. ProQuest.

Morgan, T. A. and Mahin, S. A. (2011). *The use of base isolation systems to achieve complex seismic performance objectives*. Pacific Earthquake Engineering Research Center.

Naeim, F. and Kelly, J. M. (1999). *Design of seismic isolated structures: from theory to practice*. John Wiley & Sons.

Newmark, N. M. and Rosenblueth, E. (1971). "Fundamentals of earthquake engineering." *Civil engineering and engineering mechanics series*, 12.

Pant, D. R., Wijeyewickrema, A. C., and ElGawady, M. A. (2013). "Appropriate viscous damping for nonlinear time-history analysis of base-isolated reinforced concrete buildings." *Earthquake Engineering & Structural Dynamics*, 42(15), 2321–2339.

Pennucci, D., Sullivan, T., and Calvi, G. (2011). "Displacement reduction factors for the design of medium and long period structures." *Journal of Earthquake Engineering*, 15(S1), 1–29.

Petrini, L., Maggi, C., Priestley, M., and Calvi, G. (2008). "Experimental verification of viscous damping modeling for inelastic time history analyzes." *Journal of Earthqukae Engineering*.

Pietra, D., Pampanin, S., Mayes, R. L., Wetzel, N. G., and Feng, D. (2015). "Design of base-isolated buildings: An overview of international codes." *Bulletin of the New Zealand Society for Earthquake Engineering*, 48(2).

Priestley, M., Calvi, G., and Kowalsky, M. (2007a). "Direct displacement-based seismic design of structures." *2007 NZSEE conference*.

Priestley, M., Calvi, G., and Kowalsky, M. (2007b). *Displacement Based Seismic Design of Structures*. IUSS Press.

Priestley, M. and Grant, D. (2004). "Viscous damping in seismic design and analysis." *Journal of Earthquake Engineering*.

Priestley, N., Calvi, M., Petrini, L., and Maggi, C. (2007c). "Effects of damping modelling on results of time-history analysis of rc bridges." *1st US-Italy Seismic Bridge Workshop, Pavia, Italia*.

Rai, D. C., Singhal, V., S., B. R., and Sagar, S. L. (2016). "Reconnaissance of the effects of the m7.8 gorkha (nepal) earthquake of april 25, 2015." *Geomatics, Natural Hazards and Risk*, 7(1), 1–17.

R.I. Skinner, W. H. Robinson, G. M. (1993). *An Introduction to Seismic Isolation*. John Wiley and Sons Inc., New York, NY, USA.

Robinson, W. (2011). "Lead-rubber hysteretic bearings suitable for protecting structures during earthquakes." *Seismic Isolation and Protective Systems 2.1*.

Roussis, P. C. and Constantinou, M. C. (2006). "Uplift-restraining friction pendulum seismic isolation system." *Earthquake engineering & structural dynamics*, 35(5), 577–593.

Ryan, K. L., Dao, N. D., Sato, E., Sasaki, T., and Okazaki, T. (2012). "Aspects of isolation device behavior observed from full-scale testing of an isolated building at e-defense." *20th Analysis and Computation Specialty Conference*, 25–36.

Ryan, K. L. and Polanco, J. (2008). "Problems with rayleigh damping in base-isolated buildings." *Journal of structural engineering*, 134(11), 1780–1784.

Victor Zayas, S. L. (1990). "A simple pendulum technique for achieving seismic isolation." *Earthquake Spectra*.

Victor Zayas, Stanley Low, S. M. (1987). "The fps earthquake resisting system experimental report." *Report No. UCB/EERC 87/01*, University of California, Berkeley Earthquake Engineering Research Center.

Warn, G. P. and Ryan, K. L. (2012). "A review of seismic isolation for buildings: historical development and research needs." *Buildings*, 2(3), 300–325.

Wolff, E. D. and Constantinou, M. C. (2004). *Experimental study of seismic isolation systems with emphasis on secondary system response and verification of accuracy of dynamic response history analysis methods*. Multidisciplinary Center for Earthquake Engineering Research.